A NOVEL ACTUATED DIGIT WITH TACTILE FEEDBACK FOR CLINICAL APPLICATIONS

BETTY KIT YEE TAM

Doctor of Philosophy

ASTON UNIVERSITY

January 2006

ASTON UNIVERSITY

A NOVEL ACTUATED DIGIT WITH TACTILE FEEDBACK FOR CLINICAL APPLICATIONS

BETTY KIT YEE TAM
Doctor of Philosophy
January 2006

Thesis Summary

This thesis describes the work carried out on the development of a novel digit actuator system with tactile perception feedback to a user and demonstrated as a master-slave system. For the tactile surface of the digit, contrasting sensor elements of resistive strain gauges and optical fibre Bragg grating sensors were evaluated. A distributive tactile sensing system consisting of optimised neural networking schemes was developed, resulting in taxonomy of artificial touch. The device is suitable for use in minimal invasive surgical (MIS) procedures as a steerable tip and a digit constructed wholly from polymers makes it suitable for use in Magnetic Resonance Imaging (MRI) environments enabling active monitoring of the patient during a procedure. Minimal invasive surgical procedures have come to the forefront of clinical treatment medicine. Advantages for using this type of treatment include reduced pain, blood loss and briefer recovery times for the patient. However, for the clinician, visual and tactile senses are hindered due to complexity movement through narrow openings and complex internal geometry of the human beings, coupled with poor feedback and possibly the control of complex delivery mechanisms. To provide a realistic template of the work, the research responded to the needs of two contrasting procedures: palpation of the prostate and endotracheal intubation in anaesthesia where the application of touch sense can significantly assist navigation. The performance of the approach was demonstrated with an experimental digit constructed for use in the laboratory in phantom trials. The phantom unit was developed to resemble facets of the clinical applications and digit system is able to evaluate reactive force distributions acting over the surface of the digit as well as different descriptions of contact and motion relative to the surface of the lumen. Completing control of the digit is via an instrumented glove, such that the digit actuates in sympathy with finger gesture and tactile information feedback is achieved by a combination of the tactile and visual means.

Keywords
Distributive Tactile Sensing, Clinical Diagnostic Tools, Endoscopy, Minimal Invasive Surgery

Dedicated to My Parents and Family

Acknowledgments

I would like to acknowledge the help and guidance from my supervisors Prof. Peter Brett and Dr David Holding.

Grateful acknowledgement is made to
Prof Guiseppe Tritto and Prof Mansell V Griffiths
for their support on clinical matters.

Thank you to the staff from Aston University for their technical assistance.

Finally I would like to thank my family, friends and colleagues for all their encouragement and support during this work.

Contents

List of Tables

List of Figures

Nomenclature

Symbol	Description
A	Area of the cross section of the tube
a	Length
b	Breadth
$b_j^{(1)}$	Bias of first layer
$b_j^{(2)}$	Bias of second layer
D,d	Diameter of Tube
$Diff$	Moment Difference
E	Young's Modulus
F	Load Magnitude
f	Transfer function of the process, Unit Force
$f(z)$	Function z
GF	Gauge Factor
h	Beam Thickness
i	intensity at a specific wavelength
I	Intensity, Second Moment of Inertia
$_i$	Target
$_j$	Source of connection
K	Pressure
L	Length
l	Load position
M	Number of hidden units, Torque
m	Unit Mass
N	Number of input units
NA	Neutral Axis
$o_{(i)}^{(2)}$	Output vector
$_{ORG}$	Origin
P	Pressure, Position Vector
R	Resistance, Radius of Curvature, Rotation Matrix

s	Sector of a Circle
S_1	Original length of the digit
S_2	Length of the digit when subjected to pressure
S1	Sensor 1
S2	Sensor 2
S3	Sensor 3
S4	Sensor 4
SG	Strain Gauge
t	Thickness of Tube
v_a	Deflection about a
W	Load
w	Unit Width
x_k	Input signals from the sensors
$\omega_{jk}^{(1)}$	Weight of the first layer
$\omega_{ij}^{(2)}$	Weight of the second layer
θ	Angle of Curvature
λ	Wavelength
λ_p	Peak Wavelength
ε	Strain

List of Abbreviations

Abbreviation	Description
ADC	Analogue Digital Conversion
ANN	Artificial Neural Network
BPH	Benign Prostatic Hyperplasia
BSE	Bovine Spongiform Encephalopathy
CJD	Creutzfeldt-Jakob Disease
DRE	Digital Rectal Examination
FBG	Fibre Bragg Grating
FPGA	Field Programmable Gate Array
MAT	Minimal Access Therapy
MIS	Minimally Invasive Surgery
MIT	Minimally Invasive Therapy
MRI	Magnetic Resonance Imaging
PDA	Personal Digital Assistant
PTFE	Polytetrafluoroethylene
SG	Strain Gauge
SoC	System on a Chip
UV	Ultra Violet
VCJD	Variant Creutzfeldt-Jakob Disease
VRML	Virtual Reality Modeling Language

Chapter 1

Introduction

This thesis describes the research into a new approach for retrieving tactile sensory information in minimal invasive surgery (MIS). A flexible digit actuator (end tool digit) with tactile perception feedback to a user was developed and demonstrated within a master-slave system. The research uses the distributive tactile sensing method to create a digit for clinical applications that is simple and minimalist in solution. It is unique as it is capable to register position with respect to the tissue, enabling spatial positioning and sensing shape. In the research, studies have drawn the requirements for palpation and navigation through touch sense for clinical procedures such as palpation of the prostate for diagnoses and endotracheal intubation in airway management. The digit has been demonstrated in a series of laboratory experimental phantom trials of individual elements of a whole system, so as to isolate the different facets of measurement of touch. It has been shown to increase the perception of the working site to the user when using an instrumented glove developed for the system. Control of the digit is via the glove, such that the digit actuated in sympathy with finger gestures and tactile

information feedback is achieved by a combination of tactile and visual means. The overall aim of this research is to build an actuated digit system with feedback, focusing on the implementation of the distributive tactile technique that will infer parameters of contact, and to relay this information back via though tactile and visual means. This chapter provides a brief overview of the objectives and overall outcome of the project. It also sets the scene to the challenges involved in developing such a system.

1.1 Research Objectives

The principal objectives of this work are to:

- Ascertain the challenges in designing a medical device for minimal invasive surgical procedures and to identify potential applications where tactile feedback is beneficial to the enhancing the performance of the procedures involved.
- Develop a distributive tactile technique suited for use in an actuated tool end.
- Determine how touch can be classified within a set of computational algorithms using logical systems.
- Construct an actuated tool end with the distributive tactile sensing system on board and test its performance when actuated.
- Create a phantom test rig that will model the information within touch to test the tool end tactile sensor's performance over a set of criteria required to identify characteristics of clinical procedures.
- Construct an intuitive input device that will drive the actuation of the tool end and provide feedback to the user.
- Demonstrate the complete system for controlling the movement of the tool end with tactile and visual feedback to show the how the system can be utilised for a specific applications.

1.2 Research Outcomes

The results of the research demonstrated the development, construction and testing of a novel digit actuator system with tactile perception to user and demonstrated as a master slave system for use in clinical applications.

- Evaluation of the clinical needs resulted in the classification of the endoscopy and the lead to the identification of the clinical applications appropriate for the distributive tactile sensing technology placed in an actuated digit; navigation in endotracheal intubation and palpation in transanal examination of the prostate.
- The dimension of the potential digit could range from 0.008 mm up to 65 mm in diameter (based on the lumen size a human adult), though a hydraulic actuation method will have to be used for smaller diameter digits as a pneumatic system is more suited for low pressure, large scale digits.
- Distributed tactile sensing systems consisting of contrasting sensor types; strain gauge sensors and Fibre Bragg Grating (FBG) optical sensors were created and evaluated for their performance. The results for a distributed tactile sensor consisting of four sensing elements on a cantilever beam showed that on average, FBG sensors outperformed strain sensors in accuracy by 8.2 % due to lower signal noise.
- FBG sensors are inert to electromagnetic interference, making them suitable for use in magnetic resonance scanning environments, an alternative to higher risk x-ray scanning.
- FBG sensors are also significantly smaller than strain gauges and when produced in high volumes, low in cost, making this type of sensing element highly suitable for use in disposable clinical applications where sterility of instrumentation is a critical factor in health care.
- The performance of the FBG sensors indicated an improvement in the output of optimised neural network systems developed for evaluating

parameters of touch. Optimising the neural networks also resulting in a taxonomy of artificial touch which categorises touch into different characteristics functions that are invoked in a hierarchical order according to the type of touch motion.

- The reduction of a single sensing element from the four sensing elements used in the cantilever experiment showed only a slight reduction in the performance of the distributive sensor, by a factor of 0.5 % difference in accuracy in determining contact presence, 3.7 % reduction in load magnitude and a slight improvement of 0.4 % load position, and due to size constraints on the manufactured digit, three was the number of sensing elements used.
- The digit was manufactured and tested in experimental phantom trials based on the tactile parameters required for the clinical applications, developed from the taxonomy of touch. The parameters were the presence of contact, orientation of contact load, multiple contacts, load magnitude, static and dynamic load positioning, contact stiffness and palpation.
- The digit was able to evaluate force distributions acting over the surface of the digit and discriminate different descriptions of contact and motion relative to the surface of the lumen for speeds up to 20 mm/s.
- A glove input device that provided input motion and tactile feedback prompts was created and tested, resulting in successful sympathetic motion of digit with finger gestures provided for input motion.
- Visualisation techniques were used to describe the side profile of the digit deformation when under pressure and to indicate parameters of contact such as contact region and the direction.
- A complete system with a central controller was produced and demonstrated the envisaged master slave system.

1.3 Background Information

Minimal invasive surgical (MIS) procedures are increasing in frequency in surgery. Advantages of this for treatment are reduced pain, reduced blood loss and potentially lower costs as a result of the shorter recovery periods. For the clinician, visual and tactile senses are hindered because of unnatural control of movement through narrow openings and complex internal geometry of the human body. This provides new challenges, and these are set to increase with miniaturisation of access and size of the working target. In practice, vision feedback is derived by microscope or relayed via a miniature camera to a display screen. By comparison, tactile feedback is more difficult to retrieve from the working site. Tools such as laparoscopes, endoscopes and other micro-surgical tools are used manually with little tactile sensation as changing forces are not readily detected through the long scoped mechanisms involved and are often beyond perceptible thresholds of human sensation.

The human body is far more dexterous and complex than any robotic substitute. There are 206 bones in the human body with 27 in each hand. In the hand there are bones called phalanges which are fourteen in number, three for each finger, and two for the thumb (Gray, 1995)[1] which allow the fingers to curl all the way around to make contact with the palm allowing humans to grasp things tightly. The thumb, when used in conjunction with fingers, enables even very small items like sewing needles to be picked up. However, when MIS and microsurgery is performed, the instrument tips are inside the body, and the clinician is outside, so a system to translate large movements from ex-vivo into tiny movements has to be developed. When the shaft for endoscopic can be from 30 cm to 50 cm in length (Li, 2001)[2], there is loss of tactile feedback from the site of the wound to the clinician caused by relative distance. It would be constructive if the discrepancies in tactile feedback and enhancements to visual–motor feedback and control could be addressed. Human skills take many forms such as the control and coordination

of muscle groups (Schmidt, 1991)[3]. The capabilities of basic skills such as the ability to walk, balance and eat are biologically inherited skills required for survival. Other experiences from childhood shape the skills human are able to perform as adults. Human life can be conducted with more efficiency by gaining proficiency in skills. A surgeon has a high level of manual skill and dexterity to perform life-enhancing procedures, but nevertheless the development of the next generation of minimally invasive surgical instruments needs to include greater sensory feedback to augment control by the clinician.

The challenges of this research are to develop a master-slave system consisting of a user providing motion for a tool to perform a procedure on remote tissue and then relaying perception feedback to the user. The envisioned system consists of a series of functions in a control strategy as shown in the overall strategy diagram (Figure 1.1).

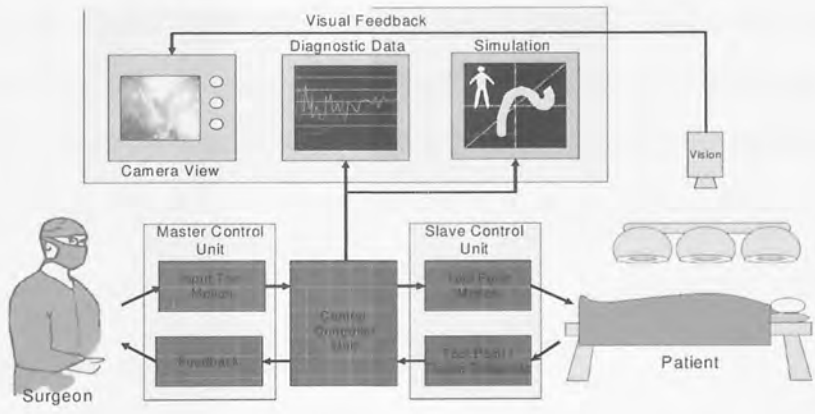

Figure 1.1 A schematic diagram of the master-slave system

The human operator is the clinician, who provides input motion for the tool that is sensed by the master system and is transmitted as a control demand to the tool point operated by the slave system. The reaction of the tissue is sensed by the tool and transmitted to the master system where controlled actuators are applied to the resist the motion of the input device and send other sensory feedback to the user. Examining Figure 1.1 more closely, the roles of the clinician, tactile information,

the tool point, the input device, visualisations and the central control are the main themes examined in this thesis.

1.3.1 The Clinician

A human has five senses, hearing, sight, touch, taste and smell. In traditional surgery, the clinician will use visual and touch feedback to perform operations, as he/she will have full access to the site requiring intervention. In minimal invasive surgery, both these sensations are restricted. The clinician is reliant on visual feedback provided by a camera incorporated into the operating device. Touch feedback is also restricted as there is no direct tactile feedback from the tissue to the clinician. The clinician must manoeuvre the instrument through a body with limited sensations and is able to do so with training and experience. However, the type of manoeuvres will be limited to the instruments available. It is important to establish what sensations are critical when developing the input and feedback devices. The needs of the clinician are incorporated into the design of a new device and this information is explored in greater detail in Chapter 2.

1.3.2 Tactile Information

Tactile sensors can be incorporated into the tool point of the system to give touch information to the user. The tactile requirements are based on the needs of the clinician in order to enhance the performance of an examination or procedure. A tactile sensor is a device or system that can measure a given property of an object or contact event through physical contact between the sensor and the object (Lee & Nichols, 1999)[4]. Building on the surveys carried out in the 1980s by Harmon (Harmon, 1982)[5] and (Nicholls and Lee)[6] and in the early 1990s by Nicholls (Nicholls, 1992)[7], the growth of tactile sensors in the 1990s as well as the types

and uses of contemporary tactile sensors was described. Tactile sensors have been used in robotics and medicine. Tactile sensing is defined as the continuous sensing of variable contact forces. The majority of tactile sensors used are array or matrix types, which use large numbers of sensing elements, however in this research; a distributive tactile sensing technique is implemented and designed for a flexible actuated digit. This methodology is described in Chapter 3 of this thesis.

1.3.3 The Tool Point

One of the primary goals for this project is to produce a robust working prototype of a flexible tool end and demonstrate that the mechanism can be operated with a closed loop control system. It has been demonstrated that it was possible to manufacture a flexible device that could replicate finger-like movement (Brett & Stone, 1997)[8]. Distributive tactile sensors were incorporated into this design and tested to determine its suitability for clinical applications. Material considerations, construction techniques and mechanical robustness of a prototype are discussed in Chapter 4. In Chapter 5, the digit is evaluated for its suitability for use in specific clinical procedures.

1.3.4 The Central Controller

Bridging the gap between the end tool and input device is the central controller. In this research, the controller is operated from a desktop PC using MatLab, Simulink and Real Time Workshop to compile an executable program for control through an A/D card. This is the heart of the system, controlling the decisions and appropriate responses required for an intelligent system described in greater detail

in Chapter 6 as descriptions how the input device and visualisations are incorporated into the system.

1.3.5 The Input Device

The clinician will need an input device to drive the system. Conventional minimally invasive instruments are held in one hand, either with a handle (Figure 1. 2A and 1. 2C) or with a thumb and finger (scissor) configuration (Figure 1. 2B). The tool point is in contact with the tissue. The master input tool, via the central controller, controls it. Contemporary tool tips are usually pincer like (Figure 1.3). If alternative designs of tool tips were developed, they will have to offer more dexterity than current designs. In Chapter 6, different modes for inputting motion are examined as well as obtaining tactile feedback information from the tool point.

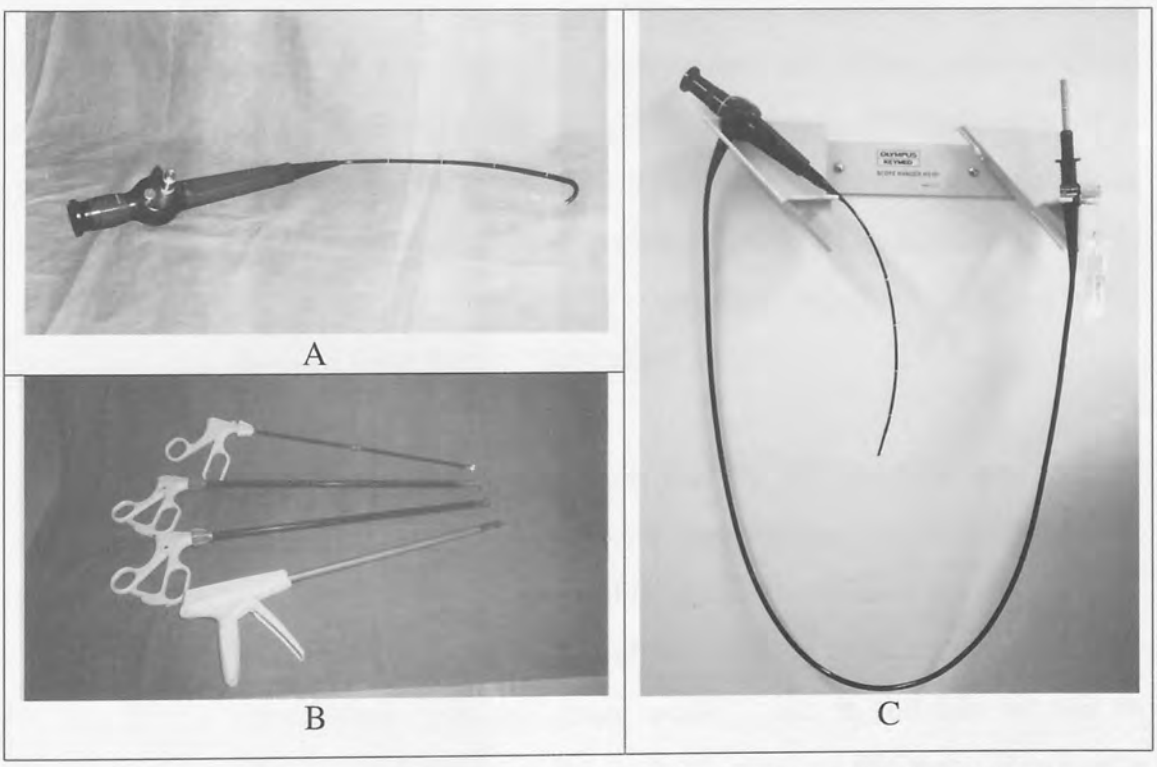

Figure 1. 2 Instruments used in minimally invasive surgery: (A) Rigid Stortz Endoscope, (B) Laparoscopic Tools and (C) Flexible Nasal Endoscope

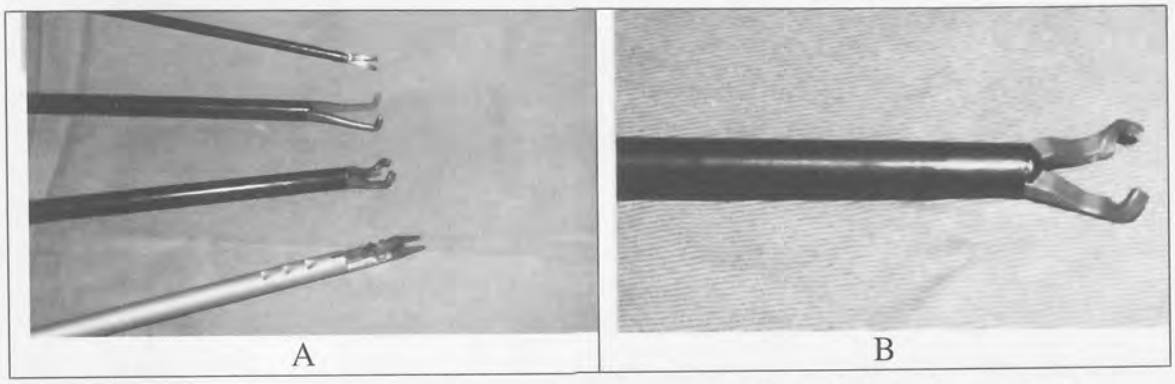

Figure 1.3: Figure 1.3A shows an array of laparoscopic tool tips. Figure 1.1B shows a laparoscope tool tip in greater detail

1.3.5 Visualisations

It is important for the clinician to see where the instrument is located inside the body. At present, the viewing apparatus that enables the clinician to see the image directly in front of the lens, although as the camera approaches the point of contact, the intensity of the light from the camera can often cause a visual *whiteout*. Currently, if the clinician would like to see a different view, it is possible to crudely manoeuvre the instrument tip to another angle, provided there is enough space. Other methods of visualisation can be used in addition to simple vision devices. Computer generated or computer enhanced imaging offer positional data obtained from tactile information.

The technology developed in this research can be incorporated into current medical instruments such as endoscopes and laparoscopes or the technologies developed further to produce novel medical devices. In addition, this technology could be used for a wider range of industrial and military applications. A design of the device, constructed from polymers would make it suitable for use in electromagnetically hostile environments such as used in Magnetic Resonance Imaging (MRI).

1.4 Thesis Structure

This thesis is organised into six further chapters. Following this introduction is an overview of each of the chapters.

Chapter 2 focuses on clinical systems and the supporting technologies are discussed to provide a setting on which this research is based. This chapter starts with a brief overview of the history surrounding Minimal Invasive Therapy (MIT) and endoscopy. Following on from this are some general clinical design considerations for a digit like device, such as the working environment, actuation and the significance of scaling, size and access. A review of endoscopic clinical procedure is carried out and classified to identify the technical functional capabilities required of endoscopic tools leading to the conclusion that a tactile digit that used for palpation and navigation can be developed. Potential applications that this digit can be used are described, both clinical and non clinical. The digit is an element of a complete system and tactile feedback. The system can be evaluated within a phantom evaluation device and how this can be achieved is discussed towards the end of this chapter.

Chapter 3 explores the uses of tactile sensors, in particular distributive tactile sensing systems. The methodology of the distributive tactile sensing technique is explained, with emphasis on the implementation of artificial neural networking techniques. Sensing elements integral to all tactile sensing systems are discussed, focusing on two types; strain gauge sensors and photonic sensors constructed from optical fibres etched with Bragg gratings. Experiments on a cantilever that resembles the dimensions and movement of a digit-like device were carried out on the contrasting sensor types and described and their performance quantified in terms of successful detection of contact, load magnitude and load position.

Chapter 4 shows the process of how the prototype digit was developed, incorporating the distributive tactile sensing technique described in Chapter 3. Initial design concepts, the materials for construction, actuation and modelling of the prototype device are discussed before the final design is described. The digit is tested and for reliability of structure when the sensors are integrated and implementation of manufacturing techniques for volume production is discussed.

Chapter 5 introduces the philosophy behind the taxonomy of touch; that touch can be defined over a range of different characteristics in a hierarchical format, dependent on the application. From this hierarchy, characteristics relevant to palpation and navigation were extracted. Individual phantom experiments to measure the performance of each of these characteristics when using the tactile digit developed in Chapter 4 are described in three sections as fundamental touch, navigational and palpation characteristics.

Chapter 6 integrates all the functions required for the master-slave system for an actuating digit with tactile feedback and describes the central control system. These components are the master input device and the slave digit. Methods of inputting and receiving data are reviewed. Feedback methods are discussed and a survey of contemporary tactile feedback devices is made. The solution for the input device suited to the actuating digit; an instrumented glove input device is introduced. The construction method, input and feedback output are described. To complete the picture of the system, a method of graphical visualisation auxiliary to the system is described, demonstrated and explored.

Chapter 7 concludes the thesis with the principal contributions and findings from these studies. Suggestions for further work to enhance the performance of this system are also made.

Chapter 2

The Context of Clinical Procedures in Design Evaluation

This chapter reviews the background information relating to the clinical application and context of this project. The history of surgery preceding the advent of minimal invasive therapy (MIT) is described. Factors affecting the clinical working environment such as gamma radiation or electromagnetic interference and the merits of inert materials and instrumentation are discussed. The importance of sterility and disposability of clinical instruments as well as practical issues of actuation, access and scaling issues are examined when considering designing endoscopic like devices. Endoscopic devices are used in internal examination of the body and the functions they perform are described and findings show that endoscopy can be used for a wide range of activities with respect to diagnosis and treatment. In diagnosis, the instrument tips of endoscopic devices are distanced from the hand of the clinician, leading to the absence of tactile information. Tactile information can be used to navigate or to palpate, and a clinical digit was envisioned. Clinical applications of transanal examination of the prostate and in endotracheal intubation are examples that demonstrate a tactile feedback digit's use in palpation and navigation.

2.1 Surgery and Minimal Invasive Therapy

Surgical procedures carried out by hand have been performed for thousands of years. Apart from dealing with wounds and fractures, early surgeons carried out operative procedures such as cutting for bladder stones, circumcisions and trepanning (Ellis, 2001)[9], where a hole was drilled into the skull to relieve pressure in the brain. This procedure was performed as early in the Neolithic Age (about 10,000 to 6000 years BC) (History of Surgery, c 2004)[10]. Over the centuries, as clinical skills developed, more complex surgical procedures were developed. By the twentieth century, technological advances such as anaesthesia, diagnosis by X-ray and the use of antibiotics were commonplace. Microsurgery and organ transplants could be carried out in the 1950s.

2.1.1 The History of Endoscopy

Endoscopy is a term used to describe examining the inside of the body using a thin lighted, flexible instrument called an endoscope. Access to the body would have been via a natural opening. Hippocrates in Ancient Greece first described endoscopy with reference to a rectal speculum. Roman medicine also produced instruments with which they could inspect internal organs. In the 1806, Philipp Bozzini developed a light conductor called the *Lichtleiter* (Miller, 1986)[11]. This early endoscope directed light into the internal cavities of the body and redirected to the eye of the observer. However, it was not until the mid twentieth century that the rod-lens system and fibre-optics were developed by Harold H Hopkins and later still, in the 1970s and 1980s when the technique of performing laparoscopy (abdominal surgery) through a miniature incision (keyhole) was developed and practiced. (History of Minimally Invasive Surgery , c 2004)[12].

2.1.2 Minimally Invasive Surgery

The term for Minimal Invasive Therapy (MIT) refers to the all diagnostics and surgery procedures which employ instruments inserted into the body through natural orifices or small artificial punctures (Dario et al, 1996)[13]. Minimally Invasive Therapy involves minimal physical disturbance in accessing the site of treatment which may also include non invasive procedures such as ultrasonic waves directed from the skin surface in shattering kidney stones, allowing the stone fragments to pass through the body naturally. Within the term MIT is minimal access therapy (MAT), which aims to preserve all tissues and organs not involved in the pathological processes of the organs being operated on. Minimal Access Therapy is encompassed in the definition of MIT but suggests that using naturally occurring entry points or small incisions into the body to promote faster healing, but this restricts access to the site of treatment.

The aim of MIT procedures is to provide health care with reduced trauma to the patient. Damage causes to muscular tissue, nerves and blood vessels, bleeding from complex organs in conventional surgery leads to changes in the biochemistry and haematology. Hence the use of minimally invasive and micro-endoscopic surgery avoids any iatrogenic damage with negligible disturbances to the patient's homeostatic mechanisms (Wickham et al, 1986)[14]. The advantages this therapy compared to traditional open surgery are the reduction of tissue trauma, scarring and post-operative pain levels, and patient recovery times. (Minimally Invasive Surgery Defined, c 2004)[15]. There is overall potential to achieve lower economic costs due to reduced hospital stays, lower bed occupancy during recovery. Hence there is pressure to increase the use of micro-surgical procedures and procedures of minimal invasion.

While there are benefits to the patients and the benefits from the perspective of cost efficiency, this type of surgery creates additional challenges, to the surgeon.

He will require additional skills to deal with the precision needed in tool actuation with limited sensory feedback of the state of the tool point. Since minimally invasive surgeries (MIS) are performed through small apertures either a natural opening or as a small incision. Operating with limited access can be awkward for surgeons, who have traditionally relied heavily on dexterity, tactile feedback and excellent hand-eye co-ordination. This creates a different working environment compared to open surgery. Due to the size and access restrictions caused by MIS, the tools used for these procedures differ to those used in conventional open surgery. In MIS, surgeons must operate using distended instruments while looking at a television monitor showing anatomical visual images coming from a camera that is usually pointed by an assistant. (Taylor et al, 1996)[16].

Achieving visualisation may also require the creation and maintenance of an optical cavity, commonly created using carbon dioxide insufflation, particularly in abdominal surgery. Minimaliy invasive surgical procedures can also be carried out through a small natural orifice if there is one available, otherwise small incisions are made into the skin for narrow tubes to be inserted so that instruments can slide through them to perform surgical manoeuvres. Trocars (hollow styli with a triangular point) inserted into an inflated abdomen for laparoscopic surgery will allow access for instruments with diameters of 10 mm or less.

Endoscopic instruments are often used in other minimal invasive procedures. These instruments are frequently long scoped instruments with small tool tips or cameras at the end that are manipulated by mechanical movement at the held end. In comparison, tactile feedback is more difficult to retrieve from the working site (Tam et al, 2004)[17]. The distance between the tool tip operating on the tissue and the hand of the surgeon can be between 30 cm and 50 cm (Li, 2001)[18], leading to reduced haptic feedback required to perform operations compared when operating in general surgery.

The threshold of sensory perception in small-scale surgery, used in MIT and microsurgery is different from general surgery. Kinesthetics, the perception of the body part position and movement in space is challenged since spatial perception of small distances is spanned by the index finger and its opposable thumb regardless of whether the eyes are open or closed (Schiffman, 2001)[19]. In small-scale surgery, small distances are differentiated with the assistance of mechanical levers, but this distorts tactile and force information. Ideally, a system that aids sensory feedback and has control actuation that utilises natural input motion to the system is desired.

From this background information, we can consider specification when designing a novel clinical device, focusing on the needs of required for use in minimally invasive surgery such as the working environment, regulatory requirements for sterility and disposability, dimensions and location of access points to the inside of the body for a endoscopic like device.

2.2 General Clinical Design Considerations for a Digit

In this research, a clinical digit was developed. The device has to be appropriate to the practices in a clinical environment and bridges the gap in technology and perception where we respond to information not the data. By making the device more natural to use, it becomes more intuitive, complimenting the skills of the clinician and becoming an extension of the senses. This section discusses the clinical working environment, issues of sterility and disposability, actuation of the device with respect to its environment, the challenges of scale and size of the device

2.2.1 Clinical Working Environment

Practical design considerations include factors such as device manufacture to its use in practice, such as the environment the device is expected to operate in. This would include how to keep the instruments sterile and any working environment considerations such as electromagnetic interference or use of radiation for scanning the body during procedures, such as those used in x-ray fluoroscopy.

Some surgical interventions carried out in minimal invasive surgery would rely on pre-operative scan data visualise the access and site where the procedure is to be performed, obtained in various ways including x-rays, ultrasound and magnetic resonance imaging. Those procedures that scan the body during an operation are limited to either x-rays or the ultrasound.

The harmful effects of exposure to gamma radiation can lead to interactions with DNA and lead to damage such as carcinogenesis, genetic defects or congenital abnormalities (Skuldt, 2001A)[20]. There are safety guidelines in place that limit

the quantity of radiation that the patient and the clinical personnel should be exposed to, causing limitations such as time to perform a procedure.
There is potential for a device to be developed to enable clinicians to work wholly in a more inert environment such as in a magnetic resonance environment that do not pose the same danger in exposure as x-rays. Magnetic Resonance Imaging (MRI) is relatively non-invasive compared to methods that use ionising radiation and is able to provide superior soft tissue differentiation (Skuldt, 2001B)[21].

Following this direction would mean that any devices and systems within the area of the operation would have to be suitable for a magnetic environment. This may include avoiding the used of ferrous and other magnetically attractive materials, pushing device design into considering polymers as alternative materials for manufacture. This also increases the likelihood for the device to be mass produced and considered as disposable.

2.2.2 Sterility and Disposability

Any equipment used in surgery needs to be sterile. There are two methods; either to thoroughly cleanse the multi-use equipment after every use and in the case of high capital medical equipment that cannot be immersed in chemical cleansing agents, or high heat treatment, drapes are usually used. However, if drapes are use, they must sufficiently protect the equipment without impeding any functionality of the equipment.

Chemical disinfectant is commonly used to clean endoscopic devices where the instrument is taken apart and then placed in a bath of cleansing solution for several hours. Heat treatment using high temperature steam is also used to clean instruments. However both methods have require time to complete and in a busy clinical environment, where outpatient surgeries are being held this is often not practical as instruments would be out of commission for the duration of cleaning.

Both cleaning treatments may also cause damage as from either chemical erosion or heat damage. Irradiation is a commonly used sterilisation technique when producing medical devices in mass quantities. However, radiation can cause damage to instrumentation. For example, optical fibres will darken when irradiated (Berghmans et al, 2000)[22]. It should also be considered that scanning by x-rays during a medical procedure may also cause potential damage to instrumentation containing optical fibres.

An alternative for heat treatment may be cold plasma that works at room temperature and atmospheric pressure. Plasma is a collection of electrically charged and non charged particles and is usually produced by superheating a gas. By injecting a mixture of helium and oxygen into the gap between two electrodes supplied with voltage, cold plasma is created. Experiments with this plasma carried out on two classes of bacteria were lethal (Laroussi et al, 2003)[23]. Cold plasma could potentially be used to sterilise heat sensitive reusable medical equipment, however this technique is still in a development phase and has not generally been adopted.

The draft recommendations from the National Institute of Clinical Excellence that surgical instruments be made disposable to reduce the possibility of infection, in particular that of the brain disease Creutzfeldt-Jakob Disease (CJD). Variant CJD (vCJD) was discovered in 1996 and is believed to be the human form of bovine spongiform encephalopathy (BSE). It is believed that molecules of protein called prions transmit CJD and vCJD, and unlike other microbes they cannot be easily disabled or killed with disinfectants or by heating. In the rare case that a patient with CJD or vCJD is operated on there is a possibility that the instruments used may become contaminated with prions, that cannot be removed by cleaning and sterilisation leading to infection of the next patient operated on with the same equipment. The only way that surgery can be made completely safe is to use disposable instruments where possible for all operations (NICE, 2004)[24].

Sterilisation by chemical, heat, irradiation and cold plasma can still be used during the manufacturing process of disposable instruments.

2.2.3 Actuation of the device

Since the device is intended to work inside the body, methods of supplying power for actuation have to be considered. The simplest MIS instruments provide purely mechanical motion. More complex instruments can be driven by electrical power. The potential for the device to work in a magnetic environment brings to attention an alternative method of supplying power to the system and actuating the digit. Cable driven, mechanical systems would require electrical power at the point of use to the digit, hence when in a magnetic environment, the system could be affected. Alternatives such as localised pneumatic and hydraulic actuation can be explored.

2.2.4 Scaling, Size and Access Issues

The size of an access points in the body for MIS is small compared to cutting open the body for better access in conventional surgery. In MIS, an instrument is inserted into naturally occurring orifices, which include the pelvic region (including the urethra, vagina, and rectum), the nasal and sinus passage and the outer ear. In all these cases, the surgical devices have to travelling directly through lumen. When artificial openings are created, wound sites are generally chosen where there is already a natural route close to the site of access. For example, access to the heart during angioplasty is at an artery near the groin. A trocar is used to pierce the skin and tissue to access the artery. A balloon catheter then inserted at this point uses the natural path of arterial lumen to reach a location of blockage, which may be some distance away from access site and inflated.

The size of lumen within the human body needs to be considered when choosing the application for the device during the design phase. Research into the approximate range of adult human lumen was carried out (Appendix 2.1). From (Figure 2.1) we can see that the largest anatomical sizes are that in gastrointestinal tract and the upper respiratory tract as well as some concurrent research involved in the navigation of lumen. However, the length of these tracts complicates navigation through these passages. The human intestine is about 7 m in length, with the large intestine being 1.5m long (Gray, 1995)[25]. The narrower the lumen, the longer it tends to be, adding to the complexity of navigating a device to the site of treatment without causing compounded damage from dragging a long umbilicus supplying power to the device. For endoscopy, complex solutions such as an inchworm device (Dario et al 2000)[26] have yielded useful results. However, a solution that is low cost and suited to a range of environments, including magnetic and miniature environments will be more advantageous.

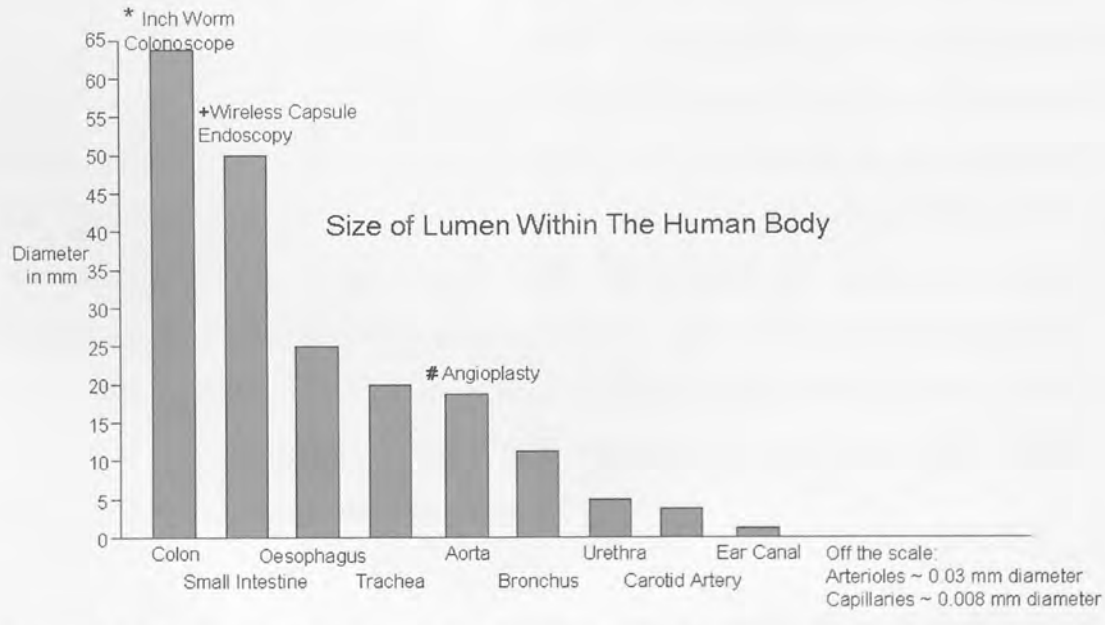

Figure 2.1 Approximate size of a range of lumen in an average adult human male body and some current research and procedures carried out within the lumen. (* MIAS Inch Worm Colonoscope (Dario, 1996)[27], + Wireless Capsule Endoscopy (Rabstein et al, 2002)[28] # Angioplasty (Anderson et al, 1985)[29])

The size of the lumen, and hence the size of the device and the number of tools or instruments that might be fed down it will be restricted. Manoeuvrability can be improved inside the body by creating pockets of space in body cavities. For example, an incision into the peritoneal cavity (located beneath the umbilicus) is sealed with a valve and then the cavity is inflated to allow for more manoeuvrability of surgical tools during abdominal surgery.

From a device prototyping and manufacturing stand point, it would be simpler to make a device such as a probe or digit that is of the order of magnitude of the lower gastrointestinal or gynaecological tracts as it would only need to investigate shallow depths, in relation to the diameter of the device. This reduces the complexity of how to retrieve the device in the case of failure during a procedure.

As the lumen reduces in diameter, the relative depth that the device must investigate is longer, and thus may also require more navigation. The average size of the adult male colon is in the order of magnitude of 60 mm (when filled). However, the ring of muscles surrounding the entrance restricts access to this lumen. In an examination, once, the device has bypassed this circle of muscle, the lumen diameter is wider, and hence, the question that needs to be addressed is whether to make the device the diameter of the colon, allowing for the fact that muscles can be stretched and will hold the base of the device in place for examination. If the probe device is smaller than the cavity it is examining, then it is possible to focus contact on the area of examination without forces from the other side of the lumen coming into contact with the probe and possibly interfering with identification of contact.

For narrower lumen, such as small arteries, smaller probe devices could feasibly be produced; provided either smaller components could be manufactured, or it may be necessary to use different types of sensors or materials than those proposed in the following chapters. Probes into very small lumen, in the order of magnitude of arterioles and capillaries, approximately 30 microns and 8 microns

would venture out of the range of microsurgery and into the realms of nano-surgery. At this size, the number of vessels will be significantly greater than for larger scaled lumen. Actuation would also be particularly challenging on this scale.

2.2.5 Design Solutions: Robotic Medical Device Systems

During long or highly skilled procedures, after period of time fatigue will occur and inevitably decrease clinician's ability to perform, regardless of expertise and may cause any natural tremor to increase. Natural tremor may also be exaggerated when small-scale procedures are performed. An example is that it is easier to thread a large needle with than a small needle. Hand-eye co-ordination will enable a person to see the large needle clearly and is spatially aware of where to locate the hole. As the needle gets smaller, more attempts are usually made to thread a needle through the hole. There may be an element of tremor in the hands causing the thread to miss the mark.

Indeed there is also an element of tactile interpretation when the edge of the hole is felt through a perceived deflection on the thread when it misses the hole. Robotic systems have been implemented within operating theatres, which could reduce the effects of this. Over the last decade, robotic technologies have explored a range of potential applications in surgery (Drake et al, 1991)[30] and (Taylor et al, 1990)[31], with some systems emerging in practice (Harris et al, 1997)[32] and attempting to utilise the benefits of consistent and precise machine motion over that of human operators. From the latter section, most invasive systems have been guided by pre-operative scan data. However there are some notable exceptions that have operated as master-slave systems by (Davis et al, 1994)[33]. Master-slave is a term used to describe a robot where the clinician

provides the physical effort to drive the surgical tool within the body of the patient. However, all of these solutions with their own additional problems, be it inherent machine control issues or legislative constraints over the use of fully automatic robotic medical systems. All these issues will have to be considered and overcome before the device finally makes it into the operating theatre. In this research, the focus is on proving the concepts of distributive tactile sensing into a digit device and returning feedback to an input device using an envisaged master-slave system as described in Chapter 6.1 using clinically appropriate design considerations.

2.3 The Endoscope: An example of a minimal invasive device

Endoscopy is a term used to describe examining the inside of the body using a lighted, flexible instrument called an endoscope. Endoscopy is the examination and inspection of the interior of body organs, joints or cavities through an endoscope. Access to the body would have been via a natural opening. Hippocrates in Ancient Greece first described endoscopy with reference to a rectal speculum. Roman medicine also produced instruments with which they could inspect internal organs. In the 1806, Philipp Bozzini developed a light conductor called the *Lichtleiter* (Miller, 1986)[34]. This early endoscope directed light into the internal cavities of the body and the image redirected to the eye of the observer. However, it was not until the mid twentieth century that the rod-lens system and fibre-optics were developed by Harold H Hopkins and later still, in the 1970s and 1980s when the technique of performing laparoscopy (abdominal surgery) through a miniature incision (keyhole) was developed and practiced. (History of Minimally Invasive Surgery , c 2004)[35].

An endoscope is a device that uses fibre optics and lenses to provide lighting and visualisation of the site inside the body. The device that is inserted into the body may be flexible or rigid depending on the medical procedure. A typical endoscope uses two optical fibres; one to carry light into the body cavity and another to the carry the image from the cavity back to the viewing lens of the clinician (Figure 2.2). There may also be separate ports for administering drugs, applying suction and irrigation. This port may also be used to introduce small instruments such as forceps, brushes and other similar tools for excision of tissue for sampling or biopsy or other therapeutic work. Many endoscopes are used in conjunction with image recording systems to document procedures and enhance visual images to assist in diagnosis.

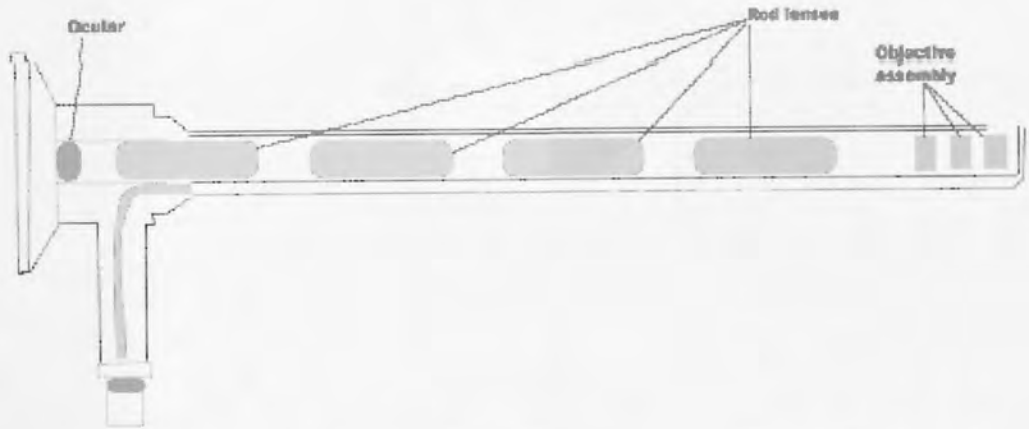

Figure 2.2 An example of a rigid endoscope: an image fibre leads from the ocular to the inserted end of the endoscope. The light fibre returns from the light source to the working end of the endoscope.

The range of medical procedures that can be carried using a minimally invasive method is extensive, and could be categorised by the areas of the body involved. Some of the medical disciplines that use or could use endoscopic examination and surgery are listed in (Appendix 2.2) and (Appendix 2.3)

2.3.1 The Function of Endoscopy in Diagnosis and Treatment

Research into the use of endoscopes identified a wide range of clinical applications (Appendix 2.4). The functions of these endoscopic procedures can be divided into two main branches, that of diagnosis (Figure 2.3) and that of treatment (Figure 2.4). Along each of these branches, there are further sub functions relating to how diagnosis and treatment could be carried out. In the case of diagnosis, visual inspection, tactile inspection and biological inspection are examined further.

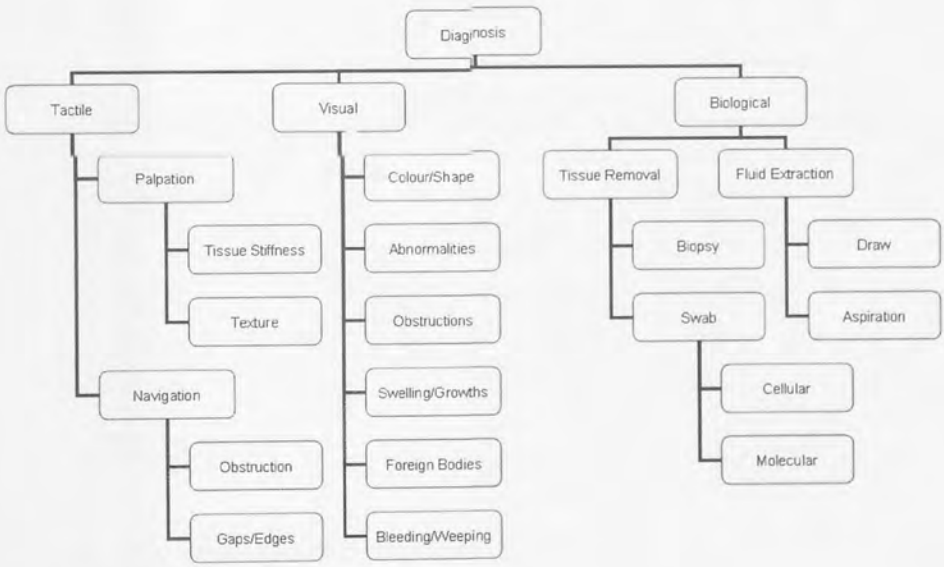

Figure 2.3 A Tree Diagram of Diagnosis

In diagnosis, there are three ways that an endoscope could be used for visual examination, tactile examination and obtaining biological specimens for later diagnosis. In tactile examination, pressing the tissue to assess its properties can be used. Kinisthetic information can be used in navigation and to search for obstructions or pathways. However, tactile information may be lost due to the sheer distance of the site of examination to the hand of the clinician holding the instrument. However, what information that can be obtained is used in

conjunction with visual examinations to make more informed assessment. Much of the prominent works on endoscopic devices have been for vision systems on improving visibility to enable the clinician to diagnose by sight. The camera-in-a-capsule (Rabenstein et al 2002)[28] overcome navigational problems by allowing the device to be swallowed, pass through the body naturally and provide a complete visual investigation of the small bowel. However, this is only provides visual feedback.

In treatment, endoscopic devices are used to remove, repair or palliate (alleviate) and depending on the modality of treatment, different combinations of tool tips can be used.

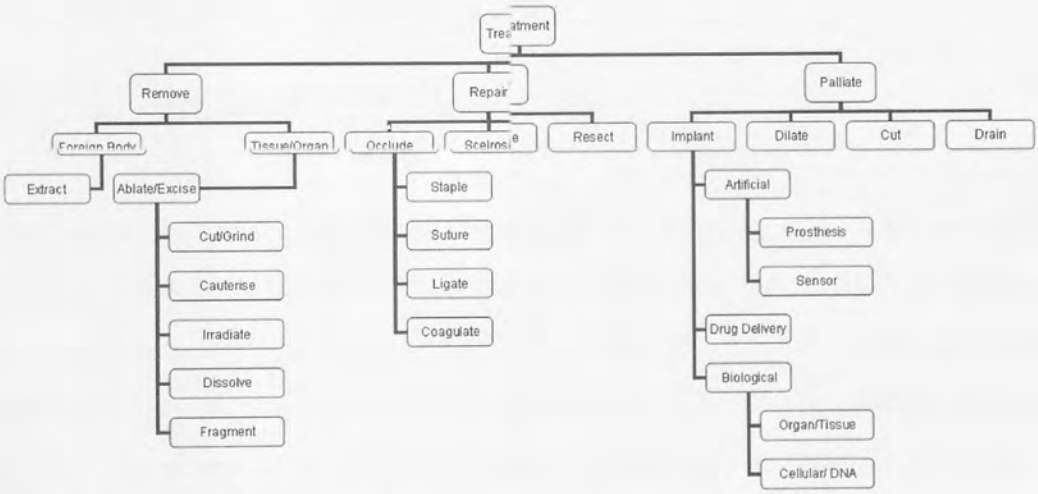

Figure 2.4 A Tree Diagram of Treatment

Of the two functions of diagnosis and treatment, the area of interest in this research is the in diagnosis; in particular the role tactile information is used in clinical examination of the patient.

2.4 Diagnosis by Touch

The absence of tactile information retrieved from the instrument tip leads to interest in developing a device is that can navigate and diagnosis using tactile feedback using a sensing technique described in Chapter 3. The sensor being developed is capable of detecting load, load position and load magnitude, which are used to detect contact. This contact information could be used in two ways:

- Navigation: using touch to find paths through lumen to the site of investigation
- Palpation: diagnosis by touch to determine abnormalities or changes in tissue or organs

2.4.1 Navigation

Navigation comprises being able to detect contact along a surface reference points within the body to relate position. Most of the tissue in the human body has pliable consistencies that make it difficult to navigate around. Too much force applied will displace the tissue and depending on the tissue type, it may take some time for it to return to its original shape or position. In navigation, when the instrument is in contact and what position it is within the body is information the digit must be able to provide. In fact, what the digit must do is *feel* its way through the lumen, therefore the digit is required to palpate.

2.4.1 Palpation

"Palpation is a method of feeling with hands during physical examination and the examiner feels the patient's body to examine the size, consistency, texture, location and tenderness of an organ or body part"(A.D.A.M., 2002)[36].

In essence, palpation is the mechanical property of differentiating changes in stiffness. For this particular project, work on palpation would be beneficial. Internal palpation of tissue or organs can be difficult and the use of physician's hands in diagnosis is very important. For example, in the diagnosis of endometriosis (inflammation of the mucus membrane of the uterine wall), manual palpation is more successful in detecting nodules that need removing than using visualisation (Martin, 2002)[37].

There are many ways, in which changes in stiffness and hardness can be perceived, such that a region of tissue can be hard, but set into softer matrix. Using force feedback measurements may not be able to distinguish if the region is hard if the underlying matrix gives way when pressed. There are also hard regions beneath softer tissue, or hard tissue on less pliant tissue.

2.4.3 A Clinical Palpating Device

A device with capabilities of palpation could be used for difficult to access parts of the body, such as the sinus ducts, which are millimetres in diameter, narrower than the fingers that are used in performing palpation. There are also internal cavities, such as the uterus, bladder and stomach that could be examined internally with palpation. Endoscopes currently can see inside these cavities, if there is an abnormality beneath the surface seen, the problem may not be detected. Using palpation on interior of these organs or cavities may improve the detection of problems, particularly those that lie beneath the surface.

2.5 Potential Applications for a Palpating Device

The use of tactile feedback has a myriad of possibilities for medical devices. In this section we examine the how the presence of tactile feedback might enhance the ability of a clinician to diagnose and present a case for the use of a tactile device. The depth in which the digit can reach to examine a site of investigation will limit the type of application that the device can initially deal with. The following clinical application is for use in classification of prostate problems. The access to the site of investigation is shallow and large compared to some body locations discussed earlier, but many of the design considerations are relevant.

2.5.1 Prostate Enlargement: A growing problem in the aging western society

The prostate is a male sex gland that surrounds the urethra and is located below the bladder and in front of the rectum. As men age, the prostate can become enlarged, causing problems such as problems with urination and interference in sexual function. The possibility of being diagnosed with prostate cancer increases with age. The majority of men over 80 will have an enlarged prostate (Kirk, 1999)[38]; this common condition is called benign prostatic hyperplasia (BPH), which is not cancer, though it can cause many similar symptoms. Coincidentally, many men with tumours will have BHP in the inner part of the gland. Prostate cancer is the second most diagnosed cancer in the UK for men. There is a 1 in 14 risk of being diagnosed with prostate cancer over the lifetime of a UK male, with the risk of developing cancer increasing with age. (Cancer Research UK, 2002)[39] Globally, there were over 540000 cases and over 200000 deaths from prostate cancer in 2000, with three quarters of these cases from more developed countries. (GLOBALCAN, 2000)[40].

Initial diagnosis for prostate cancer would involve a prostate specific antigen (PSA) test, which though is not an absolute test, as other conditions in the prostate can give elevated antigen levels, so this is given in conjunction with a digital rectal examination. Part of the diagnosis of BPH and prostate cancer is with a digital rectal examination (DRE), in which the physician feels the prostate through the rectum to find hard or lumpy areas. The physician inserts a gloved, lubricated finger a few inches into the patient's rectum and gently palpates the prostate gland to feel for a nodule or lump, change in size, hard tissue, or any abnormality that might be a tumour. The differences between cancer of the prostate and BPH can be defined in a digital rectal examination and are summarised in (Table 2.1) and based on this information, initial diagnosis would be made (Family Practice Notebook, 2000)[41]. Training for clinicians to diagnose prostate problems can include models of the male pelvic region. Limbs and Things (Limbs and Things, c2005)[42] provide a diagnostic prostate trainer with five interchangeable prostates: normal, bilateral benign, unilateral benign, bilateral carcinoma and unilateral carcinoma. This provides some measure of shape and texture of the prostate; however, the conclusions still are suggested by feel and experience and there are no quantifiable values in the classification.

Suggestion of cancer of the prostate	**Suggestion of benign prostatic hyperplasia**
Asymmetry	Symmetric prostatic enlargement
Iduration (pathological hardening or thickening of tissue)	Smooth
Nodularity	Firm but elastic
Diffuse Firmness	

Table 2.1 Symptomatic criteria for examination of an enlarged prostate gland

Screening for prostate cancer using DRE is often recommended, but DRE is not a sensitive screening test for early disease. DRE may miss some prostate cancers since the DRE relies on the experience of the physician for diagnosis, as this touch is subjective. A tactile digit can be used to determine tissue properties and to collect data that could be used to improve diagnosis using the DRE method. The digit could quantify what are the significant parameters for diagnosis of

prostate problems and record this information for future reference. With the correct implementation, provision for recording, comparing and more detailed analysis would be possible. This will have the advantage over current method of DRE since the results would be firmly quantifiable.

2.5.2 Endotracheal Intubation

A contrasting procedure that could use a tactile feedback incorporated into the instrumentation could be used for the pharyngeal area, in particular intubation devices. This is a navigational application, enabling the clinician to feed a device down the throat of an immobilised patient. Intubation is the introduction of a tube into part of the body for the purpose of diagnosis or treatment. For example, gastric intubation may be performed to remove a sample of the stomach contents for analysis or to administer drugs directly into the stomach. In endotracheal intubation a tube is inserted through the mouth into the trachea to maintain an airway in an unconscious or anaesthetized patient. It requires expert knowledge for insertion, using a laryngoscope, and has a small cuff at the far end for inflation inside the trachea. It affords the best level of protection of the airway from vomiting. (Concise Medical Dictionary)[43]

The purpose of endotracheal intubation is to serve as an open passage through the upper airway. This prevents inadequate oxygenation in an unconscious patient by permitting air to pass freely to the lungs in order to ventilate the lungs. The intubation tube is sometimes connected to an artificial ventilator. The patient is often incapacitated when intubation is taking place and would be able to respond verbally to discomfort felt by the insertion of the tube. This procedure is used widely when a patient is operated on, whilst under general anaesthetic.

2.5.3 Alternative Clinical Uses of a Palpating Digit

Digital rectal examination is also used as part of the diagnosis of colorectal problems and abnormalities in female reproductive organs such as the uterus and ovaries. So in effect, there is scope for a device designed for detecting prostate problems can also being applied to a wide range of clinical diagnostic practices for the lower gastrointestinal, urological and gynaecological tracts. Endotracheal intubation is one of many interventions that require navigation. Examination of the digestive tract and guidance of catheters through blood vessels are other alternative uses.

The aim for developing a novel flexible digit with tactile feedback is to focus on a couple of clinical procedures that can be quantifiably measured, but leaving the design open for resizing for other potential applications, clinical and otherwise. A single flexible digit tip can be paired with another to form grasping tool tips, or more ambitiously, more tips can be co-ordinated to form a multi-dexterous end tool either to perform remote surgery or to form a prosthetic hand for amputees.

2.5.4 Non Clinical Uses of a Palpating Digit

Industrial applications for a navigating, palpation digit include investigation of pipes and chambers in manufacturing systems for routine maintenance or repair, with minimal disruption of processes. Endoscopic devices are already used to visually inspect of aircraft engines to check for cracks and leaks. By introducing the additional feature of touch to such inspections, non-visible faults may also be detected. A digit with sufficient tactile feedback can be used in bomb disposable. Navigational properties can be used to explore sites too dangerous to life such as collapsed buildings or contaminated areas. Forms of the digit could be used in

remote deployment, particularly useful for military applications where sending personnel into the field may be more dangerous.

2.6 Tactile Feedback for a Clinical Flexible Digit

The tactile flexible digit system is a master slave system with the clinician imparting motion of the digit through movement of the finger or hand. An instrumented input device can achieve this. The design of such devices needs to build on the response of tactile receptors of the hand, which are transient in their response. Measurements corresponding with tactile stimulus have been carried out in investigations on user response (Brett & Guild, 2000)[44], with respect to needs in surgical practice. This showed that slip is identified by touch through a combination of movement and vibration (the vibration disturbance may reach many 100Hz), whereas the identification of unexpected transients requiring a physical response by the human system at best mimics a first order dynamic system with a break frequency of 1.5Hz. Also the absolute accuracy in sensing is not as important as the detection of changes in contact conditions, since the human operator will be more responsive to discrimination than measurement. The challenge here is to avoid a cumbersome system that would impair the freedom of motion by the clinician, and of course there is the need to achieve a device at low-cost and suited to the sterile environment

2.7 Clinical Evaluation of the System

Once each element of the system has been developed, they have to be tested in a manner that is in context with its clinical application. A phantom test rig that enables some of the features listed below to be tested on the digit device is developed. The phantom test rig is described in greater detail in Chapter 5 of this thesis.

- Contact Presence
- Size and Magnitude
- Location of Contact
- Stiffness of Contact
- Load Magnitude
- Load Position
- Force applied to the phantom test rig

For example, a digit that is developed for detecting changes in the prostate the identifying features for any physical prostatic examination is changes in size, stiffness and location of any nodularity, which can be translated into phantom tests. Initial tests focus on the sensor and consequently the digit's and input device's ability to detect or relay the following criteria.

The tactile sensor can fulfill not all the criteria, but other auxiliary sensing systems can be used. These include biosensors, specimen collection by collecting cell, fluid or tissue samples or other non-invasive diagnosis systems such as ultrasonic probes that that generates high frequency sound waves that scan surfaces of tissues and organs to detect abnormalities. The common needs for flexible tips are summarised in Table 2.2 and these are the prime indicators of how a novel tool tip can be evaluated.

Common Needs for Flexible Tips	Prostate Diagnosis	Endotracheal Intubation
Greater degrees of freedom in manipulation and navigation	To introduce a digit with sensors to the location of the prostate	To introduce tube down the airway
Measurement of contact resistance and displacement relative to feature	To ensure excessive force is not exerted and to measure firmness of the prostate	To ensure excessive force is not exerted
Shape discrimination	To check for any asymmetry of prostate	N/A
Contour mapping for shape and texture identification	To check for any nodularity of the prostate	N/A
Detecting end reactive load	To detect digit is in correct position	To detect tube destination reached
Detecting motion relative to feature	N/A	To navigate down the airway

Table 2.2 Common needs for flexible tips

2.8 Conclusion

This chapter brings into context of clinical evaluation in the design process and demonstrates that an instrument can be multifunctional and versatile. The design solution needs to offer measurable, quantifiable diagnosis on a large scale.

The idea of providing tactile feedback such as touch and tool force information presents an ongoing challenge in surgery. The most apparent need in minimal invasive surgery is where sensory feedback from the operating site is extremely constrained and clinicians are often working at the threshold of tool control. For example during endoscope navigation, in conjunction with visual perception through the end of the endoscope, the sense of the point of contact of the digit, the discrimination between hard and soft contact, and the identification of edges, should allow the clinician to achieve greater control and perception of position

targets compared with current methods. Similarly, diagnostic methods will benefit, in conjunction with ultrasound imaging, from palpation where a form of tactile perception will enable greater control of the action against the surface. In all these cases the requirement is to utilise the outer structure of the digit or tool as a means of providing tactile sensory feedback. For endoscopy, complex solutions such as that by Dario et al (2000)[26] have yielded useful results, however a solution that is lower cost and suited to a range of environment will be more advantageous.

In considering general design considerations for designing a minimally invasive device in the context of a widely used device, the endoscope, certain criteria can be determined. An actuated device applied in the detection of problems of the prostate using palpation would be an appropriate focused application because the incidence rate of prostate problems in the developed world is high, and with an aging population, the number of incidences is likely to grow. Diagnosis by digital rectal examination carried out by a physician is also dependent on medical experience. If an actuated digit has a tactile surface and a system of feeding back this information to the clinician, he is better informed to make a diagnosis and the results can also be recorded for future analysis and for improving diagnostic techniques. Taking into consideration the clinical requirements for a flexible digit with tactile feedback, the following chapters focus on the technological requirements and capabilities for developing such a medical device.

Chapter 3

Tactile Sensors

In this work, the success of this research is dependent on a novel approach to tactile sensing. This is compatible with the clinical needs of small access devices. This chapter describes a distributive tactile sensing technique suitable for the clinical requirements of the research. The two types of tactile sensor that can cover large surface areas are the matrix and the distributive types. These are reviewed at the beginning of this chapter, focusing on the requirements of a distributive tactile sensing system. These are the material required for the contact surface, the sensing elements used and the computational algorithms required in the distributive technique. The placement and number of the sensing elements are important in the performance of the distributive system and a mathematical model of sensor placement is described. Finally, transducers are a key component in all tactile sensors and there are is a myriad of choice. Two contrasting transducers, strain gauges and optical fibres etched with Bragg gratings are used to build distributive tactile sensors. These sensors are tested and the results show that the sensors are able to detect tactile information in terms of magnitude and position of

load using both types of sensing elements, with improved overall performance with the use of fibre Bragg grating optical sensors. This distributive tactile sensing technique can then be implemented into a clinical tool.

3.1 Tactile Sensing

Tactile sensing relates to the sense of touch and is a developing technology. A tactile sensor is a device, which measures parameters of a contact interaction between the devices and some physical stimuli. The interaction is normally confined to the touch sensitive region of the device surface (Lee & Nicholls, 1999)[45]. Touch sensing occurs when touch probes that measure a single contact point is sufficient for contour following and is often used in guiding a robot into position for another critical operation or for detecting flaws in a substrate. Tactile sensing can be defined as the continuous measurement of contact pressure within an array of *tactels* or tactile elements and is distinct from *touch sensing* which is defined as a single contact pressure measurement (Ruocco, 1987)[46]. Tactile sensing allows for continuous measurements of pressure distribution across the whole tactile array, providing a pressure image of an object at any point in time and hence be able to detect slippage. Slippage detection is useful when handling delicate materials to prevent excessive forces being exerted. However in clinical applications, a tactile system that can derive information, rather than data would be suitable. Data needs to be processed into information relevant to the user. By ensuring that the system has pre-processed data, the system becomes more user-friendly. In touch, descriptive states can be generalised, whereas quantification in values such as force and dimension are more difficult for the clinician's mind to differentiate. The two types of tactile sensing systems are described, and although both can be used in a clinical context, their construction and outputs make them suitable for different applications.

3.1.1 Matrix Tactile Sensing

Tactile sensors have traditionally been based on direct measurement of force transducers, that is to say devices that measure the mechanical deformation produced by force acting directly on the transducers themselves. Traditional tactile sensing systems have utilised multiple sensing elements to provide information of contact in a map like form. This type of sensing is known as array or matrix style sensing and its output is discrete. The resolution of the tactile sensor depends on the number of sensing elements used in this type of sensing system. The regions between sensing elements are sometimes referred to as *dead areas*, which have no sensitivity (Dargahi et al, 2000)[47] so by increasing the number of sensing elements in the array, the sensitivity of the sensing surface is increased.

One of the most well known matrix style tactile sensors on the market is the Tekscan pressure measurement system which is a 0.1 mm flexible tactile force sensor in either grid based or single load cell configurations. Each sensor is able to measure pressures between 0.15 and 0.175 kPa and the resolution of the sensor location can be up to 0.14 mm^2. The sensor consists of two thin flexible polyester sheets with electro-conductive electrodes deposited in various pattern according to the sensor application. When the two sheets are placed on top of each other, a grid pattern is formed to create the sensing location at each intersection and by measuring the changes in current flow at each of these points the applied force distribution can be interpreted (Tekscan, c2004)[48]. The F-Scan sensor made by Tekscan is used to measure pressures and force in shoes. The sensor is cut to fit the shoe; meaning measurement of smaller shoe sizes will be affected adversely as the resolution decreases (Woodburn & Helliwell, 1997)[49].

3.1.2 Distributive Tactile Sensing

The distributive tactile sensing system is an alternative to the array approach and has some similarities with the human system of tactile touch. It relies on the coupling between sparsely located sensing elements outputs produced by the response of the contacting surfaces to the applied load. The distributive tactile sensing technique is a means of determining complicated outputs from minimal number of coupled sensing points on a homogeneous substrate and a computational algorithm (Brett & Stone, 1997)[50].

The distributive system works by working on a surface of known behaviour and monitoring the response to contact measured by a limited number of sensor elements. The number of transducers is much smaller than with array type tactile sensing systems. The response to an applied load on the surface forms a unique characteristic signature that can be identified by algorithms that use previous knowledge of the surface's behaviour to determine contact type. Due to this method of interpretation, the response from the sensor element must be consistent, so the choice of sensor element used is important, as is the choice of computational algorithm if the distributive tactile sensing system is to be successful.

Some work on distributive tactile sensors was carried out by Stone and Brett (1996)[51]. They studied the range of potential applications for tactile sensing. Tongpadungrod's et al (2003)[52] work describes a formulation of a distributive tactile sensing technique and explores the design parameters that would affect the performance and sensitivity with work focusing on a single dimension, identifying load magnitude and position on a beam, and in two dimensions on a surface that could infer the load, position, size and orientation of an object.

The differences between the two tactile sensing techniques are summarised in Table 3.1 that shows a comparison between distributive and matrix style tactile sensing systems

Matrix	Distributive
Very high resolutions possible with high number of sensing elements	Reduced number of sensor elements for equivalent spatial resolution
Multiplexing of the sensors may be required	Low cost and low complexity
Precise in acquiring shape or profile of object	Sensing elements not necessarily in contact with surface
Dead areas in regions between sensors elements	More suited for discrimination
High computational load	Low computational load
Certainty	Probabilistic

Table 3.1 The comparison between the distributive tactile sensing system and the matrix style tactile sensing

3.2 Construction of Distributive Tactile Sensor

A distributive tactile sensor is comprised of:

- Transducers to be used as sensor elements
- Deforming a contact surface of known behaviour
- Computational algorithms for interpretation

These are synthesised through the design process in order to obtain robust performance.

3.2.1 Sensor Elements and Surfaces used in Tactile Sensing

There are three main sensor elements in tactile technology; capacitive, optical and resistive. Capacitive sensors depend on the change in capacitance between capacitor plates when pressure is applied to them. A stress-sensitive resonator is a chip proposed by Shinoda and Oasa (2000)[53] containing a coil for receiving and transmitting electrical power with wireless coupling, capacitance sensitive to stress and a ceramic resonator to provide high-Q resonance.

Some types of optical transducers respond to a change in light intensity by detecting the change in distance travelled by light from the source to the photo-detector. A simple opto-electrical sensor will consist of a light source, a modulation medium, a transmitter and a photo-detector. In the past, short-range optical infrared sensors have been used to measure the displacement of a beam in bending (Brett & Stone 1997)[50].

Other optical transduction methods include the use of the optical fibres. Optical fibres have been used in opto-electrical tactile sensing schemes which work on the principle of changes in light intensity caused by attenuation of light when a fibre is curved can be measured. This is based on the micro bending of optical fibres, which causes light to attenuate at the core of the fibre when a mechanical perturbation is applied to the outer surface of the fibre. Optical fibres offer immunity to electromagnetic interference, are lightweight and are isolated electrically, which are ideal attributes in telecommunications and sensing applications.

Resistive sensing devices are the most popular for tactile sensors because of they have high sensitivity and Cartesian resolution (Ruocco, 1987)[46]. They are made from resistive compounds such as carbon fibres, conductive rubbers and other polymer films that have been impregnated with conductive dopants. These change resistance in response to applied pressure. The latter are the most popular because of low hysteresis and larger dynamic range. Popular resistive devices include strain gauges and piezo-resistive transducers. In this work, two types of sensor elements are trialled. Strain gauges and an optical fibre with Bragg Gratings etched onto it.

The contact surface materials that the sensing elements are measuring are typically uniform with a homogenous substrate being ideal surface on which to mount the sensors on or under. Previous work carried out showed that materials such as mild steel (Brett & Stone, 1997)[50] and aluminium to be effective contact surfaces.

3.2.2 Computational Algorithms

Computational algorithms are used to deduce meaning from the sensory data by forming relationships between the sensory input and expected output. Artificial neural networks are a form of computational algorithm that can be used to process data from the sensors in this technique and has been shown to be successful in outputs on a simply supported beam (Ma & Brett, 2002)[54]. Neural networks have been used where sensor inputs are highly non linear. Small deflections in beam bending can be considered as linear; however, when a beam deflection is great, the output from a simple beam equation becomes unstable, resulting in deflections greater than the length of the beam. Other computational algorithms include the genetic algorithm, and fuzzy logic, used in which are used in classification and decisive systems. However, ANNs are generally considered best suited in classification reflected in decision theory and can obtain an exemplar pattern from a noise or incomplete one (Eberhart et al, 1996)[55].

3.2.2.1 Neural Networks

An Artificial Neural Network (ANN) is system that processes information, inspired by the way biological nervous systems, such as the brain, processes information (Picton, 1994)[56]. It is composed of a large number of highly interconnected processing elements called neurons working together to solve specific problems. ANNs, learn by example and is configured for a specific application, through a learning process, such as pattern recognition or data classification. Learning in biological systems involves adjustments to the synaptic connections that exist between the neurons, a method an ANN imitates.

The neural networks used for these experiments are based around the NETLAB software toolbox*, which is written and can be modified in MatLab. Various types of neural networks can be employed, but for the following experiments, a single layer feed-forward neural network (Figure 3.1) is employed and the equation for this neural network is described in equations (3.1) and (3.2). Single layer networks use statistical techniques of linear regression and generalised linear models, which consist of a linear combination of input variables where the coefficients are the parameters of the model followed by an activation function. The activation function used depends on the type of data being modelled and is described in greater detail in Section 3.2.2.2. There are four standard steps in using a neural network (Figure 3.2).

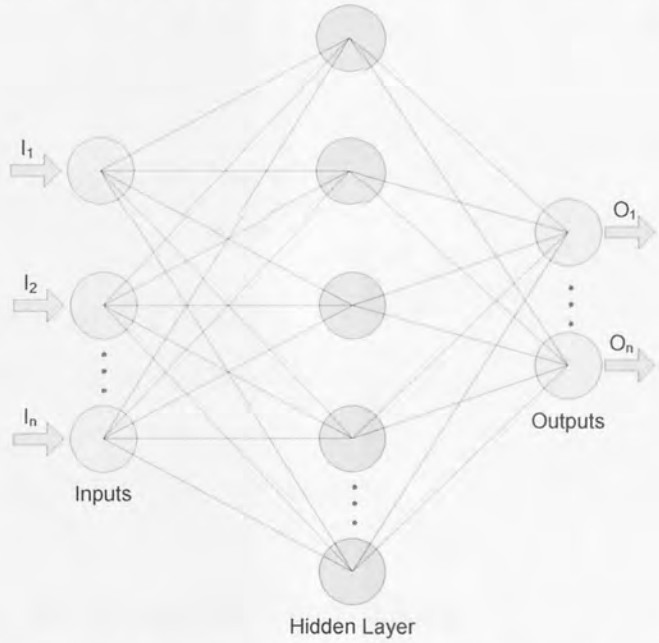

Figure 3.1 A typical single layer feed forward neural network structure

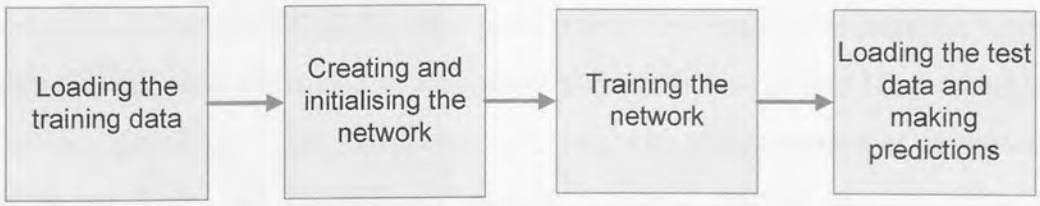

Figure 3.2: Standard steps for implementing a neural network

* The NETLAB toolbox is available from the Neural Computing Research Group website at http://www.ncrg.aston.ac.uk/netlab/index.php [04/01/2006]

The equation for a single layer feed forward neural network is:

$$o_{(i)}^{(2)} = f\sum_{j=1}^{M} \omega_{ij}^{(2)} f(\sum_{k=1}^{N} (\omega_{jk}^{(1)} x_k)) \qquad \textbf{(3. 1)}$$

Where $o_{(i)}^{(2)}$ = Output vector
N = Number of input units
M = Number of hidden units
f = Transfer function of the process
j = Source of connection
i = Target
$\omega_{jk}^{(1)}$ = Weight of the first layer
$\omega_{ij}^{(2)}$ = Weight of the second layer
x_k = Input signals from the sensors

Simplifying this equation gives:

$$o_{(i)}^{(2)} = \sum_{j=1}^{M} \omega_{ij}^{(2)} f(\sum_{k=1}^{N} (\omega_{jk}^{(1)} x_k) + b_j^{(1)}) + b_j^{(2)} \qquad \textbf{(3. 2)}$$

Where $b_j^{(1)}$ = Bias of first layer
$b_j^{(2)}$ = Bias of second layer

The purpose for bias is for better convergence.

3.2.2.2 The Activation Function

A neural network can be made more powerful if non-linearity is introduced since without it, the network would work simply as a linear function of linear functions, which remains linear. Any non-linear function, with the exception of polynomials (which are finite and have no asymptotic features) can be used as activation functions for the hidden units. An activation function that resembles a smooth step function is often chosen as they tend towards infinity (Bishop, 2002)[57]. The most common choices are the Gaussian functions and sigmoidal functions, such as

logistic and hyperbolic tangent. The hyperbolic tangent activation function described in equation (3.3) produces negative and positive values and yields faster training than a function that only produces positive values, such as the logistic functions (Bishop, 2002)[57].

$$f(z) = \tanh(z) \qquad \textbf{(3. 3)}$$

Choices for the activation function in NETLAB for a single layer feed-forward neural network outputs include *linear*, *logistic* and *softmax*, which provide different models for outputs.

- **Regression Outputs (Linear Model)**

The linear regression uses the hyperbolic tangent activation function and ensures that the output will be in continuous numerical form, for example, a position output would be any position along a beam up to a reasonable measurable resolution. This means the output will be predicted up to a certain amount of measurable resolution.

- **Two Class Model (Logistic Model)**

Logistic is an S-shaped (sigmoid) curve and the output for this model is in 1-N encoding (0,1). For example, this assigns input data into one of two classes; this model was used to determine the presence or absence of a load. The use of the logistical sigmoid activation function allows the discriminant to be interpreted as posterior probabilities, providing more than simply a classification decision (Bishop, 2002)[57].

- **Three or More Classes Model (Softmax Model)**

Softmax is an exponential function, with results normalised so that the sum of activations across the layer is 1.0. This allows the output data to be discrete.

The output for this model is in 1-N encoding. (Table 3.2) shows 1-N encoding for a three-class model. It can be used in the output layer of multilayer perceptrons for classification problems, so that the outputs can be interpreted as probabilities of class membership (Bishop, 2002)[57]. A softmax model puts output data into two or more classes; for example this was used to classify the load magnitude.

Class 1	1 0 0
Class 2	0 1 0
Class 3	0 0 1

Table 3.2 1-N Encoding for three class softmax model

3.2.2.3 Neural Network Strategies

There are various strategies that can be applied to neural networks to achieve predicted outputs:

- **A Combined neural network**

A combined neural network uses all the sensory input data to determine several output parameters simultaneously. In this case, four sensor inputs, S1, S2, S3 and S4 are fed into a single neural network to output three parameters of contact, load magnitude and load position simultaneously as is shown in Figure 3.3.

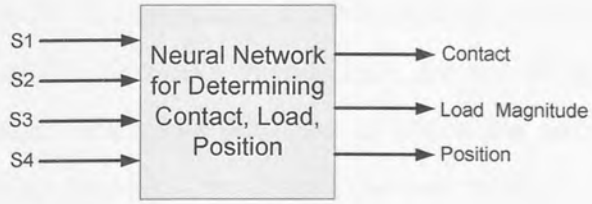

Figure 3.3: A Combined Neural Network to predict three output parameters where S denotes the sensor input channel number

- **A Parallel neural network**

A parallel neural network comprises of parallel neural networks to output parameters simultaneously. In this case, the sensory data from the four inputs, S1, S2, S3 and S4 are simultaneously fed into individual neural networks for each output parameters; contact, load magnitude and load position as is shown in Figure 3.4

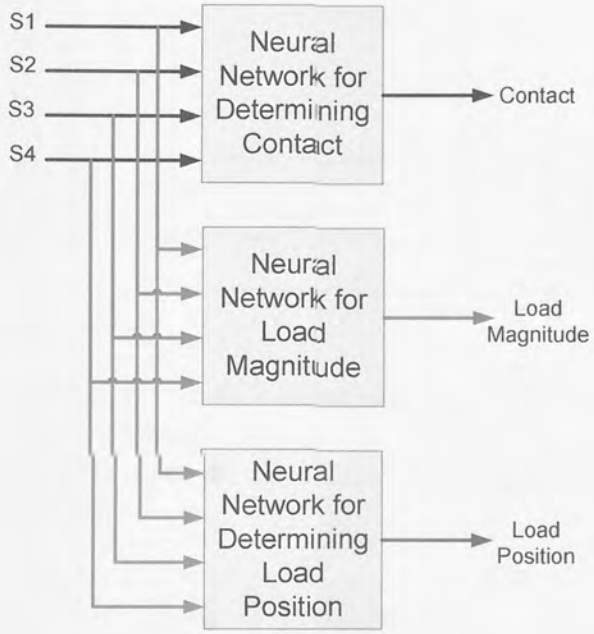

Figure 3.4: A Parallel Neural Network using three networks to predict three output parameters where S denotes the sensor input channel number

- **A Cascaded neural network**

A cascaded neural network will predict the output of a series of neural networks in sequence, using the output from the previous neural network in the chain as an additional input as is shown in Figure 3.5. Cascaded neural networks however are dependent on the outcome of the strongest results, and if the results of earlier networks in the chain are not satisfactory, errors are further compounded. Therefore the order in which the output parameters are processed should be considered to achieve the best results.

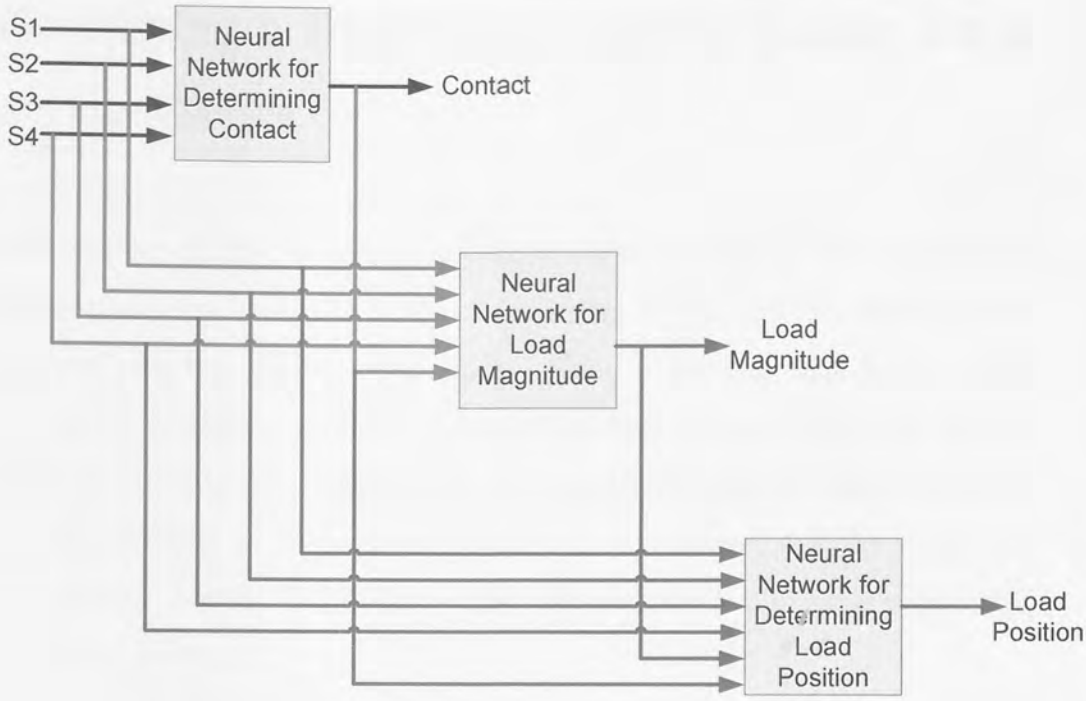

Figure 3.5: A Cascaded Neural Network using three networks to predict three output parameters with each subsequent network utilising the output from the previous network as an extra input for more efficient training. S denotes the sensor input channel number.

3.2.2.4 Neural Network Training

Training the neural networks consists of obtaining training data, which contain both the input values and also the output values. From all sensory data gathered during the experimentation phase, for each type of neural network to be implemented, all the data is first scaled as described in greater detail in Section 3.5.2.3. The data is then randomised before being divided into three sets of data. The first set of data is used to optimise the architecture of the neural network, as described in Section 3.5.3. Once the neural network has been optimised, this optimisation data is added to the second third of the unused data to be used as training data, where the neural network is given the output values to learn from. The final third of the data is then used to test and validate the neural network.

3.3 Developing a Distributive Tactile Sensor for a Digit Type Device

Placement and the number of sensing elements are dependent on the structure of the device the tactile sensor is to be appended onto. In this research, the tool end of the device is a flexible actuating digit. Since a flexible digit is long and narrow, a sensor with these proportions would indicate few sensing points placed in a single array along the axial length. A simplified approximation a flexible digit can be modelled as a cantilever beam as it is assumed that the digit will curve in a similar manner. From this model, the position and number of sensing elements can be determined.

The digit is modelled as a cantilever beam of length L with a moment M applied at the flexible end. The objective is to measure the applied load having a different magnitude and position using as few sensing points as possible. The optimum position for each of the sensing points can be determined by considering a cantilever beam and assuming that it is under linear deflection (Figure 3.6).

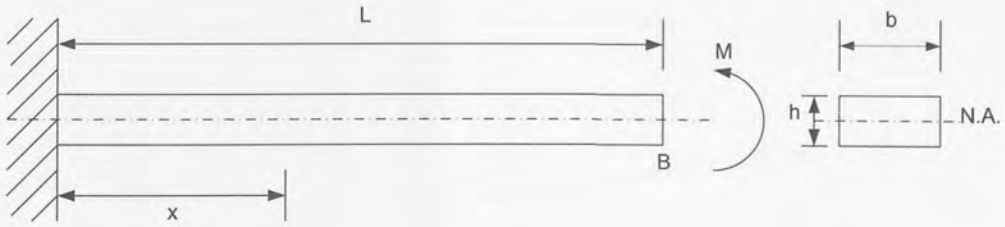

Figure 3.6 The Cantilever beam under consideration

From the bending moment diagrams (Figure 3.7) we can see that only three sensors are needed to determine load position and magnitude. Sensing points 1 and 2 can be used to determine load magnitude F. With the information provided

by sensing point 3, the loading position l can be decided (junction of the slope and horizontal line in Figure 3.7).

The moment difference (*Diff*) between a pointed load and a distributed load with same force amplitude can be sensed by the strain gauge within the load range, this is shown in Equation (3.1). The distributed load has unit force f and width w, the load magnitude $F=fw$. The load width can therefore be decided through the sensing point within the load width. In order to determine load width of more than a quarter length of the beam, the sensing points should be no more than every *L/4* apart. However, since our interest is on the free end half of the beam (closest to the tip), the sensors can be arranged at the position at approximately 0.1L, 0.4L, 0.6L, and 0.9L from the root as denoted by the * symbol in Figure 3.7. This way we can determine any load applied on the free end half of the beam with more than L/4 width, its position and its magnitude.

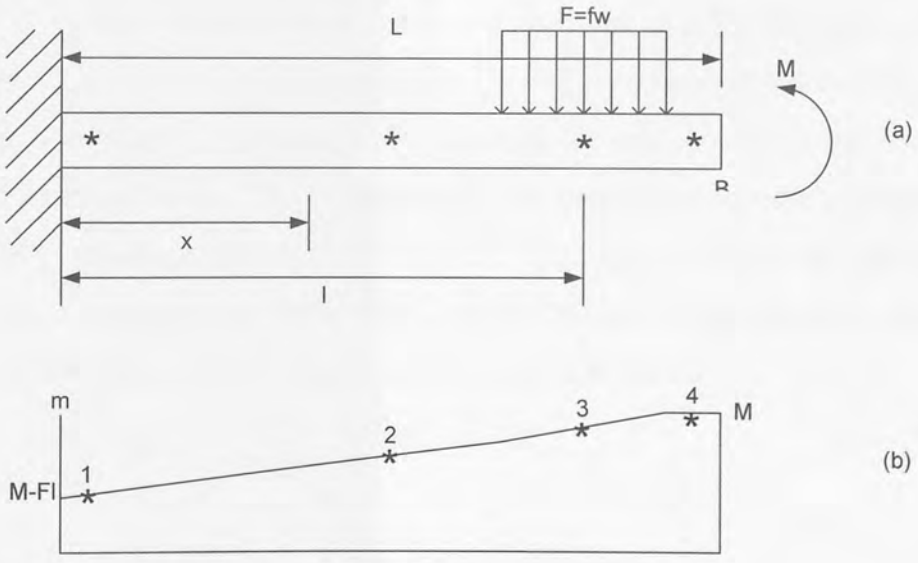

Figure 3.7 Bending Moment Diagram

$$Diff = \begin{cases} -\frac{f}{2}(l+\frac{w}{2}-x)^2 + Fl - Fx, & when \quad l-\frac{w}{2} < x < l \\ -\frac{f}{2}(l+\frac{w}{2}-x)^2, & when \quad l < x < l+\frac{w}{2} \end{cases} \qquad \textbf{(3. 4)}$$

Where *Diff* = Moment Difference

3.4 The Sensing Elements

A beam with four sensing positions is able to detect all the parameters of a distributed load and a test rig was constructed to demonstrate the capabilities of the distributive sensor arrangement using strain gauges and with an alternative type of sensing elements. These are a photonics solution using fibre Bragg sensors, where a change in the wavelength between a grating is related to a change in stain.

3.4.1 Strain Gauges

A strain gauge is a device that experiences a change in resistance when it is stretched or strained and physicaily consists of length of material that is etched onto a flexible backing sheet. Strain gauges are usually bonded to the object where displacement is to be measured using cyanoacrylate adhesive. As the strain is applied to the gauge, the material distorts, changing the shape of the cross-sectional area. The resistance of this material is inversely proportional to the cross sectional area (Morris, 1993)[58]. This relationship in the strain gauge is expressed as the gauge factor (*GF*), which defined as the change in resistance *R* for a given value of strain ε and is shown in equation 3.2.

$$GF = \frac{\delta R}{\delta \varepsilon} \qquad \textbf{(3.5)}$$

The resistance of the gauge is measured by direct current (d.c.) bridge circuit and the displacement is inferred from the bridge output measured. As the resistance output from the strain gauge is very small, bridge output is also very small, so amplification is essential. The specification of the strain gauges is 2 mm long with a gauge resistance of 120 Ohms +/- 5 % and stated measurable strain of 3 – 4 %. Further details of these sensors can be found in Appendix 3.1.

3.4.2 Fibre Bragg Grating Sensors

Fibre Bragg gratings (FBG) can be integrated into the basic infrastructure of normal optical fibre instrumentation making it possible the incorporate the two types of fibres for use in medical applications such as endoscopy, which currently use optical fibres for vision system.

In its most simple form, FBGs consists of a periodic modulation of the index of refraction along the core of the fibre. The Bragg gratings are written on a nanometre scale with Ultraviolet (UV) light and result in minimal disturbance of the fibre's structure and no measurable loss to the mechanical strength of the host material. This makes it possible to place a large number of Bragg gratings at predetermined locations in the fibre to create a distributed sensor network for monitoring structures (Orthonos & Kalli, 1999)[59]. As a broadband light source is directed into a fibre optic fibre with such gratings in it, the reflection intensity at specific wavelengths will be constructively interfered, whilst all other wavelengths will be destructively interfered. As the material on which the fibre is fixed elongates, the spacing between gratings become greater. These results in a wavelength shift of the constructively interfered light intensity (Figure 3.8). Typical shifts in wavelength are in picometer range. The diagram illustrates how the strain applied to a Bragg grating alters the wavelength of reflected light λ with intensity I. The left picture shows the original position of the etched gratings and the right describes the change in the grating positions after the fibre has been deformed, leading to a change in the wavelength. The diagram shows exaggerated distances between gratings to demonstrate the changes in wavelength. In reality, the distance between wavelengths is very small on the scale of picometers.

Fibre Bragg gratings have the advantage that multiple sensors can be placed on each optical fibre which can be very long. Optical fibres are also very small, light and will not interfere with external electrical or magnetic environments. There is also a linear relationship between the sensor signals. FBG sensors can give absolute measurements that are insensitive to any fluctuations in the irradiance of the illuminating source as the information is directly obtained by detecting the wavelength shift induced by strain or temperature change (Yang et al, 2001)[60].

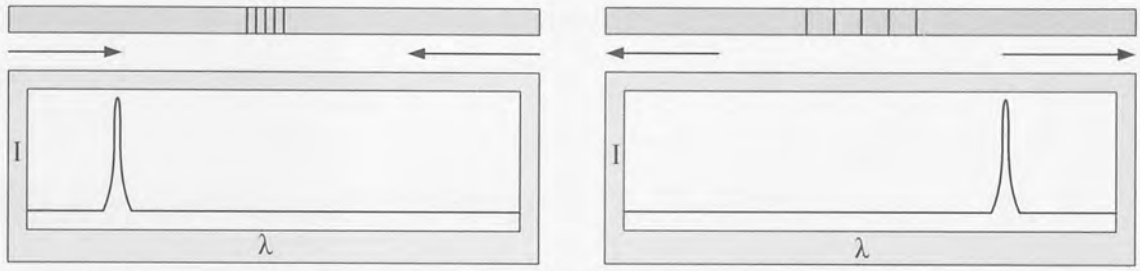

Figure 3.8 Illustration of how the strain applied to a Bragg Grating alters the wavelength of reflected light λ with intensity I.

There are many benefits for using FBGs. One such benefit is their multiplexing ability; many gratings be used on a single fibre, and can be interrogated simultaneously using a single spectrum analyser. Fibre Bragg gratings are created by exposing the optical fibre to UV light. Once the non-reoccurring manufacturing setup is absorbed, FBGs cost substantially less to produce than conventional measuring devices, such as strain gauges. Another benefit to these measuring devices is their size. They can be applied to a measuring surface with very little protrusion, as they are generally as small as a quarter of a millimetre in diameter. Other benefits include their electrical immunity, their long-term stability, and their fatigue durability. However, there is an initially high capital cost outlay of UV photo masks and interrogation equipment for FBG sensors.

3.5 The Distributive Tactile Sensor Cantilever Experiment

An experiment was carried out to determine if a distributive tactile sensor based on the position and number of sensing elements described in Section 3.3 would be able to characterise the presence, size and position of a load placed on it. Two contrasting types of sensors (strain gauges and fibre Bragg grating sensors) were manufactured and tested for these parameters in order to make comparisons between the sensing element types.

3.5.1 Experimental Setup

The experiment consists of two pieces of spring steel (Appendix 3.3) 0.381 mm thick and 24.25 cm long, and is supported at one end. The sensor element locations are at 10 mm, 90 mm 150 mm and 220 mm from the root of the beam (Figure 3.10). Four strain gauges (Appendix 3.1), each in a quarter bridge configuration (Figure 3. 9) are placed along the positive side of the neutral axis as shown in (Figure 3.11). On another similar beam, a fibre optic cable with four fibre Bragg gratings was positioned along the centre of the beam (Figure 3.12) and connected to a broad band light source and the reflected spectrum being measured using an Optical Spectrum Analyser, described in greater detail in Section 3.5.2.2.

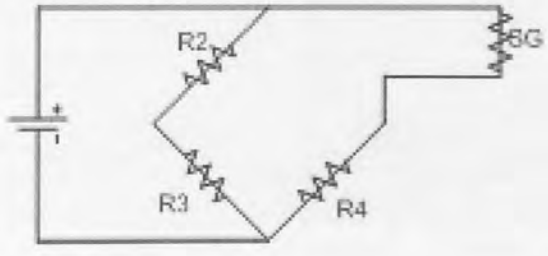

Figure 3. 9 Quarter bridge circuit configuration, where SG = Strain gauge, R2, R3 and R4 = resistors of 120 Ohms each

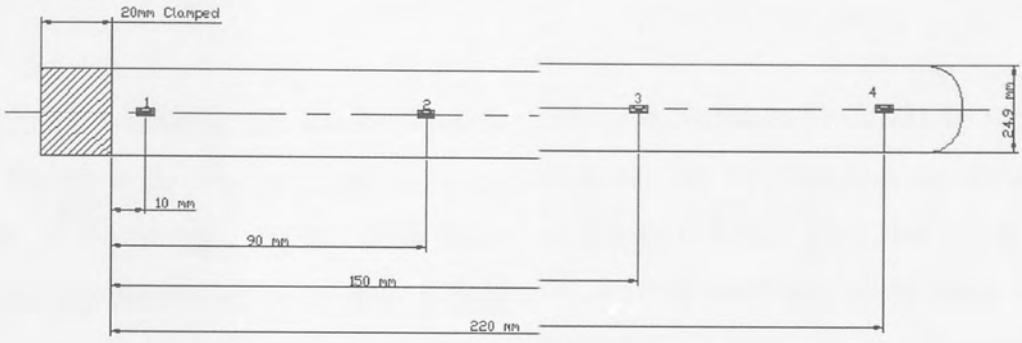

Figure 3.10 Layout of sensing elements on beam

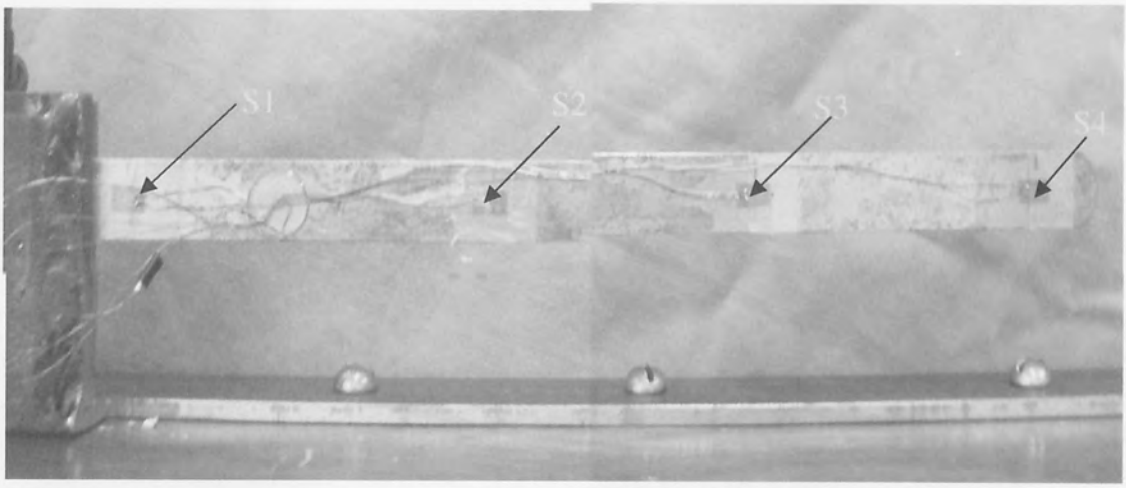

Figure 3.11: Four strain gauges, S1, S2, S3 and S4 attached to a clamped beam

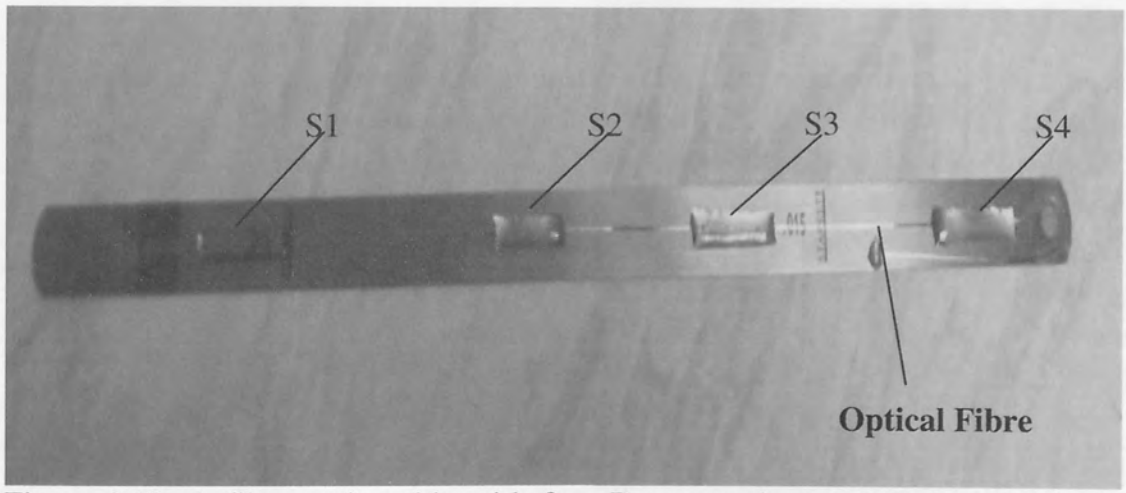

Figure 3.12: A fibre optic cable with four Bragg gratings attached to the beam with a soft epoxy resin gel. The gel restrains and protects the fibre without interfering with the output, as the cladding protects the core with etched gratings.

3.5.2 Data Collection

The beam is divided and inscribed into 24 positions, numbered from 0 (the root of the beam) to 23 (the tip of the beam) where loads can be placed on the dividing lines. A single load (0.024 N) is placed at thirteen chosen positions along the beam. The loads required to deflect the beam are very small and so the loads used are small single units, consisting of uniform buttons as they are manufactured to the same size and loads with good tolerances. The sensors outputs were measured for each loaded condition five times to ensure repeatability results. This data collection is then repeated with double loads and triple loads (Figure 3.13). These test positions are predominantly in the half of the beam nearest the tip along with a couple of test positions close to the root of the beam for completeness of measuring the range of the tactile sensing system (Table 3. 3).

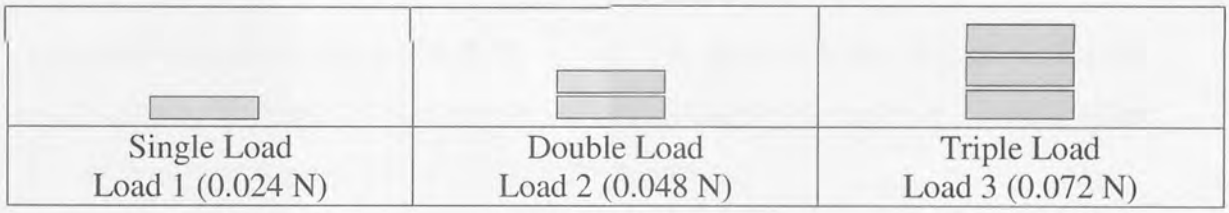

Single Load Load 1 (0.024 N)	Double Load Load 2 (0.048 N)	Triple Load Load 3 (0.072 N)

Figure 3.13 Load Configurations

Position of load from the root of the beam	**Load Type**
0	Load 0 (No Load)
5	Load 1, Load 2 & Load 3
10	Load 1, Load 2 & Load 3
14	Load 1, Load 2 & Load 3
15	Load 1, Load 2 & Load 3
16	Load 1, Load 2 & Load 3
17	Load 1, Load 2 & Load 3
18	Load 1, Load 2 & Load 3
19	Load 1, Load 2 & Load 3
20	Load 1, Load 2 & Load 3
21	Load 1, Load 2 & Load 3
22	Load 1, Load 2 & Load 3
23	Load 1, Load 2 & Load 3

Table 3. 3 Position and Loading combinations for the experiment

The results obtained from the strain gauges are given as amplified voltage outputs and from FBG sensors as a stream of wavelength values. Both these sets of data then have to be processed in a standardised format readable for the neural network program to analyse. The method for obtaining the data from both the strain gauge and fibre Bragg sensors is described in the following section.

3.5.2.1 Strain Gauge Data

The strain gauges readings are amplified using three RDP 628 strain gauge amplifier channels (sensors 1, 2 and 3) and one Strainstall strain gauge amplifier (sensor 4) (Appendix 3.2) and the data was acquired through a Computer Board PCI-DAS 1602/16 10 bit ADC at a sample rate of 125 samples per second using MatLab Real Time Workshop and XPC Target tool boxes (Appendix 3.4). There is a small amount of noise which can be minimised by obtaining a mean value for each sample. Figure 3.14 shows a sample strain output, in the range of 0-0.1 volts for strain sensor 4 when loaded with different loads.

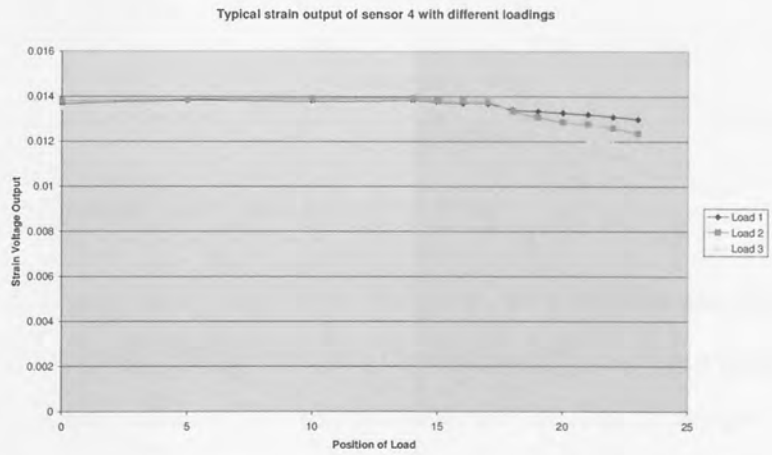

Figure 3.14 Typical strain output for sensor 4 with different loadings

3.5.2.2 Fibre Bragg Grating Sensor Data

The gratings were interrogated using a broadband light source connected to the fibre via a 50-50 coupler, the reflected spectrum being measured using an Optical Spectrum Analyser with a resolution of 0.1nm. The spectrum analyser was connected to a data acquisition card in a PC controlled with Labview. A plot of typical spectrum analyser data for the sensor array is shown in (Figure 3.15). This shows that there are four Bragg gratings etched into this optical fibre with wavelengths significantly far apart (within nanometres) so that the even with extreme strains, and the resulting wavelength shift (within Pico metres), one of the Bragg gratings will not shift into another grating.

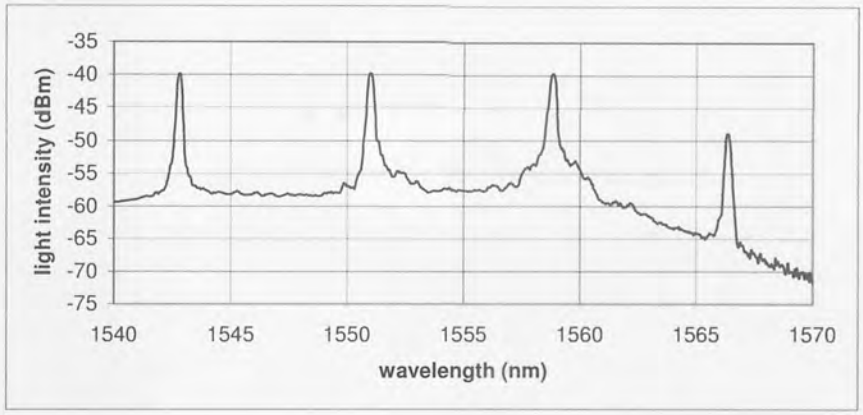

Figure 3.15 Spectrum of fibre Bragg grating array.

As the load is moved along the beam, the peak wavelengths are shifted as well. This is equivalent to the change in strain during loading. It is not enough however to take the maximum value of wavelength intensity as it is necessary to look at an entire region and determine the average of the data. For this, however, it is necessary to define a region first for which we are interested in the all wavelengths within it. The peak wavelength is in a certain region, and since the wavelengths for the whole fibre are measured, the peak wavelengths for each sensor can be determined by one of several methods. The first being the least

squares method, which approximates a second order polynomial to the region of interest, the second, and the ones used for these tests, is the centroidal detection algorithm (Ezbiri et al. 1998)[61]. This algorithm relies on examining all wavelengths and their intensities within a pre-defined region, and calculates the peak intensity from their intensity weightings, using equation (3.6). A typical example of the outputs obtained from this algorithm is shown in (Figure 3.16). This graph shows that the centroid detection sensor 4 with different loading positions of a single load.

$$\lambda_p = \frac{\sum_j \lambda_j i_j}{\sum_j i_j} \qquad \textbf{(3. 6)}$$

Where λ = wavelength in the pre-defined region
λ_p = the peak wavelength
i = is intensity at a specific wavelength

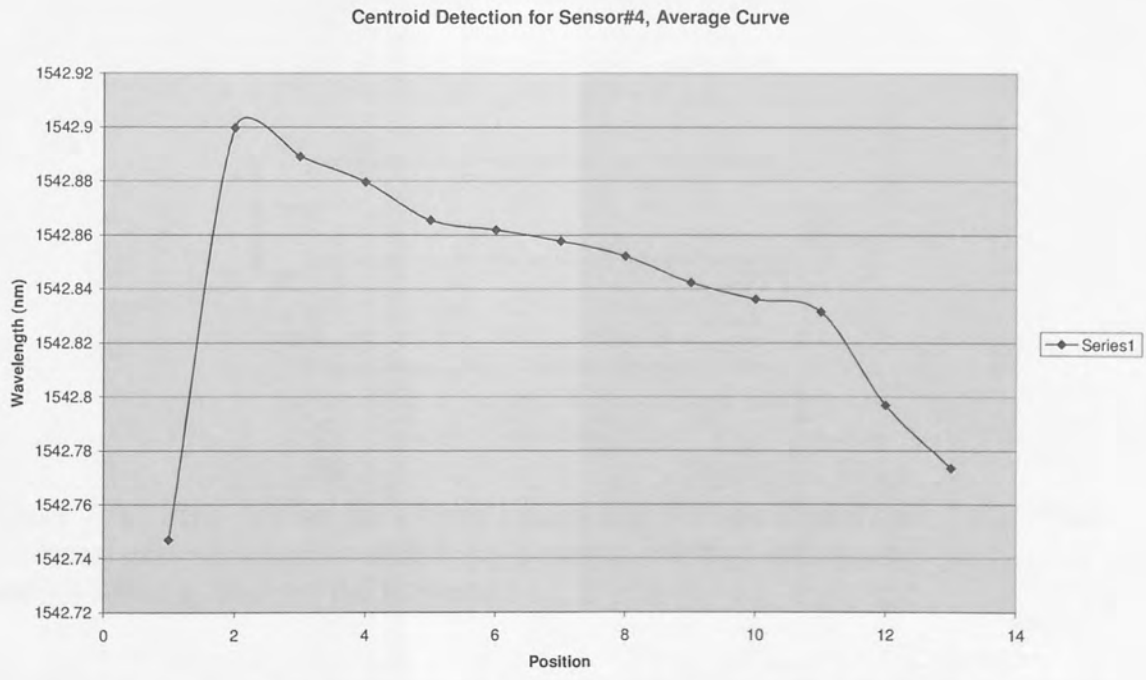

Figure 3.16 Centroid detection for sensor 4 with different loading positions

3.5.2.3 Data Scaling

The two sets of strain and FBG data are then scaled so that the input variables for the neural networks have similar magnitudes. This means that the network weights can be expected to have similar values if the inputs are equally important and can be initialised randomly. Without normalisation, network training often gets stuck in a local optimum because some of the weights are a long way from their best values. (Nabney, 2002)[62]

For example, examining the data produced from loading the beam with a single load at various positions along the load (Figure 3. 17), the magnitude in the variance for each sensor is very small in comparison to the variance in the wavelengths of the gratings. There is very little perceptible difference between readings.

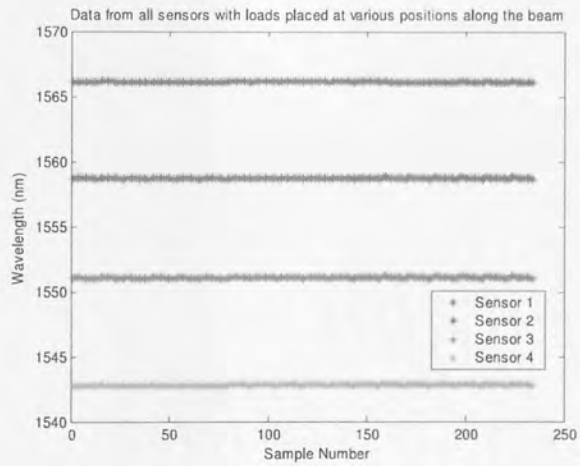

Figure 3. 17 FBG data set for a beam loaded with a single load (Load 1) at various positions shows no distinct differences between readings and requires normalisation to observe the variance.

Examining the data for each sensor in more detail, we can see there is greater variance, but all the data sets have to be scaled to the same range. (Figure 3.18a) shows the variance in pico-meters of the samples for sensor 1 and this data is normalised so that the mean is zero and there is unit variance (Figure 3.18b). The

data for each sensor is scaled in this way independently thus increasing the spread of the overall variance. Figure 3.18c shows the all the normalised and scaled data from all the FBG sensors with varied beam loadings and positions. It can be seen that there is a greater range in variance. The same method of scaling is carried out for the expected output values dependent on the format of the output based on the type of neural network used. This process was also repeated for the strain gauge data.

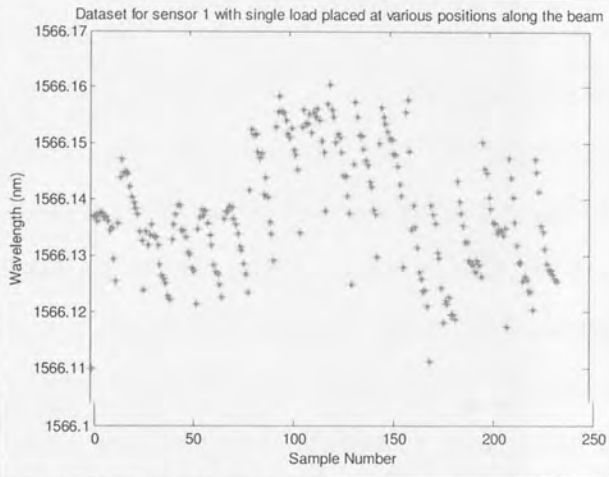

Figure 3.18a Variance of dataset for FBG sensor 1 after normalisation

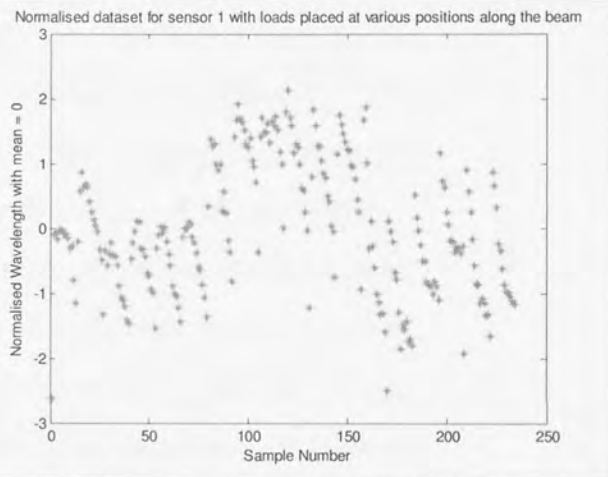

Figure 3.18b normalised variance of dataset for FBG sensor 1 after scaling

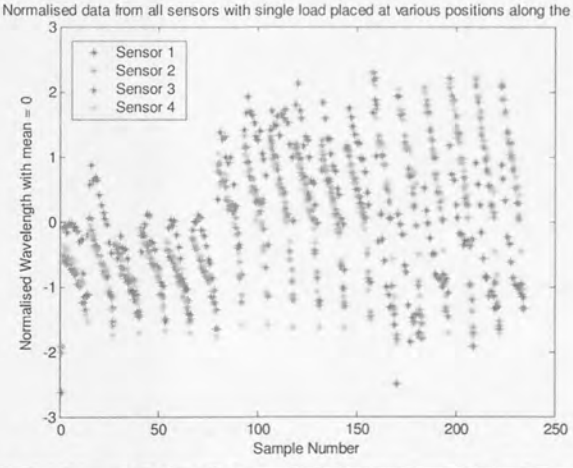

Figure 3.18c Normalised data for all the FBG sensors for all load and load position combinations

Figure 3.18 Scaling for FBG sensor data

3.5.3 Optimising Neural Network Architecture

In preparation for training the neural networks, the optimal architecture can be estimated by to gather information about the convergence of the error for different number of nodes. In this exercise, a third of each dataset is taken in a random sample and fed into a neural network with changing parameters. Another third is used to validate the results of testing. The number of hidden nodes tested is increased in intervals of 5, and the error is measured every 2000 iterations, for 50 epochs. The error is measured as the negative log of the likelihood. The likelihood assumes that all the elements in the data sample are mutually independent and by finding the minimum of a scalar function of several variables, starting at an initial estimate, this is generally referred to as *unconstrained nonlinear optimisation*. Figure 3.19 demonstrates that the optimal number of hidden nodes for convergence is around 45 nodes for determining whether contact is present using a FBG sensor data and a logistic activation function. A table of the optimised node parameters used are given in Table 3.4.

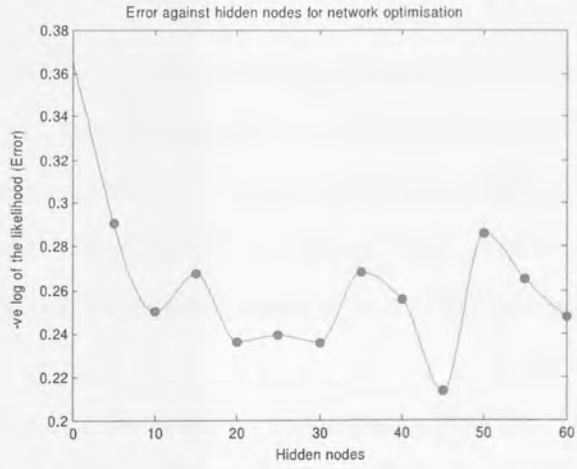

Figure 3.19 Example of neural network architecture optimisation for a FBG data set

Neural Network output	Output Type	Optimal Number of Hidden Nodes for Strain Gauges	Optimal Number of Hidden Nodes for FBG Sensors
Logistic	Contact Presence	60	45
Softmax	Load Magnitude	15	10
Linear	Load Position	5	15

Table 3.4 Number of optimal hidden nodes to train single neural networks that are used in a parallel net configuration

3.6 Results of Experiments

When the neural network architectures for each of the contact parameters have been determined, the results for detection of contact, load magnitude, and load position are evaluated.

3.6.1 Detection of Contact

The first step in identifying the load characteristics is to find out first if there is any load contact. For this application, there are only two states that the load can be in; no contact and contact. Due to the fact that different types of loads are placed onto the beam at different positions with different loading profiles, a classification neural network can be used to detect the presence of contact.

The type of neural network used in this case is simple classification, with two classes which are outputs in a 1-N encoding (Table 3. 5), using the logistic neural network model. The optimal number of hidden nodes to run the neural network was determined to be 60 for strain sensors and 45 for FBG sensors.

1 0	No Contact
0 1	Contact

Table 3. 5 1-N Encoding used to distinguish between 2 classes

To train the neural network, each sensor dataset were randomised and two thirds of the data was used for training and one third for testing the optimised neural network for required output and sensor type. The results in Figure 3.20 show that the neural networks using strain gauge data correctly detected 98.5% of contact conditions, but with the FBG sensors neural network performing better with 100% of contact conditions correctly identified. By inference, the ability to detect the presence of contact with one sensor would also be used as an input to a *second stage* cascaded neural network. By identifying the presence of contact, the non-contact datasets can be set aside, whilst the remainder can be processed by other neural networks to identify load magnitudes and load positions.

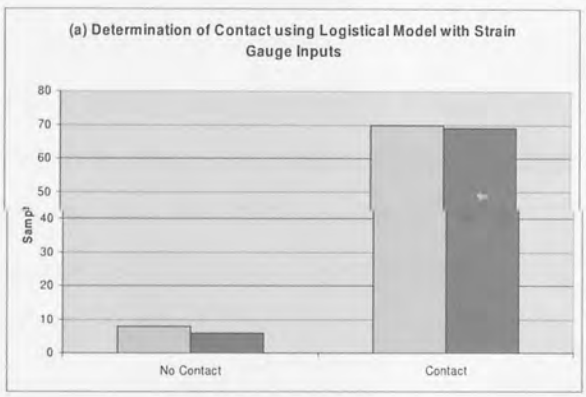

Real/Predicted	No Contact	Contact
No Contact	6	2
Contact	1	69

Confusion matrix for strain gauge

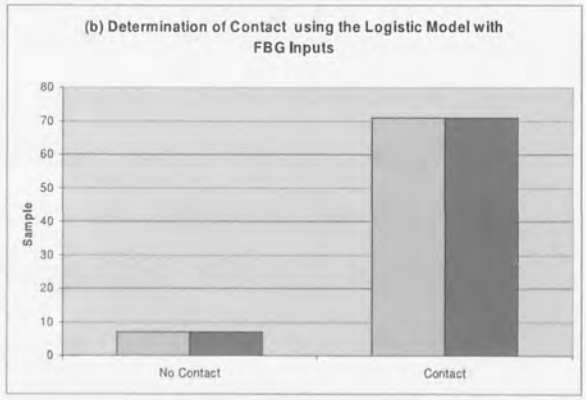

Real/Predicted	No Contact	Contact
No Contact	7	0
Contact	0	71

Confusion matrix for FBG

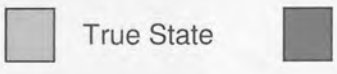

Figure 3.20 Results and confusion matrices of a neural network trained with (a) strain gauge input data and (b) FBG sensor in put data

3.6.2 Load Magnitude

The load magnitude can be determined in two ways, either by using neural network with a regression (linear model) or by using a classification technique (Softmax model) for three or more classes. In this case, as the loads magnitudes are discrete values, a classification type neural network was appropriate. The loads were placed on the beam in increments that lends itself to a classification technique rather than the regression technique. The outputs were classed as no load, one, two or three loads as described in Table 3. 6.

Comparing the results between strain gauges and FBG, the neural network using FBG sensor data was more accurate in three cases out of four than that using resistive strain gauge data when detecting load magnitude (Table 3. 7). This table shows that the FBG neural network is overall more consistent than the strain gauge neural network in determining the load magnitude with 86 % accuracy to 70 %.

Class	**Output for Regression**	**1-N Encoding for Classification**
Class 0	0 Load = 0 N	1 0 0 0
Class 1	1 Load = 0.024 N	0 1 0 0
Class 2	2 Loads = 0.048 N	0 0 1 0
Class 3	3 Loads = 0.072 N	0 0 0 1

Table 3. 6 Load Classification

Load Type	**Resistive Strain Gauge % Accuracy**	**FBG sensors % Accuracy**
No Load	70.0 %	100 %
Load 1	96.2 %	85.0 %
Load 2	60.9 %	77.8 %
Load 3	52.4 %	82.6 %
Overall Accuracy	69.9 %	86.4 %

Table 3. 7 Comparison between the neural networks trained with strain gauge data and FBG sensor data for load magnitude

3.6.3 Load Position

The position can be determined in two ways, either by using linear regression output neural network or by using a classification network (softmax model) for three or more classes. In this thesis, a linear regression model is used to demonstrate the method. In a linear regression output neural network, the output will be in continuous numerical form, for example, a position output would be any position along the beam up to a reasonable measurable resolution.

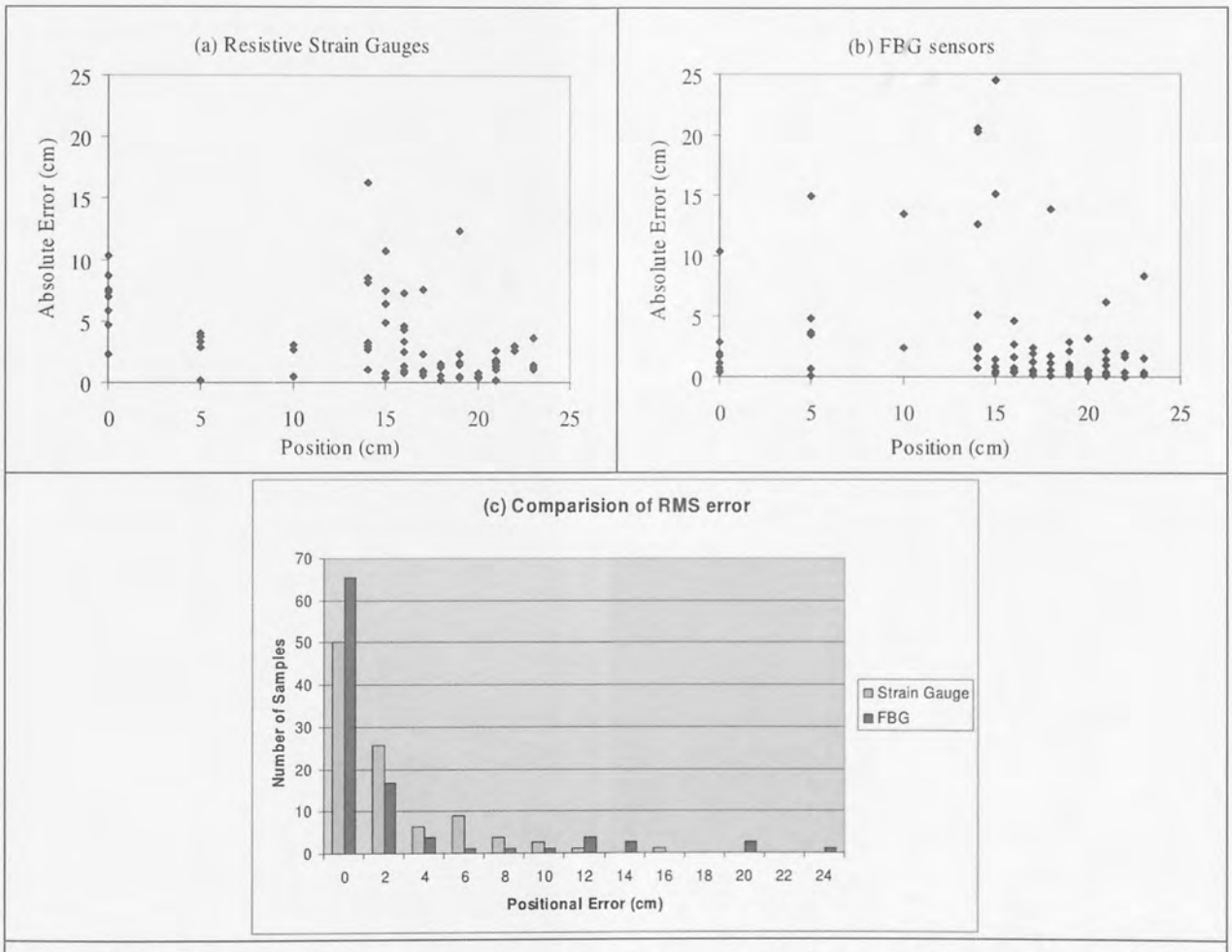

Figure 3. 21 Accuracy of a neural network predicting load position using (a) Strain Gauge data (b) FBG Sensor data, with (c) histogram showing comparison of errors.

Comparison of the data in Figure 3. 21 show that the FBG sensors have a greater percentage of outputs (within ≤2cm which is approximately 10% of the beam) of the true position; however this success is compromised by several inaccurate results with larger errors. This is due to loading directly onto the sensing element causing exaggerated readings, which give the FBG sensors an overall RMS error (6.1cm, vs. 4.5cm for the resistive strain gauges). This in percentage terms is equivalent to 74.6 % and 81.3 % accuracies respectively of the total length of the cantilever beam.

3.7 Conclusion

In this chapter, greater understanding of the distributive tactile sensing scheme for single dimension is achieved. The work carried out on a thin cantilever beam was used to simplify the behaviour of a flexible digit and the use of contrasting sensing types shows the versatility of neural networks to be able to deduce complex information from limited sets of data.

The results show that FBGs perform well in this application outperforming the resistive strain gauges in the majority of cases. These results are summarised in Table 3. 8.

	Strain Gauge	FBG
Contact Condition	98.5 %	100 %
Load Magnitude	69.9 %	86.4 %
Load Position	74.6 %	81.3 %

Table 3. 8 Performance comparison based on accuracy between neural networks trained with strain gauge data and FBG sensor data

In these experiments the data was processed after it was collected. Any data processing used in a real-time system should not cause a delay perceptible to the user; for example, the data rate for palpation is in the region of 30 Hz (Peine et al, 1997)[63]. Neural networks offer the possibility of highly efficient, parallel data processing that can considerably simplify the extraction of useful information from complex data. The study reported here demonstrates that the use of FBGs is compatible with this kind of signal processing.

Fibre Bragg Grating sensors are reliable as they produce less noise, however they are expensive to manufacture in low volume, also the interrogation equipment is

high cost and there was limited availability of this equipment during the experimental period of this research. Hence, for the majority of this thesis, strain gauges are chosen as the preferred sensing element type due to their abundance, flexibility in their application, low capital cost and availability of amplification equipment. This technique is incorporated into the tool point design described in the following chapter.

Chapter 4

The Tool Point

This chapter examines the design and manufacture of the prototype digit tool point. The deflection properties and performance are characterised for the chosen solution of a flexible digit. The digit design, materials and construction techniques were chosen on the expectation of the needs of a clinical tactile sensing digit and the requirements for endoscopes along with integration of the sensors used the distributive tactile method as described in Chapters 2 and 3 respectively. The techniques used to construct an operational end tool point to serve as an actuated digit with distributive tactile sensing are detailed and the material selection, construction techniques and validation of the final constructed device are described.

4.1 Design Requirements

Contemporary MIS devices can be divided into two groups: rigid and flexible. Rigid instruments are essentially long structures and mechanisms with tool points at the tip. An example of such a device includes laparoscopic instruments. The feed rate of such instruments is dependent on the location of the target and the mass of tissue displaced as the instrument is pushed to its destination. In flexible MIS instruments, such as a nasal endoscope, the device is pushed through an opening in the body and the shape is partially dictated by the resistance and flexibility of the sidewalls of the lumen in which the device is travelling. In both cases, there is a possibility that the force of pushing the instrument will be greater than the force that the tissue can withstand and bruising, perforation or tearing could occur.

Navigation of the instrument inside the body should be constrained by the tissue that it encounters, but should comply with the shape of the lumen instead. The tool should find a path without forcing its way through. Detection of force is impaired through the high mechanical impedance of the long structure. Based on the requirements for the digit outlined in Chapter 2, the design criterion for the digit is established:

- Flexible, yet stiff enough to be able to move through tissue, when pushed through without causing damage
- Provide information feedback
- Should be disposable
- Ideally manufactured with non metallic components for potential use in magnetic resonance scanning
- Minimal wiring for actuation and sensory feedback should be considered

4.2 Digit Design Concepts

There are several ways in which the digit can be constructed, and in this section, we exam some of the current methods employed (4.2.1) including the chosen approach for actuating and sensing in a controlled flexible digit (4.2.2) and the materials required for construction of a digit (4.2.3).

The construction of the digit rests on the integrated methods of actuation and sensing. The digit needs to be flexible, capable of deploying tip deflection comparable to contemporary endoscopic devices in at least one axial direction for palpation, and in orthogonal directions for navigation. Current flexible endoscopes tips are actuated via cables. This type of construction has some merits, as the mechanism is a pulley and hence simple to operate. However, cable driven endoscopes are limited to the amount of deflection and curvature that can be achieved. For example, the tip deflection of a standard fiberscope manufactured by (Olympus Industrial, 2005)[64] has a typical tip deflection of 120° in the upward and downward directions. It is feasible for the tip to be constructed to deflect in more directions, but this would increase the density of cabling within the endoscope construction and winding mechanisms at the held end of the instrument, leading to inefficient use of the volume and cross section.

Yamashita et al (2003)[65] proposed a bending mechanism with a multi-slider linkage with two pin joints that could rotate ± 45° respectively enabling the rotation of ± 90°. Though the conclusion was that the multi-slider linkage mechanism was useful and highly repeatable, having been tested in an in vivo surgical experiment, the design does not incorporate tactile sensing.

Lazeroms et al (1996)[66] proposed the design of a hydraulic forceps, which consists of an inner tube made from very flexible material holding water and an

outer tube made from a stiffer material with small incisions cut perpendicular to the tube. Both the ends of the tube are connected to each other so that the deformation is consistent throughout and by increasing the water pressure in the inner tube, an axial force is introduced on the end of the tube that contributes to tube curvature since the there is a large difference in the stiffness of the outer tube compared to the inner tube.

Another solution considered was a digit made with three corrugated tubes bound together and sealed at one end (Figure 4. 1). A pressure inlet is attached to each of the tubes and the other end and is sealed off. When pressure is applied to one of the tubes; that particular tube will stretch, causing the other two tubes to contract and forcing the digit to more in the direction of the stretched tube. This allows the digit to bend in three directions. The distributive tactile sensing technique could be implemented in the central core of the three tubes.

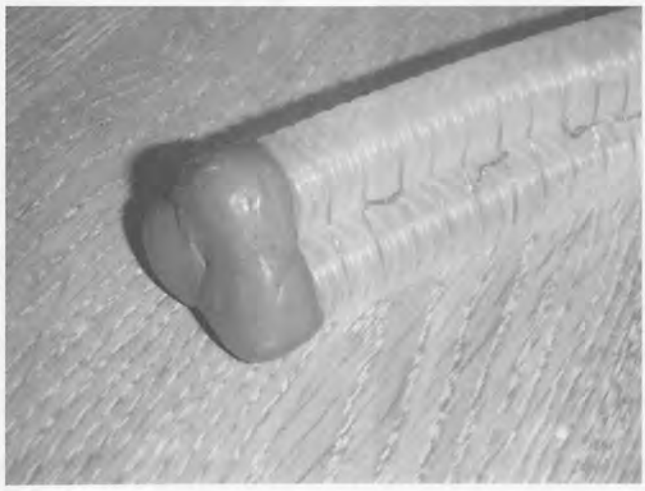

Figure 4. 1 Triple chambered actuated digit prototype

An alternative is a bellowed tube with an axial constraint was proposed by (Stone & Brett, 1996)[67] and drawing from this method, techniques for building an operational device were developed (Figure 4.2). The solution for a bending mechanism is to have a corrugated flexible tube with a constraint along one side

of the tube wall. This tube is then pressurised pneumatically. The solution of pneumatics is for practical demonstration purposes. Liquids will be heavier, but are ideal for smaller diameter tubes. As pressure increases in the chamber, the ridges of the corrugations will expand longitudinally, with little or no expansion of the tube diameter. This method is ideal for a laboratory test environment, where there the supply of compressed air was readily available and it removes the need to ensure that the device is water tight to prevent possible damage to any sensors from fluid leakage.

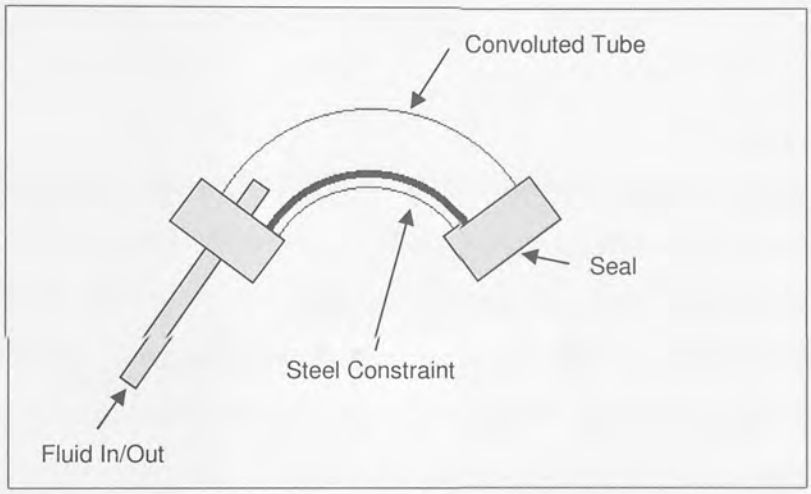

Figure 4.2 Schematic construction of the first prototype digit

Of the last two designs, the latter was chose as the solution for this research. Although the three-chambered digit could incorporate a distributive tactile sensor in a central core of the three chambers, the sensor would have to be very thin and narrow and three individual distributive tactile sensors could be employed. However, the structure of the distributive tactile sensor described in Chapter 3 is a thin beam which can only deflects in a single plane as the second moment of area for thin beam is much greater in one plane, making it too rigid for deflections in the orthogonal directions. The second design is more suitable for this type of distributive tactile sensing scheme.

4.3 Digit Construction

The main components for the digit are flexible corrugated tubing, an axial constraint, air seals and inlets. During this period of research, many combinations of materials were considered and tested. In this section, the development of the prototype digits is described, from the choice of materials for components to the construction techniques used to create the final working model.

4.3.1 Material Requirements

The bellowed tubing that provides the main structural component of the digit must withstand pressurisation. Working on the assumption that the maximum pressure available in the laboratory, the bellowed tubing required for the tubing must be able to withstand internal pressurisation up to 75 PSI or vacuum pressure. The final choice of material for the tubing was based on suitable and widely available PTFE convoluted tube, most commonly used in anaesthesia (Appendix 4.1). It is flexible and transparent, making it ideal material to be used to initial prototypes as its dimensions proportions and lightweight made it suitable. The tubes are available in two sizes of diameter; 12.5 mm and 25 mm and can be cut to length required. The pitch between convolutions is 3 mm, and this is the same for both diameters of tubing. However, there were adhesion difficulties when joining the tubing to other components to PTFE. Other types of flexible tubes such as flexible hose used and described in Appendix 4.2 were examined; however no other tubing offered the same material and structural properties required for the digit design. Most were significantly larger in diameter than the PTFE tubes and frequently incorporated coiled helix springs in the core to provide flexibility rather than convolutions and were much stiffer than simple corrugated tubes. Use of these types of tubing would lead to very large and stiff prototypes requiring

large forces to actuate flexion. In addition, many of the samples examined were not specified for use in clinical environments. It has to be noted that, whilst PTFE tubing was ideal for the prototypes, however it is not ideal in adhesion with other materials including the sensing elements. As with all potential medical devices, all the materials used in the final product will have to be tested by medical devices regulatory boards and follow clinical test guidelines before release. This will mean further changes in the materials used in the final device, but is beyond the scope of this project.

The end caps sealing the digit can be made from several materials. Moulded nylon was used initially, and although this method formed a strong seal, it required heating to temperatures that often affected the shape of the bellowed tubing. An alternative sealant is epoxy resin putty which has more pliable qualities for moulding into desired shapes without the need of a mould or heat and could equally offer an airtight seal to the digit chamber.

4.3.2 Digit Actuation

The digit is actuated pneumatically as this fluid medium is readily available in the laboratory. In the experiments, the actuator was controlled using a Norgren VP50 proportional pressure control valve (Appendix 4.3), which has linear pressure gain over the range of 10 PSI to 75 PSI as required for the digit. This linear range was determined by measuring the pressure output of the control valve with a dial pressure gauge at 0.1 V control valve input intervals. The equation over the linear range (between 0.1 V to 0.9 V) for the pressure in PSI was determined to be, $P = 94x - 11$ where x is the control valve input voltage. By controlling the input voltage to the valve, consistent changes in pressure can be maintained. We can see from Figure 4. 3 that the slope of input voltage plotted against pressure in PSI is linear. This indicates that the pressure control valve the pressure gain is constant from

0.1V to 0.9V, giving a maximum pressure of 75 PSI, with a resolution of 0.1 V per 9.2 PSI.

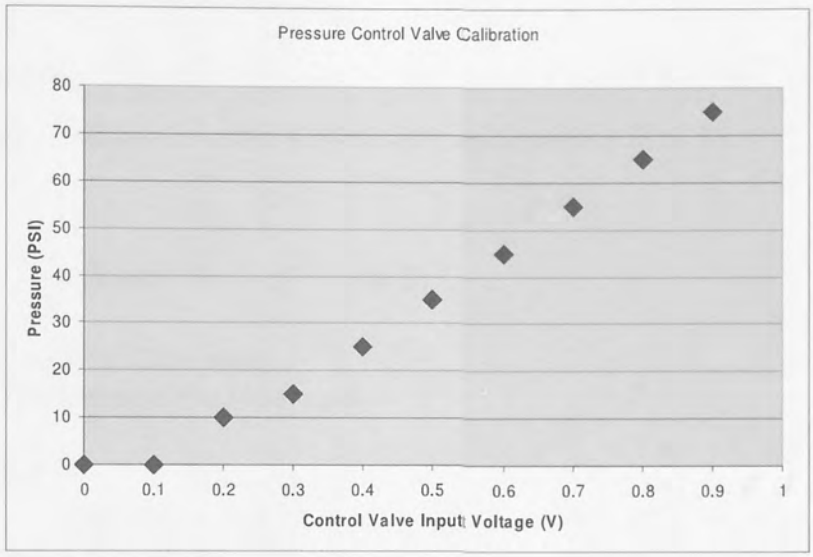

Figure 4. 3 Pressure Control Valve Calibration

4.3.3 Digit curvature based on diameter of tube

The digit curvature is dependent on the diameter of the tube can be determined by the sensitivity to curvature with respect to pressure gain. By examining the relationship between the pressure and tube diameter, the choice of actuation can be made. Currently pneumatic is used for the dimension of tubing used, but hydraulic actuation can be considered for smaller scale versions digits, as the pressure required to the cause the digit to bend increases as the digit axial diameter decreases as shown in the following formulation:

$$\frac{1}{R} = \frac{P\pi d^3}{8} \times \frac{1}{(EI)} \qquad \textbf{(4. 1)}$$

Where R = Radius of curvature
P= Pressure
d= Diameter of tube
E= Young's Modulus
I = Second Moment of Area

The assumptions that the thickness of the tube, $t << D$ and that there will be characteristic variation in a thin walled tube as described in (4.2).

$$\delta I = \frac{d^3}{8} t.\delta\theta.\sin^2\theta \qquad \textbf{(4. 2)}$$

Where θ = Angle of Curvature
t = Thickness of the tube wall

It follows that

$$I = 4\frac{d^3 t}{8}\int_0^{\pi/2} \sin 2\theta.\delta\theta \qquad \textbf{(4. 3)}$$

$$I = \frac{d^3 t}{4}\left[\theta - \tfrac{1}{2}\sin 2\theta\right]_0^{\pi/2} \qquad \textbf{(4. 4)}$$

$$I = \frac{\pi}{2}\cdot\frac{d^3 t}{4} \qquad \textbf{(4. 5)}$$

Hence (4.1) can be written as:

$$\frac{1}{R} = \frac{\pi d^3}{8}\times\frac{8}{\pi d^3 t}\times\frac{P}{E'} = \frac{P}{E't} \qquad \textbf{(4. 6)}$$

Normalising on size of curvature with respect to the diameter

$$\frac{d}{R} = \frac{d}{Et}\cdot P \qquad \textbf{(4. 7)}$$

For a given elastic proportion of (Et), the tube curvature is proportional to the diameter and pressure. Tube dimensions ranging from 5 mm to 30 mm were applied to this formulation, resulting in Figure 4.4 This shows that as the diameter of the tube narrows, the pressure required to reduce the curvature of bending increases. This indicates that for smaller diameter tubing, the operational pressures for actuation are greater, hence hydraulic pressures can be considered. It also must be noted that hydraulic pressure actuation system would increase the mass within the construction, making the digit heavier to manoeuvre. The volume of the tube increases exponentially with the diameter of the tube, so for small diameter tubing, the effect of volume of fluid is less significant.

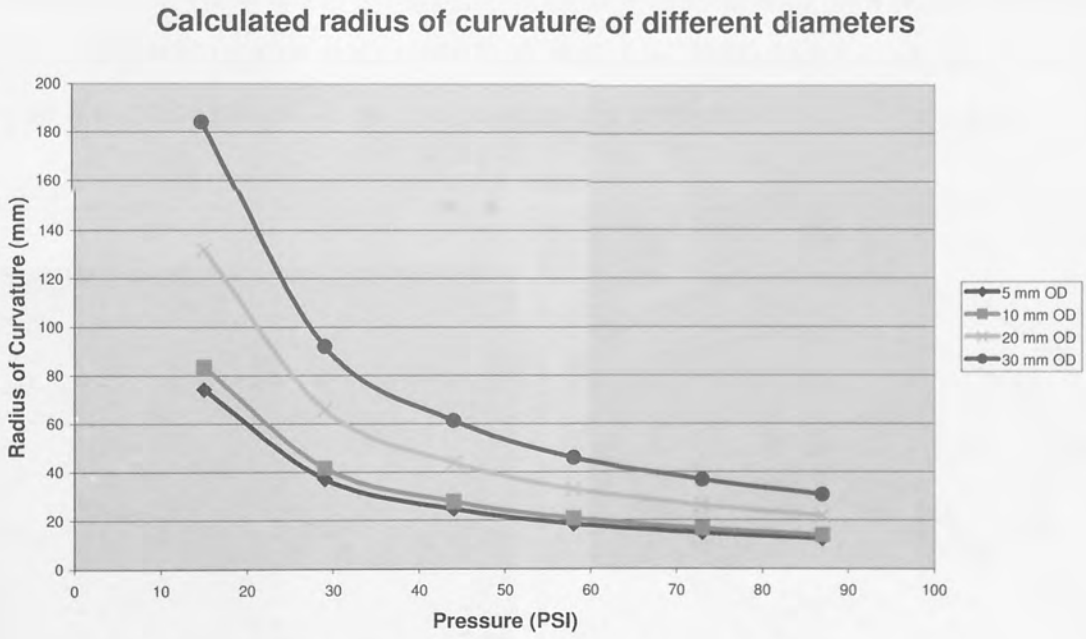

Figure 4.4 Dependency of pressure on diameter

4.3.4 Digit curvature validation

Validation of the pressure requirements of different diameter tubing can be verified by performing tests on two different diameter convoluted tubes. The tubes are readily available and are made from blow-moulded PTFE and are manufactured in two common sizes; outside diameter 12.5 mm and 25 mm and in the construction a length of 150 mm. Three test pieces for each diameter of tube were made to the aforementioned specification for repeatability. The digits were inflated at pressure intervals of 10 PSI (0.69 bar) and their average extensions after 30 seconds were measured. Both diameter of tubing have the same pitch of convolutions, which is significant as this reduces the number of variables that can cause the extent of tube extension. Both ends were sealed with epoxy putty, with an air input tube located at one end, designated as the based end (Figure 4. 5).

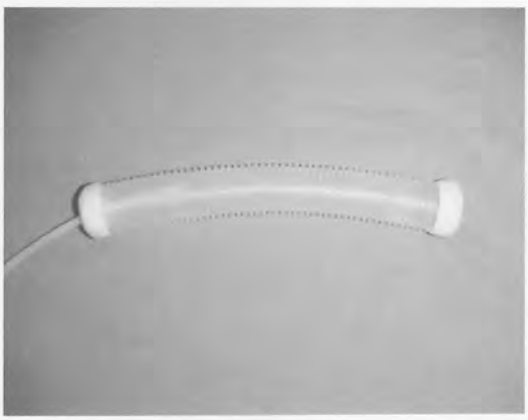

Figure 4. 5 Sealed test digit

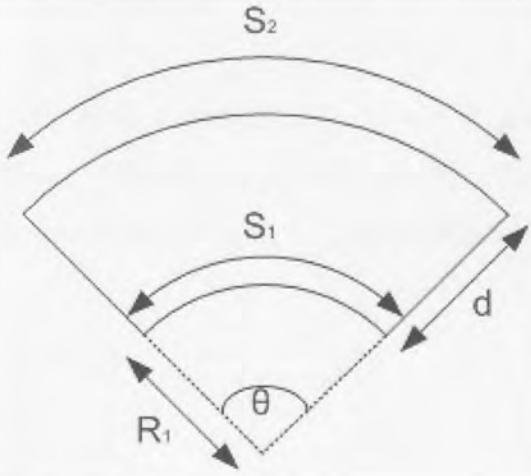

Figure 4. 6 A curved tube

The assumption is that if there is an axial constraint, there is insignificant change in axial length along the side of the constraint, which we call S_1. However, the side that is unconstrained will stretch, causing the digit to curl and designated as S_2 (Figure 4. 6). By measuring the average change length of an unconstrained

digit when it is subjected to changes in pressure and applying equation (4.11), the radius of curvature for tubes of varying diameter is approximated.

Based on the equation for the sector of a circle:

$$s = r\theta \qquad \textbf{(4. 8)}$$

Where s = Sector of a circle
r = Radius of the circle
θ = Angle of curvature (radians)

We can derive the following equations (4.10) for a constrained digit (Figure 4. 6):

$$\begin{aligned} S_1 &= R_1\theta \\ R_2 &= R_1 + d \\ S_2 &= R_2\theta \end{aligned} \qquad \textbf{(4. 9)}$$

Where S_1 = Original length of the digit
S_2 = Length of the digit when subjected to pressure
d = Diameter of the tube

This yields three simultaneous equations the three variables, R_1, R_2 and θ, the radius of curvatures and the angle of curvature. Rearranging (4.10) produces the formulae for approximation of the actual bending curvature of a digit of different diameters (4.11):

$$\begin{aligned} \theta &= \frac{S_2 - S_1}{d} \\ R_1 &= \frac{S_1}{\theta} \\ R_2 &= \frac{S_2}{\theta} \end{aligned} \qquad \textbf{(4. 10)}$$

The results in Figure 4. 7 show that thee average measured radius of curvature for both diameter of tubing were similar to the calculated values in 4.3.3. Figure 4. 7 plot the comparison between calculated and measured results digit curvature of

different diameters and they are similar and the model is validated. This shows that the feasibility of the digit design being manufactured on different dimensional scales, enabling more versatility in the range of applications that the digit can be applied to. Although pneumatic actuation is used in this research, in a clinical environment, a hydraulic solution is more desirable for higher pressures, as this limits dangers posed by high-pressure pneumatics that could lead to venous air embolism in the patient.

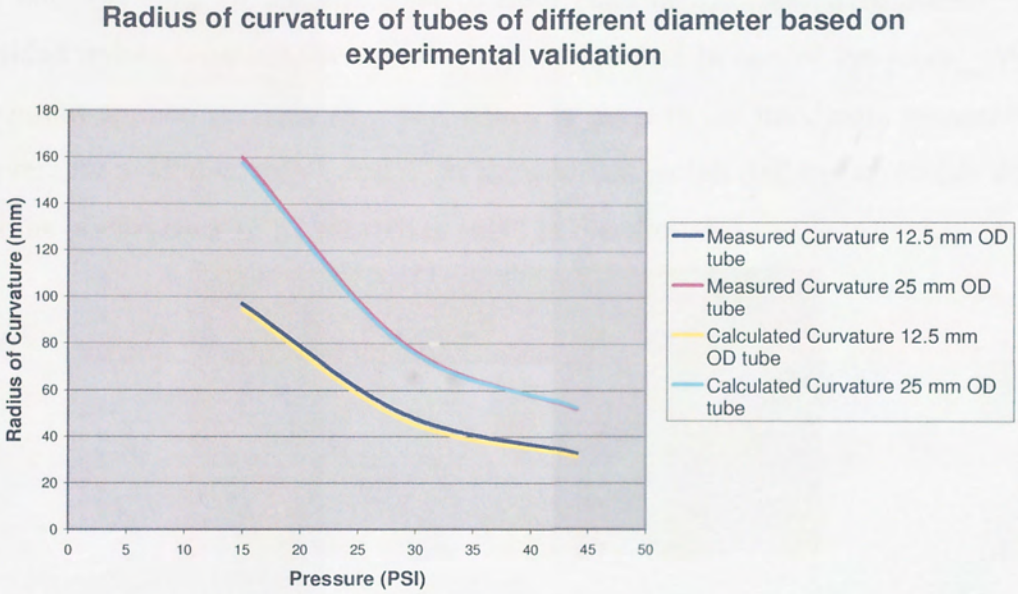

Figure 4. 7 Validation of radius of curvature

4.3.5 Initial Prototype

The first prototype flexible digit (Figure 4. 8) built was constructed from a single piece of corrugated PTFE tubing that is 12.5 mm in diameter and 160 mm in length. The axial constraint is a strip of spring steel that is 0.254 mm thick, inserted along the length of the tube and its ends embedded into the seal. Strain sensing elements were attached to the constraint in positions 16mm, 64 mm, 96 mm and 144 mm on the same side. Both ends of the tube were sealed with moulded nylon, with one air inlet/outlet tube inserted in one of the seals. With maximum applied pressure of 5 bar, which is close to the maximum compressed air pressure available, tests carried out showed that a digit deflection reaches up to a radius of curvature of 57 mm (over 160°) in one direction

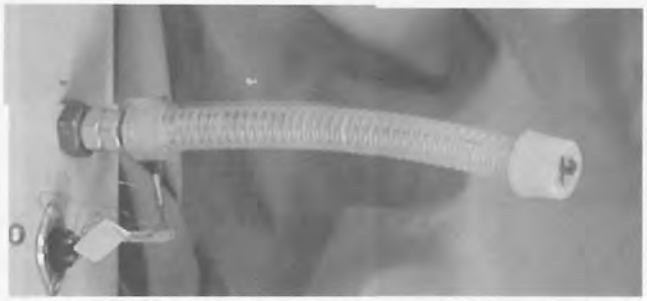

Figure 4. 8 Initial Prototype

Strain gauges adhere to the steel constraint easily, however, due to the placement of the constraint inside the tube and since it is not attached to the sidewall of the digit, there was a tendency for the digit to buckle with internal pressure applied, leading to damage to the strain gauges. Therefore, an alternative solution was needed.

4.3.6 The Number of Sensing Elements for the Digit

Since some of the strain sensors in the first prototype had failed, it was decided to test if the distributive tactile sensor could work with fewer than four sensors, allowing for the possibility of redundancy in the sensing system. The next challenge is to make a digit shorter slightly shorter in length (the original was 160 mm long) reducing the amount of additional bending to the digit from the weight of the construction itself. The new digit was 120 mm in length. However, with making the length shorter, the space available to place the sensing elements is at a minimum, hence creating problems in physically fitting the elements to the constraint. The number of sensing elements that could be placed on the axial constraint is limited by the size of the overall digit.

Returning to the data obtained during the cantilever beam sensor experiment described in Chapter Three, the number of channels of data fed into a neural network was reduced and results from these neural networks were compared with neural networks using four channels of input data (Table 4. 1). It was indicated that the removal of sensing element 4 caused the least degradation in the overall results for presence of contact, load magnitude and load position. The fourth sensor, located at 0.9L from the root of the sensor is intended for use in determining the width of the load greater than a quarter of the length of the beam (Chapter 3.3.1).

	% Accuracy		
	4 Channels	**3 Channels**	**% Error Difference**
Contact Present	98.5 %	98 %	- 0.5 %
Load Magnitude	69.9 %	66.2 %	- 3.7 %
Load Position	74.6 %	75	+ 0.4 %

Table 4. 1 A comparison of accuracy for four and three channels of strain gauge input neural networks.

4.3.7 Final Digit Construction Method

Several steps in the construction of the digit are described in Figure 4.9 and a diagram of the different layers in the digit construction is shown in Figure 4. 10. The first prototype digits used spring steel as the constraint. Suitability to magnetic environments, polymer constraints were considered. The constraint that governs the bending of the tube is a polyester boning material commercially known as 'Rigiline'. This type of material was chosen because of its porous nature, which allowed for better adhesion to the convoluted tube. Rigiline is made from a several flexible rods of nylon, woven together with polyester (Figure 4.9A). There is potential that some of these flexible rods could be replaced with optical fibre Bragg grating sensors.

The sensors used for this prototype were strain gauges that were attached to an acetate strip embedded between the tube and the boning (Figure 4.9B). Originally the strain gauge was glued directly onto boning. However, this was found to be unsatisfactory when pressure was applied to the completed digit, as the boning surface is not smooth and caused the sensing element to slip.

The constraint is glued to the tube with a silicone sealant that when cured would provide a seating for the constraint to reduce slippage of the boning. To prevent the constraint from peeling from the tube when the digit is pressurized, the device is then bound together with polyester thread, using a 'Casting' stitch that anchored the thread at each of the convolutions along the tube (Figure 4.9C).

The tube was sealed at either end with 50 g of epoxy putty at each end, which, when cured provided a strong, airtight moulded seal (Figure 4.9D). The putty replaces the nylon moulding as it proved to be more pliable to work with and is also strong enough to be used as linking material for two or more chambers.

The completed digit was connected to the pneumatic supply and valve. By changing the pressure within the digit, the bending curvature of the digit was adjusted to a range between 0 and 160° (Figure 4.9E).

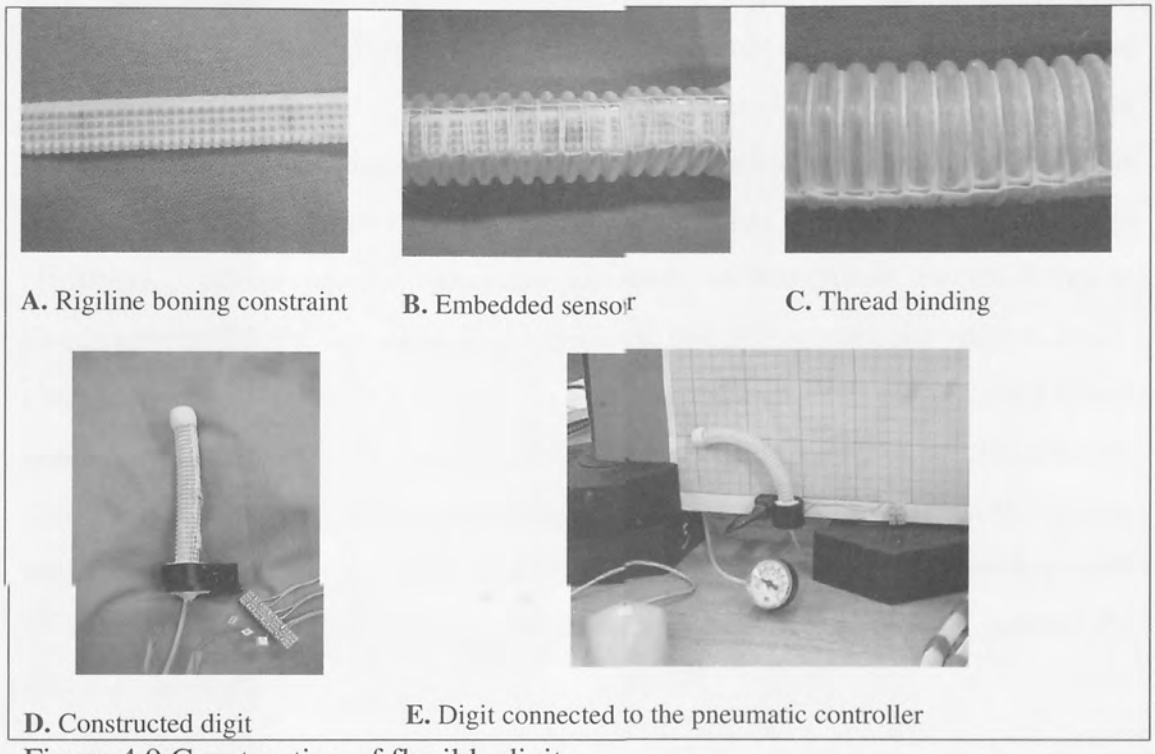

A. Rigiline boning constraint **B.** Embedded sensor **C.** Thread binding

D. Constructed digit **E.** Digit connected to the pneumatic controller

Figure 4.9 Construction of flexible digit

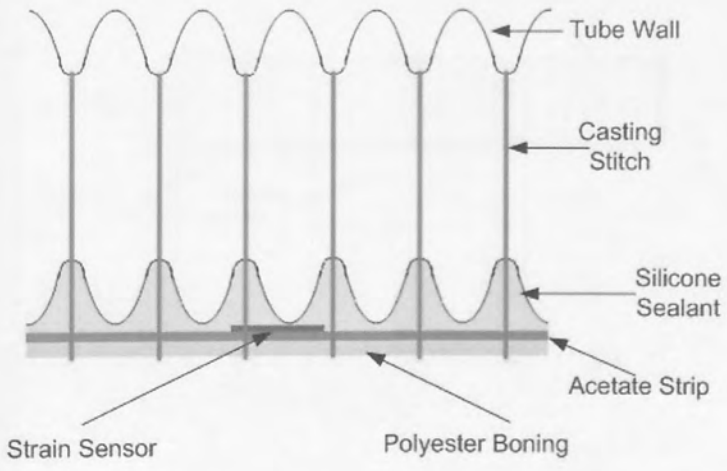

Figure 4. 10 The different layers in the digit construction

4.3.8 Multiple Chambered Digits

Using the same construction techniques and additional epoxy putty, it is possible to create more complicated digit forms consisting of several digits (Figure 4.11). If pressures in each chamber in the multi-chambered digits are controlled independently, then there is scope for the digit being more versatile for manipulation, contact and range of contact categorisation (Figure 4.12). This diagram shows the shapes produced when the digit has one, two or three pressure chambers. Manoeuvrable snake robots such as that made by OCRobotics (Buckingham, 2002)[68] are already in existence, and perform similar tasks to multi-chambered digits described here and could be used in deep navigation clinical applications. However, these snake robots are highly complex in construction with vast amounts of cabling to actuate the device. Both these types of devices are closer to conventional endoscopic devices, but by adding tactile sense to each of the chambers, the potential for its uses are enhanced for 'feeling' around the site of examination.

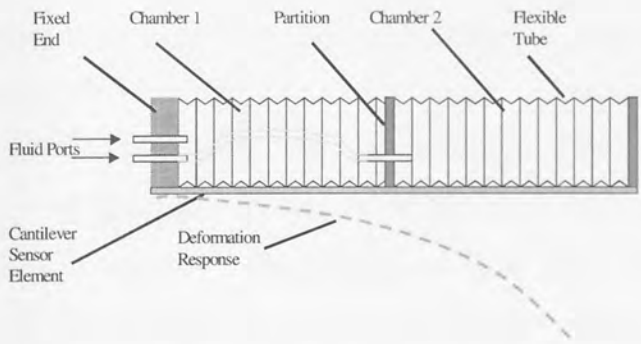

Figure 4.11 Proposed mechanism for a multi-chambered digit

Figure 4.12 Flexible digits with one, two and three chambers

4.4 Digit Characteristics

With this construction, the deformation properties of the digit were tested to evaluate its performance for durability, repeatability and sensitivity. Relevant experiments were carried out to determine mechanical properties and stability of the digit. Since many of the tests are destructive, dummy test digits of the same dimensions as the final prototype, but without the more expensive and delicate sensing elements were used for mechanical testing.

These dummy digits were used to evaluate the maximum pressures that a sealed digit chamber could maintain, the effect on pressure required to curve different diameter tubes and for measuring material stability. Having established the material properties of the digit, the effect of the construction surrounding the sensing elements is evaluated. The effects of load magnitude, position and pressure on sensing element readings on the digit are described towards the end of this section. Pressure applied to the digit showed that they are able to withstand pressures up to 75 PSI without audible leakage and when placed under water, no air bubbles were apparent.

4.4.1 Hysteresis Test

The aim of this test was to determine the operating pressure of the digit by performing hysteresis tests, which will give the elastic limit of the digit construction. Unconstrained dummy digits were inflated at pressure intervals of 10 psi (0.69 bar) and deflated after 30 seconds. The room temperature during the course of the experiment was 22 °C. The lengths of the digits were then measured at minute intervals until their lengths shrank back to their original length. It was noticed that at higher pressures, that the digits do not return back to their original length after five minutes since they have stretched beyond their elastic limit by 45 psi. Figure 4. 13 shows the time required for the dummy digits inflated to different pressured return to their original length. This means the maximum pressure that should be applied to the digit with out damage is 45 psi.

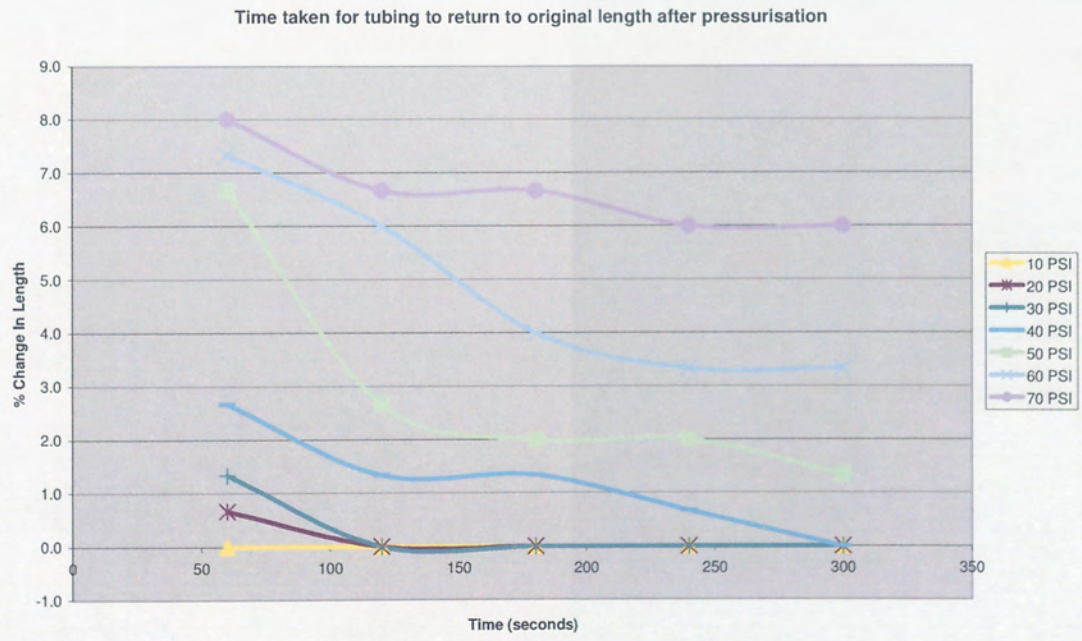

Figure 4. 13 Elastic Limit of Unconstrained Tubing

Further investigations were carried out where the unconstrained digits were inflated at smaller pressure intervals of 1.88 psi (equivalent to 0.2 v pressure control valve units) and their average extensions after 30 seconds were measured before the pressure was increased

It was found that when every dummy digit is first inflated, the overall rate of elongation is lower than for subsequent cycles of inflation and deflation (Figure 4. 14). This indicates that the tubing requires a warming interval before a repeatable cycle is achieved. Deflation of the unconstrained digit shows that in a single inflation cycle, the rate which the tube returns to its original length is greater than 30 seconds, however, during the cyclical inflation and deflation, the initial and final lengths of the digit remain at around 3.5% and 26 % longer than the original length if the cycle of inflation and deflation sustained at the rate of 4 psi per minute. This means that with an increase or decrease in pressure is maintained at 4 psi per minute, the digit will behave in a consistent manner.

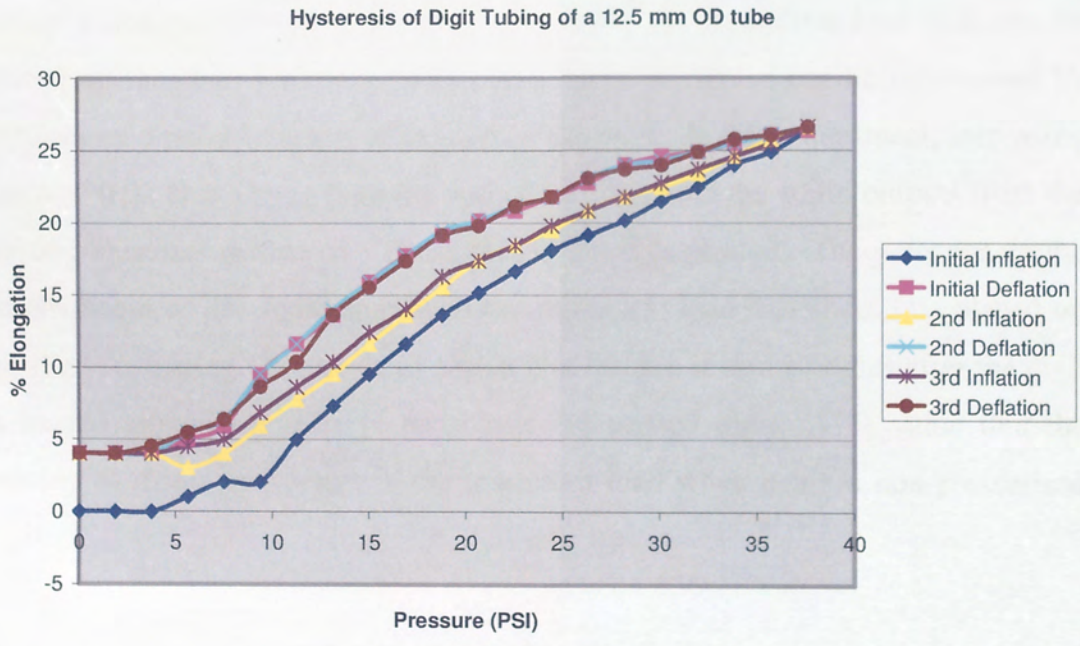

Figure 4. 14 Hysterisis of a 12.5 mm unconstrained tube when inflated and deflated

From these results, the structure of the digit is able to withstand up to 45 psi pressure internally before deformation becomes permanent. However, for digit curvature, pressure up to 40 PSI (2.76 bar) is sufficient for near full curvature (360°) and for subsequent experiments the maximum pressure was limited to 45PSI (3.1 bar). It is recommended that prior to all digits being used for the first time, that it undergoes a cycle of pressurisation of up to 40 psi.

4.4.2 Sensitivity to Load Magnitude

The objective of this experiment is to determine the sensitivity of the digit to load magnitude. From this information, the minimum loads that can be applied to the digit in further experiments can be ascertained. The sensitivity of the digit is expected to be different when the digit is pressurised.

Using a non-pressurised but constrained digit, the minimum load that can be placed on the digit for the sensing elements to recognise can be established by performing a point load test at the end of the digit. In this experiment, increasing loads of 0.02 N are hung onto the end of the digit, and the strain outputs from the sensing elements measured. These results are then plotted. The point where the strains begin to rise more sharply is the minimum load that should be placed on the digit for testing. Figure 4. 15 shows that the rise in strain begins after the digit is loaded around the 0.08 N for a non pressurised digit. This value that the sensing elements can detect is the minimum load when using a non-pressurised digit.

When this experiment was carried out when the digit pressure is varied in steps of 5 PSI, the minimum load detected by the sensing elements is 0.2 N for pressures up to 20 psi as is shown in Figure 4. 16 by the increase in the incline of the graph.

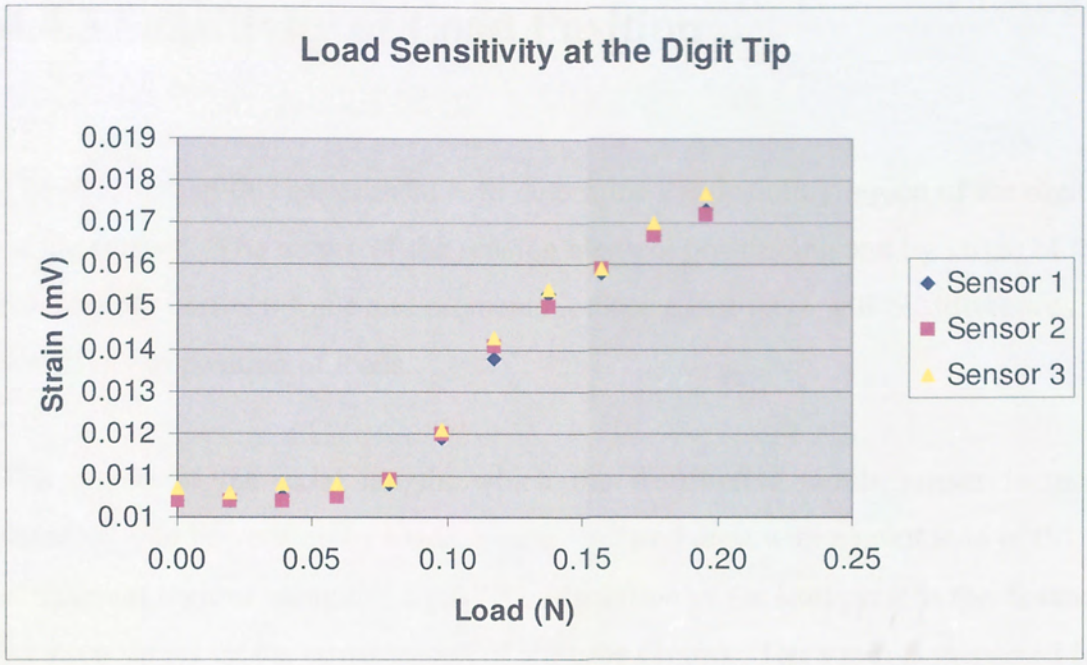

Figure 4. 15 Load sensitivity at digit tip

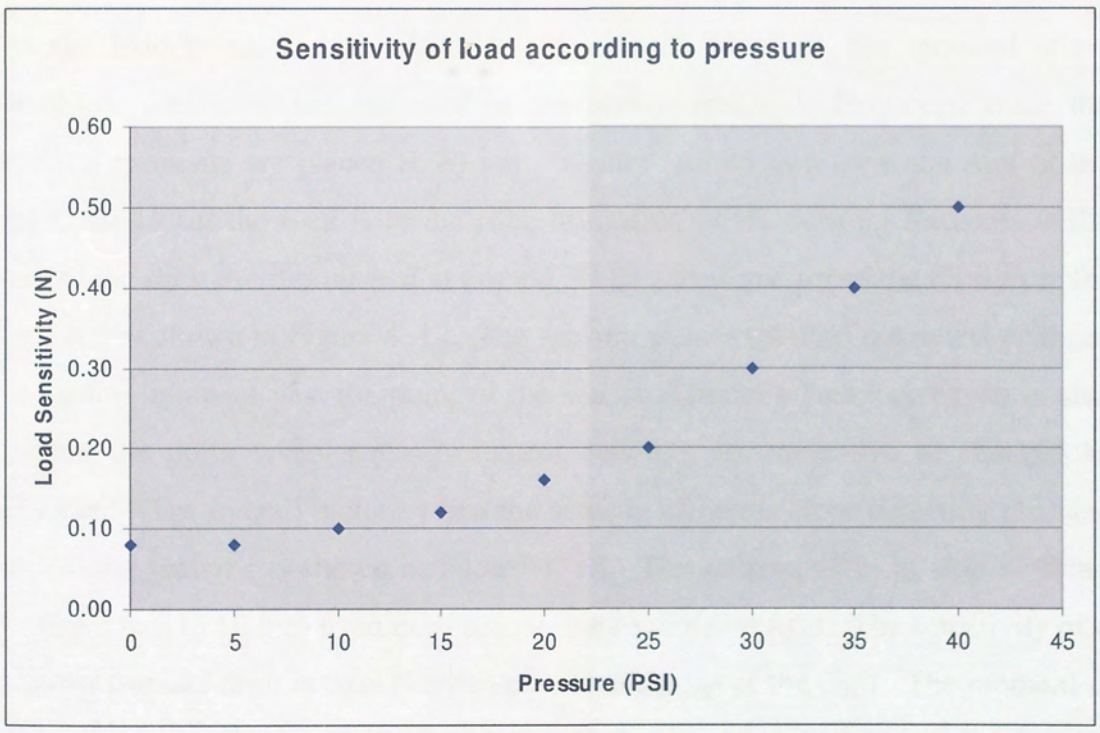

Figure 4. 16 Average load sensitivity at digit tip according to pressure

4.4.3 Sensitivity of Load Position

The objective of this experiment is to determine the operating region of the digit's tactile surface. The nature of the sensing element positioning and by virtue of the relationship between force and moments indicates that there will be differences in sensitivity to position of loads.

The region of the axial length, which the distributive tactile sensor is most sensitive, can be verified by loading an un-inflated digit with a point load of 0.1 N at different regions along the digit. The resolution of the load point is the distance between ridges on the corrugations of the tube (3mm). The strain is measured for each of the sensing elements plotted.

As the load point reaches closer to the root of the digit, the moment effect decreases, changing the intensity of the sensor reading. However, since the sensing elements are placed at 20 mm, 60 mm and 85 mm from the root of the digit, the closer the load is to the root, utilisation of the sensing elements at the end of the digit are diminished at around 20 mm from the tip of the digit as is for sensor 3 as shown in Figure 4. 17. The sensing element is does not detect changes in loading moment past the point of the sensor element's location, which is also around the point when sensing element becomes less sensitive to changes as expected. The overall picture when the sensing elements stops detecting changes in loading patterns is shown in Figure 4. 18. The sensors seem to stop working within 5 mm to 10 mm from each sensor due to moment load. The sensitivity of a non-pressurised digit is 0.08 N when placed at the tip of the digit. The moment at this point is 9.6 N/mm. If the load is 0.1 N, the point in which the digit becomes less sensitive is around 24 mm from tip of the digit, based on the effect of moments as the load approaches the sensor.

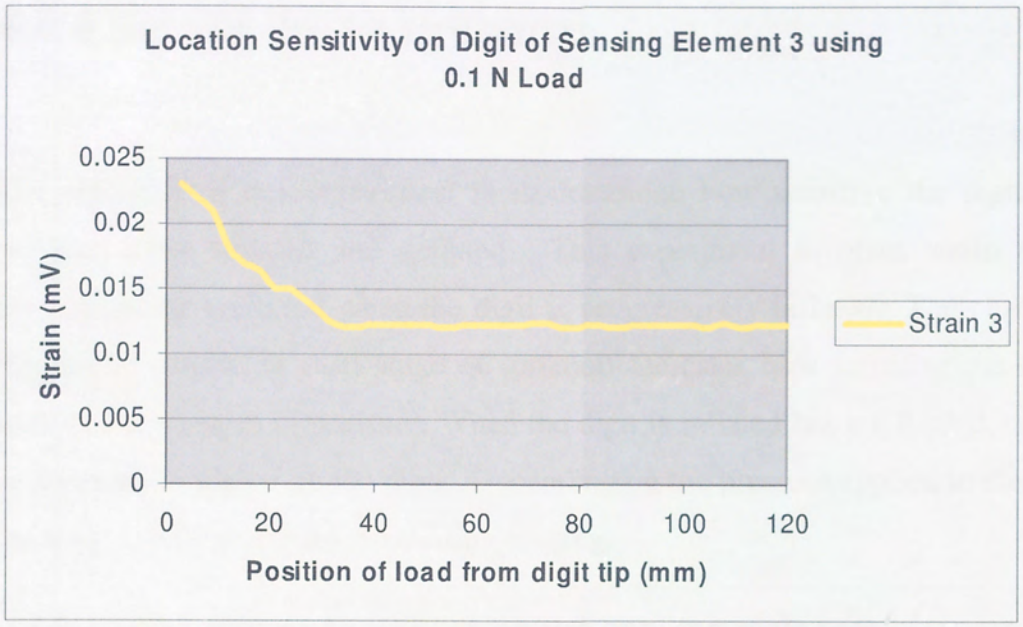

Figure 4. 17 Location sensitivity for sensor element 3

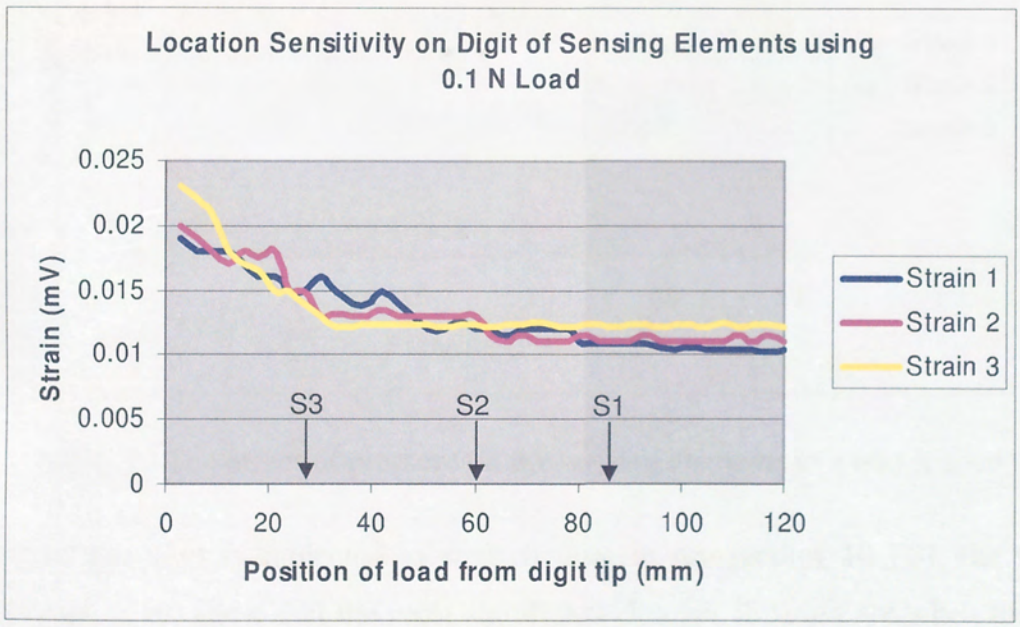

Figure 4. 18 Location sensitivity for all sensing elements, S1, S2 and S3

4.4.4 Sensitivity to Pressure

The objective of this experiment is to determine how sensitive the digit is to pressure when inflated and deflated. This experiment involves strain sensor readings being collected when the digit is progressively inflated. The change in the sensor outputs at each stage of inflation indicates how sensitive the tactile sensor is to changes in pressure. When the digit is inflated but not loaded, there is uniform strain placed on the digit. Depending on the pressure applied to the digit, the sensors will give out a correlating reading.

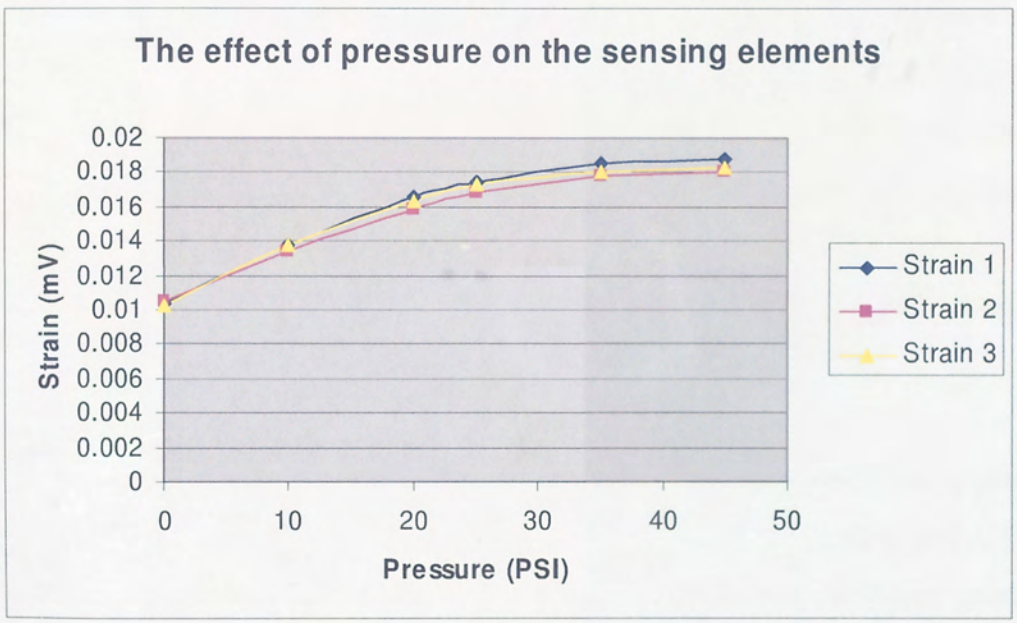

Figure 4. 19 The effect of pressure on the sensing elements in a non-loaded digit.

When the digit is subjected to step changes in pressure of 10 PSI, the results (Figure 4. 19) show that the most significant changes in strain are when the digit is at lower pressures. As the pressure increases, the changes in strain are less pronounced. This indicates that the strain gauges are capable of measuring strain when the digit is pressurised up to at least 45 psi, the established maximum working pressure. From the second experiment in 4.4.3, the load magnitude required for the sensing elements to detect the existence of load is much greater

for higher pressures, confirming that the characteristics of the digit are dependent on the internal pressure within; this creates tension in the structure. If the digit is loaded when the digit is inflated, the intensity of the sensor readings are diminished by the compensatory factor due to the pressure.

4.5 Conclusion

It is demonstrated that the digit can be constructed from polymers with a distributive tactile sensing element consisting of three sensing elements can be successfully made. The sensors can be used to determine the load and position etc, with marginally reduced efficiency and the loss of load width detection compared to the use of four sensors. However this is a trade off, as to whether load width is necessary for the application in this case. The positions of the sensor have to be in the places allocated as losing a channel of data closer to the root of the digit produces poor results.

In terms of construction techniques, the digit currently has strain sensing elements incorporated into the design. In Chapter 3 optical fibre with fibre Bragg gratings (FBG) sensors are suggested as a non-electrical alternative for future prototypes. This type of sensor is ideal for clinical applications as they removes the need of metallic components within the tool point, making it a potential contender for use in magnetic resonance imaging environments. In addition, the manufacturing process to make the tool point can incorporate strands of optical fibres into the fabric of the constraint and mould the entire constraint into the body of the bellowed tubing. End caps can be designed to be moulded separately and an airtight seal can be achieved by either heat treatment or bonding with appropriate polymer fillers and adhesives.

The potential of a construction using optical fibres with FBG incorporated within; along with many polymer constructions lend themselves towards mass manufacture. Well-managed screening is the best strategy for public health rather than on demand individual testing (EDMA, 2005)[69]. A device for mass screening, such as that for the screening for problems of the prostate in the aging population would be ideal. A simple device for screening that is efficient and low cost is vital for success of the product, particularly in a health care market that is dominated by government health services.

Like with all devices intended for clinical use, the digit will need to comply with the directives given by the Medical Devices Agency if the device is to be used in the UK, and other European and worldwide agencies for global applications. An example path, which the tool point would have to follow, would be further consideration and testing of materials, actuation, sensing, safety features and vitally the purpose of the device in performing the task it is designed for.

In the following chapter, further consideration is given to how the digit is implemented by performing phantom clinical experiments and their results a measure of how effective it will be for use in clinical applications that were described in Chapter 2.

Chapter 5

A Touch Sensitive Digit

Chapter 4 provided the methods for the production of a digit with a tactile sensor, but in order for the sensor's performance to be evaluated, investigations on the contact conditions required in clinical applications would have to be carried out. The concept of touch can be defined over a range of different characteristics depending on the application. For navigation, information about contact orientation, load magnitude and the position of loading are important and differ from the characteristics that define palpation: loading points and contact stiffness are the predominate features. The system of touch can be described as a hierarchy of characteristics, which is defined into taxonomy of touch. In this chapter, taxonomy of touch is described and used in the evaluation of the touch sensitive digit for phantom experiments in navigation and palpation. Evaluating the digit's performance yields the position each of the characteristics holds in an optimised system of neural networks.

5.1 Taxonomy of Touch

From the review of the characteristic functions of endoscopy in Chapter 3, diagnosis by touch is defined by several output parameters. Indeed, the clinical applications suggested; the examination of the prostate and endotracheal intubation share common needs as well as individual features. These needs include measurement of the contact resistance and displacement relative to the feature and detecting end reactive load. Further examination of these needs shows that the touch can be categorised into several simple, but identifiable characteristics.

- Contact versus Non Contact
- Number of Contact Points
- Orientation of Contact Load
- Position of Contact
- Load Magnitude
- Stiffness of Contact
- Shape of Contact

These are the desired output parameters that are considered in determining the type of contact encountered. However, grouping these features in a different way may convey the information of contact features in the form of a flow hierarchy. The flow path of contact information would be dependent on the application. The order in which the parameters are determined is important as there may be some masking of signals due to coupling and it is from study of each of the parameters that taxonomy for touch is derived (Figure 5. 1). The sequence in which a system of touch determines navigation and palpation is dependent on the performance of the neural networks used in the distributive tactile sensing technique. The top of this hierarchy is similar to the layout of decision trees. A decision tree takes as input an object or situation described by a set of properties, and outputs a yes/no

decision. Decision trees therefore represent Boolean functions. Functions with a larger range of outputs can also be represented (Russell & Norvic, 1995)[70]. The taxonomy is not quite a decision tree, but is a scheme applied to certain data in order to generate the information describing touch with all the subsets. The top region of this taxonomy focuses on data categorisation, which is useful for discrimination, similar to the cognitive responses for decision making in humans, whereas the lower part of the chart is more information based with parameters that are quantifiable ranges suitable for other machine learning systems.

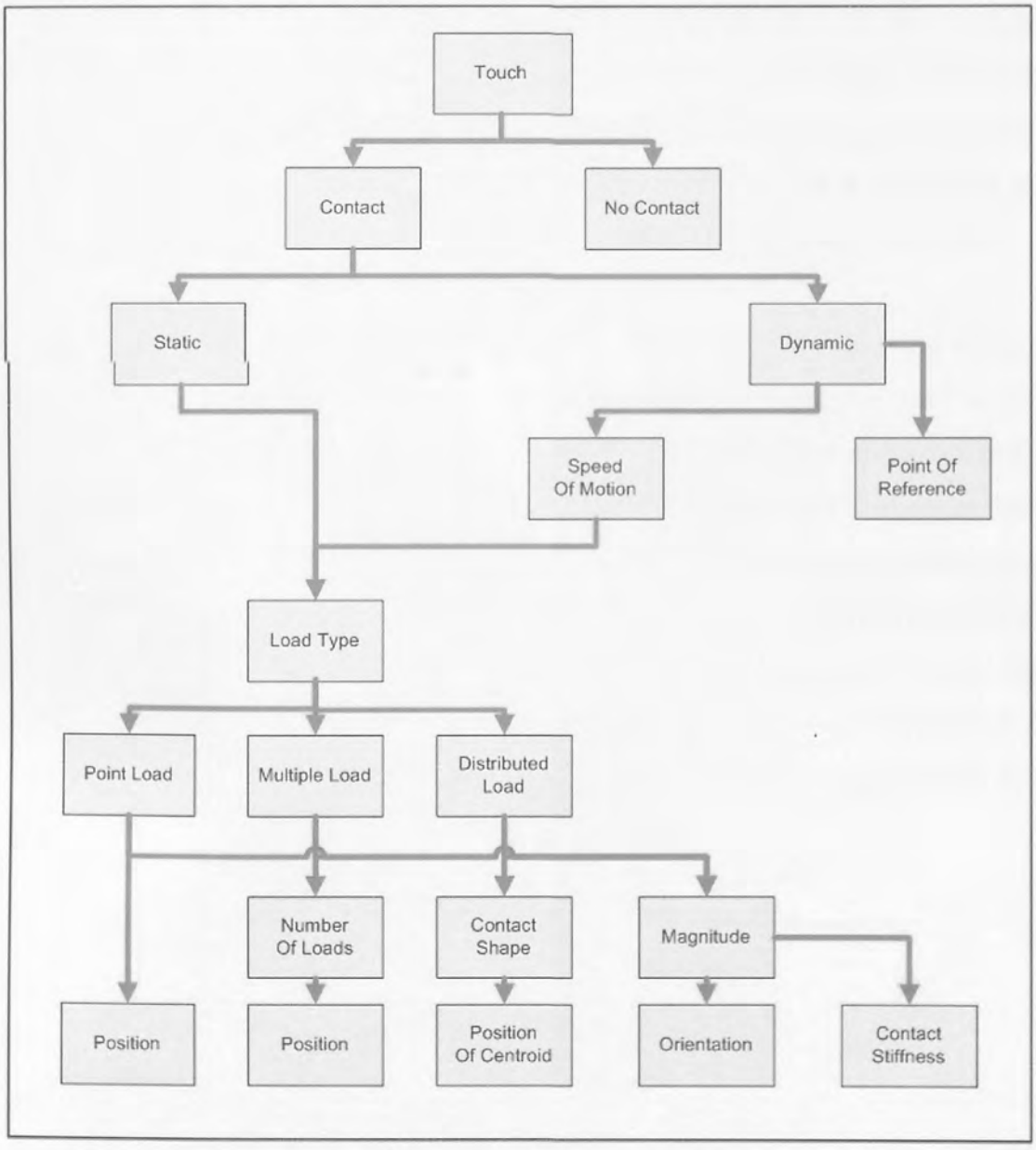

Figure 5. 1 Taxonomy of Touch: A map of subsets describing the facets of touch

The touch system is made from a number of neural networks, each dedicated to discriminating a certain type of information, sometimes in parallel, other times in a neural network cascade. On a higher level is a supervisory program that will monitor the outputs and control the decision making. This way, the processing power of the system can be concentrated into small blocks of information that, when combined, can be used to produce a better understanding of the environment that the digit is in contact with. The reality is a staggered process; the information feedback to the clinician needs to be minimal and focused on the critical parameters aiding better performance in surgery. In a real environment, this does happen and a supervisory function tries to identify the possibilities presented by the neural networks. As we know that the cognitive behaviour does not inform us what temperature a warm object is, rather if the temperature becomes intolerable.

In effect, taxonomy of touch is based on hybrid parallel and cascaded neural network architecture. The decision to as which order the contact parameters are considered depends on the dominance of each parameter during performance tests described in the next section. For example, the most dominant feature of any set of data collected from a three-transducer digit is that of contact versus non-contact. It is apparent that there is a significant difference in the data output of a digit that has contact applied compared with one that has not and it would be trivial to discriminate a position or load magnitude when there is no contact. By early categorisation of contact and non-contact loads, there is no confusion for the touch system to discriminate other contact parameters.

5.2 The Experiments

The experiments that evaluate the digit's performance are divided into three sections; fundamental touch characteristics, navigation characteristics and palpation characteristics. The characteristics that the digit is required to identify during navigation and palpation as well as common parameters are described in Table 5. 1. The first phase of experiments are, non-inflated digit tests, similar to the experiments carried out on the cantilever beam sensor in Chapter 3. Many of these characteristics of touch are common both navigation and palpation. Experiments relating to navigation of the digit follow in the next section including relative positioning and point of digit insertion. Finally, stiffness and pressurisation tests on the digit are carried out to determine the effectiveness in palpation

<table>
<tr><th>Navigation</th><th>Palpation</th></tr>
<tr><td colspan="2">Contact and Orientation of Load</td></tr>
<tr><td colspan="2">Multiple Contact Points</td></tr>
<tr><td colspan="2">Load Magnitude</td></tr>
<tr><td colspan="2">Position Testing</td></tr>
<tr><td rowspan="2">Relative Positioning</td><td>Stiffness Test</td></tr>
<tr><td>Palpation Test</td></tr>
</table>

Table 5. 1 Characteristics of Navigation and Palpation

5.2.1 The Performance Evaluation Rig

To examine the performance of the tactile digit, a rig was produced to provide repeatable and verifiable conditions based on the taxonomy of touch (Figure 5. 2). An experimental rig was designed and built to provide synthesised contact conditions for navigation and palpation. It is intended that the digit be used for dual purposes:

1. To assist in navigation through the narrow opening to the site of investigation
2. For use in palpation once at the site of investigation has been reached

Static and dynamic experiments were performed to simulate conditions of navigation and contact. The experimental evaluation of the performance of the digit to detect tactile information requires consistent motion and positioning of the digit for reliable and repeatable results.

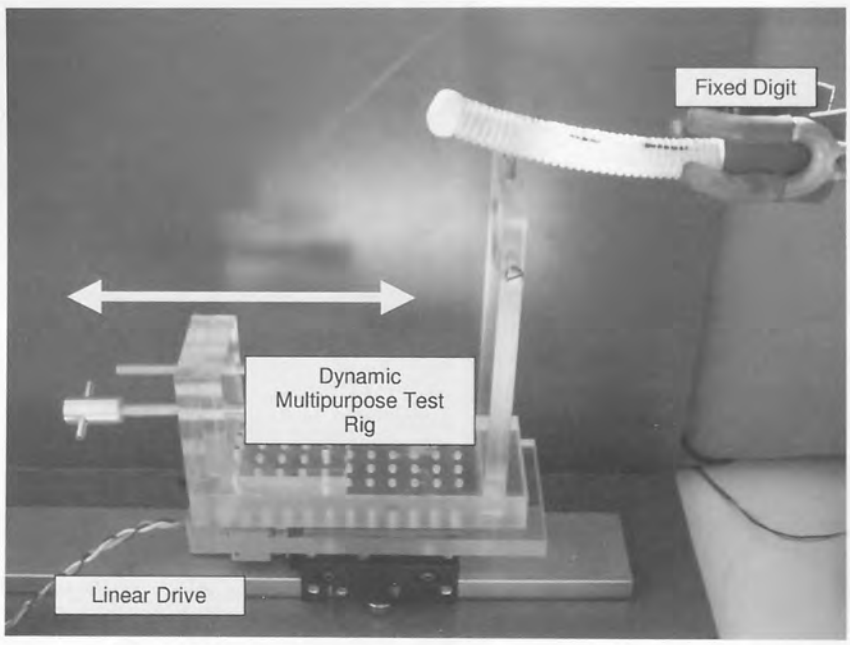

Figure 5. 2 Evaluation rig used to measure different contact parameters

The rig was manufactured in house and is made from clear Perspex for visibility. It has been designed to be functional and capable of changing the position and angle of phantom lumen made from different grades of tubing. The tubing ranges from smooth bore vinyl for smooth walls to PVC ribbed flexible tubing. Figure 5. 3 show the evaluation rig being used to hold tubing to synthesise lumen properties.

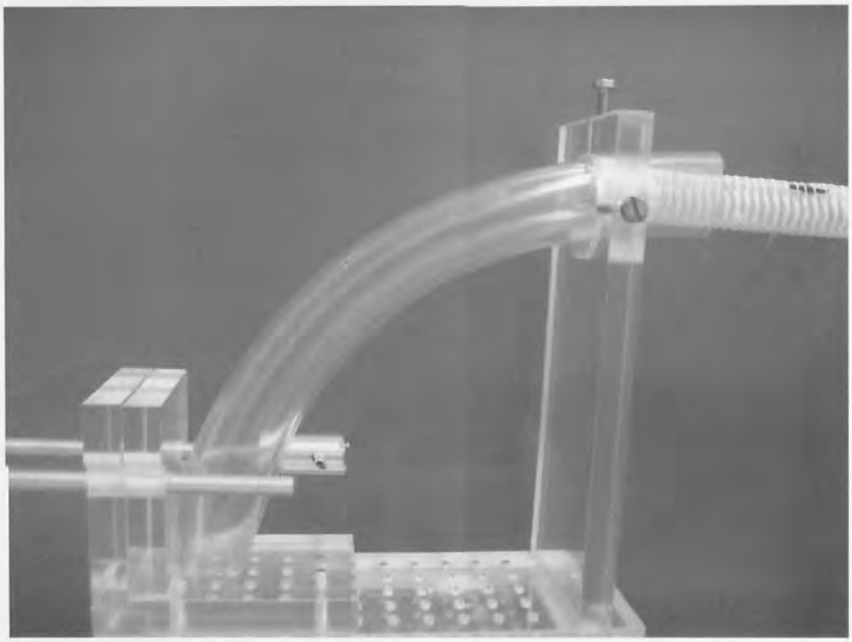

Figure 5. 3 Evaluation rig being used to hold phantom lumen

The rig is placed on a linear drive to enable the digit to be positioned. The linear drive system used is supplied by Baldor and consists of a stepper motor on a linear etched platen and controlled using NextMove ST intelligent 3-axis stepper controller (Appendix 5.1). The resolution repeatability of the linear drive and platen is +0.0004 inches (0.01 mm), Resolution +0.0001 inches (0.0025mm).

Data acquisition is set to collect 25 samples per second. Attached to the digit with three strain gauges is a RDP three channel strain gauge amplifier. Data from the amplifier is acquired using Computer Board's PCI-DAS 1602/16 data acquisition board and recorded using MatLab Simulink, Real Time Workshop and XPC Target.

The digit is 120 mm in axial length and the sensors have been placed at 20 mm, 60 mm and 85 mm from the root of the digit and connected to the amplifiers and data acquisition equipment. Actuation of the digit is controlled using a Norgren VP50 proportional pressure control valve.

After pressurisation, the minimum load that the sensing elements can detect significant changes is 0.25 N. Based on the sensitivity tests carried out and described in Chapter 4, the digit, when not pressurised will be subjected to that of at least 0.1 N to ensure that the strain sensors can detect significant changes over any noise in the signals.

The performance evaluation rig is summarised in the illustration below in Figure 5. 4 and shows that the PC via a control valve connected to an A/D board controls the digit movement. This same board is also converts the strain amplification on the gauges on the digit as well as controls the output of the linear drive used to position the performance evaluation rig which sits on top.

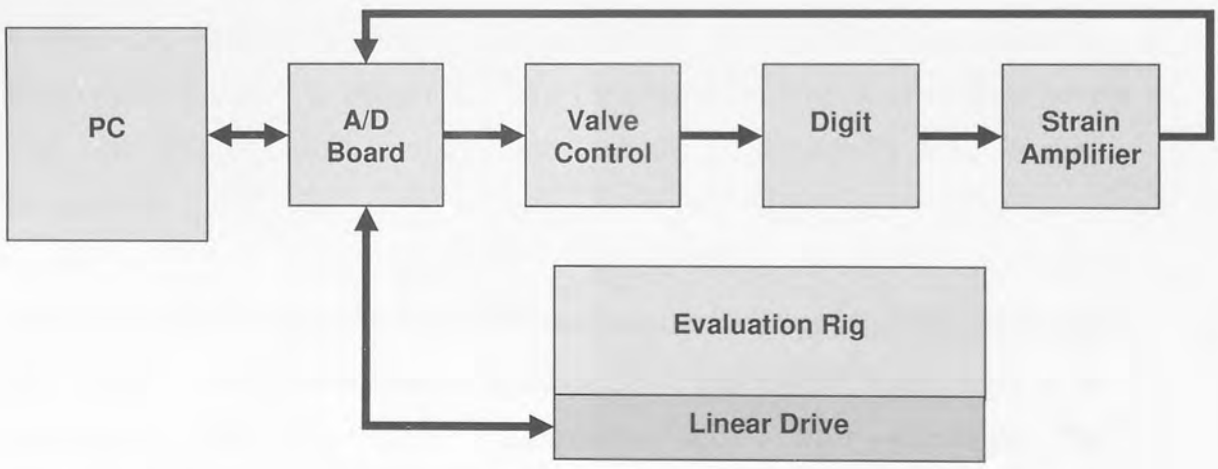

Figure 5. 4 Schematic of evaluation rig

5.2.2 Evaluating Fundamental Touch Characteristics

There are some parameters that define touch that are common in both navigation and palpation. The experiments carried out in this section are to support detection of situations relevant to the applications of:

- Contact and Orientation of Load
- Multiple Contact Points
- Load Magnitude
- Position Testing

5.2.2.1 Contact and Orientation of Load

In this experiment, contact and the direction of contact is evaluated for a digit when loaded with a single localised load. Contact and direction of load is useful for navigation as well as palpation. The parameters for loading orientation have also been included in this experiment, and are predominantly used in digit navigation.

The importance of detecting contact is paramount to defining other characteristics of touch. By early categorisation of contact and non-contact loads, there is no confusion for the touch system to discriminate other contact parameters. The most dominant feature of any set of data collected for touch analysis is that of contact versus non-contact. It is apparent that there is a significant difference in the data output of a digit that has contact applied compared with one that has not and it would be trivial for a neural network to discriminate a position or load magnitude when there is no contact present.

Method for Evaluating Contact and Orientation of Load

1. The digit is clamped at the root with the constraining strip and sensors facing upwards. This position is designated the top side of the digit as indicated in the cross sectional area in Figure 5. 5.
2. The digit is subjected to loads of 1 N being applied in perpendicular directions (at 90 degree rotations) at the tip of the digit and the strains recorded.
3. The strain sensory data corresponding to the digit is recorded to from the data acquisition equipment.
4. In addition to side loads, an end load was applied to the digit. The hard surface used for the end load is Perspex, moving along the linear drive platen at the speed of 20 mm/s, and stopping after a distance of 5 mm displacement.
5. Each loading position was repeated five times to check for repeatability of results.
6. In a similar manner of data processing, as described in Chapter 3, a neural network was produced for this application. The type of neural network used for this experiment is in a classification mode (Softmax) as the nature of the classes is very distinct.

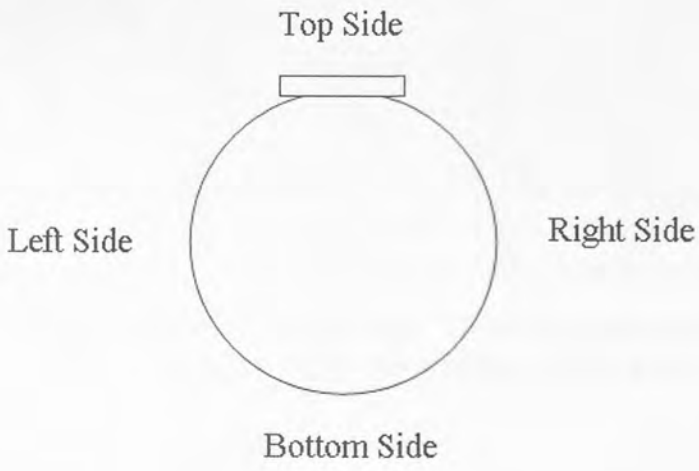

Figure 5. 5 Designation of Load Directions: Top, Bottom, Left and Right

Results for Contact and Orientation of Load

The architecture of this classification type neural network for contact and orientation is a 3 input, 6-class output neural network and was optimised to contain 60 hidden nodes. Figure 5. 6 display the quantity of each parameter of contact and orientation.

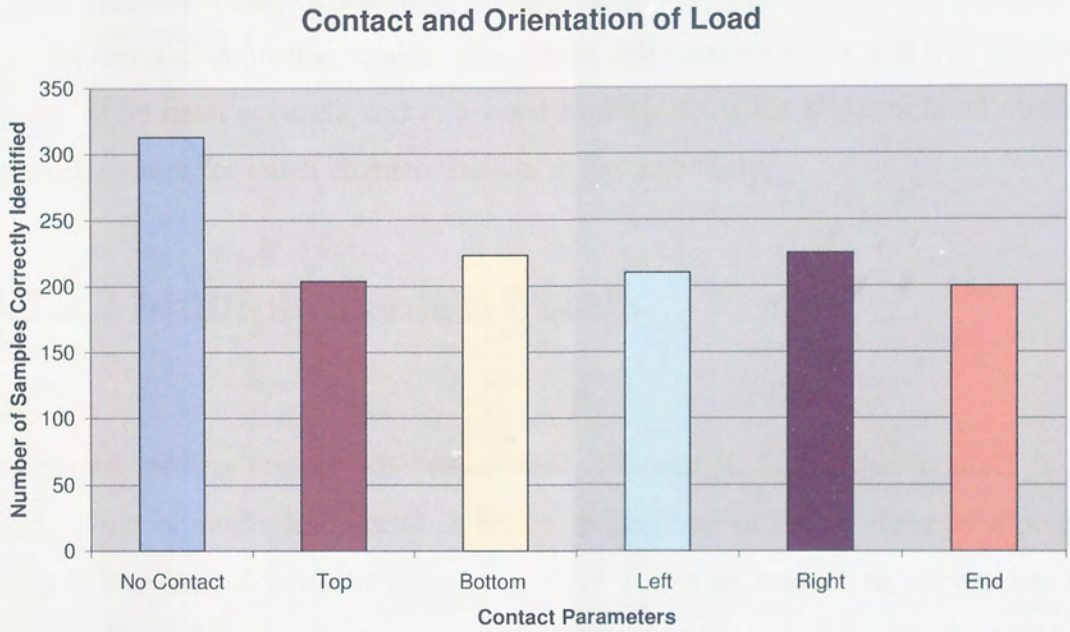

Figure 5. 6 Chart showing contact and orientation of load correctly identified

Real/Predicted	No Contact	Top	Bottom	Left	Right	End
No Contact	313	0	0	0	0	0
Top	0	204	0	0	0	0
Bottom	0	0	223	0	0	0
Left	0	0	0	210	0	0
Right	0	0	0	0	225	0
End	0	0	0	0	0	200

Table 5. 2 Load orientation classification table: This table shows that the neural network has been trained and can classify the direction of the load.

Examining the results more closely,

Table 5. 2 show a confusion matrix that states that out of 1375 samples of data, all classifications were correctly identified by using a classification type neural

network. This type of neural network will output results in only one of two ranges, contact or null contact, with the output number closer to 0 indicating a null contact and closer to a value of 1 for contact. In this case the orientations are distinct and resolvable and there is no confusion between the orientations.

The results indicate that the digit system is able to identify both the occurrence of contact and detect the orientation of the applied load placed, with a 90° resolution. The detection of contact is vital in all systems that monitor touch and this method proves to be most accurate and is a good starting point for a hierarchical neural network system for touch characterisation in the taxonomy.

5.2.2.2 Multiple Contact Points

Further to reading contact, the subsequent information is whether contact is a single point or multiple points. In human perception of touch, there is a point when it becomes difficult to resolve multiple points of contact as opposed to a single point with reduced pitch. The two-point threshold on the pad of a mobile thumb is 4 mm before it can distinguish two separate areas of touch. This can be compared with an immobile calf, where the 48 mm is the threshold (Schiffman, 2001)[71]. The aim of this experiment is to ascertain if the digit is able to distinguish more than a single point of contact and to evaluate the two point threshold. This information can be used to perceive the topology of the surface being examined.

Method for evaluating multiple contact points

1. The digit is clamped at the root with the constraining strip and sensors facing upwards and the strains on the digit when there is no load placed on it are recorded
2. Two loads of 0.25 N each are placed on the digit. The first load is placed at the tip (the last convolution of the corrugated digit). The second load is placed 20 convolutions apart (60 mm). The strains are recorded.
3. The second load on the digit is then moved 2 convolutions (6 mm) closer to the first load and strains is recorded.
4. Step 3 is repeated until there is only 2 convolutions distance apart from the two loads.
5. A second set of data is then generated, where the digit will be subjected to a single load of 0.5 N and the strain is recorded for when this load is positioned at the last convolution and then each subsequent second convolution, in the same locations as for the second load in the first part of the experiment.
6. Each loading position was repeated five times to judge the repeatability of results.
7. In a similar manner of data processing, as described in Chapter 3, and neural networks were tailored for this application.
8. First the data is filtered using a two-class type neural network to extract the sets of data that contain contact from the null contact data since the nature of the classes is very distinct.
9. Then a second two classification neural network is applied to the contact data to determine single or double contact points.

Results for evaluating multiple contact points

Filtering the data for non-contact variables proved to be 99.2 % accurate. Table 5. 3 is a confusion matrix of the neural network results. The rows indicate the predicted outcome and the columns the actual or real results. Where the network has mis-identified a data that contains contact as a null contact, on closer examination shows that the position of these loads of the lowest denominations of 0.5 N and closest to the root of the digit, which indicates that the digit was insensitive to loading at that point. Since the number of these data sets is very low, they can effectively be filtered out, leaving the rest to be considered for the next neural network. The neural network architecture for contact filtering is 3 inputs, 2 outputs system with 20 hidden nodes.

Real/Predicted	Contact	No Contact
Contact	680	5
No Contact	0	38

Table 5. 3 Table of accuracy of a contact determining neural network used as a filter.

From the set of 680 contact data sets, the second neural network with the architecture of 3 inputs, 2 outputs system with 20 hidden nodes for determining classes of single and double contact points was applied. The results indicate that the neural network is able to determine single point contact to 97.9% accuracy and double contact to 77.3% accuracy and the overall accuracy is 87.6%. Figure 5.7 shows a graph comparing the neural network outputs for single and double contact points for correctly and incorrectly identified classification.

Examining the results of for double contact loading more closely, it can be seen that the accuracy falls as the loads are placed closer together. The two point threshold for the digit has been determined to be 14 mm for 85% accuracy, falling to 40% accuracy for loads placed 7 mm distance apart. Figure 5. 8 shows the

effect of contact point pitch has on the accuracy of distinguishing double contact points.

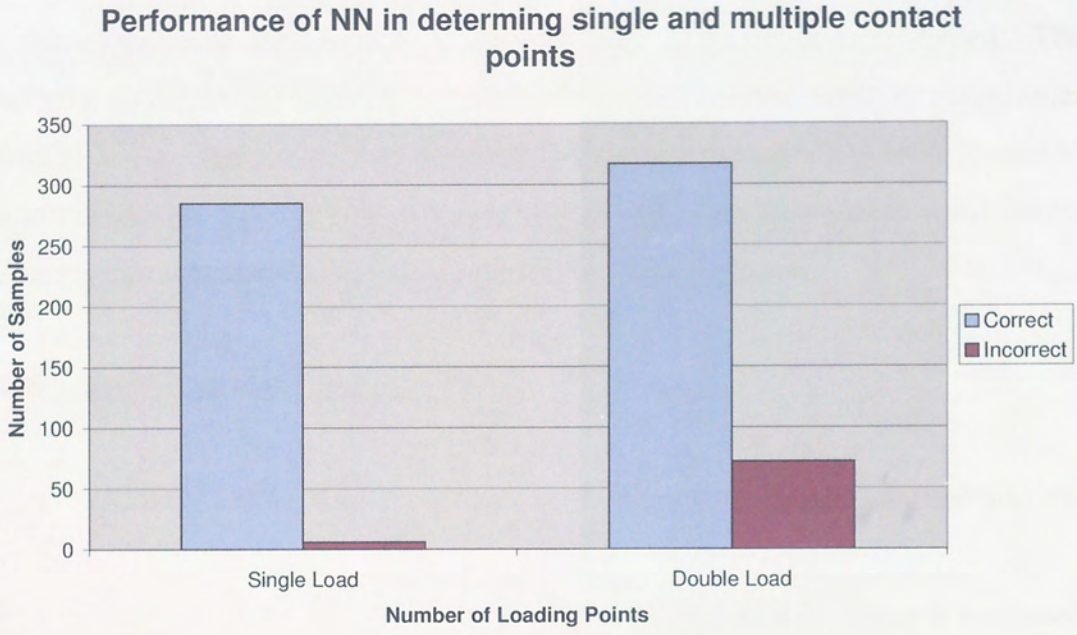

Figure 5. 7 A graph showing the results of a two class neural network in determining single and multiple point loads

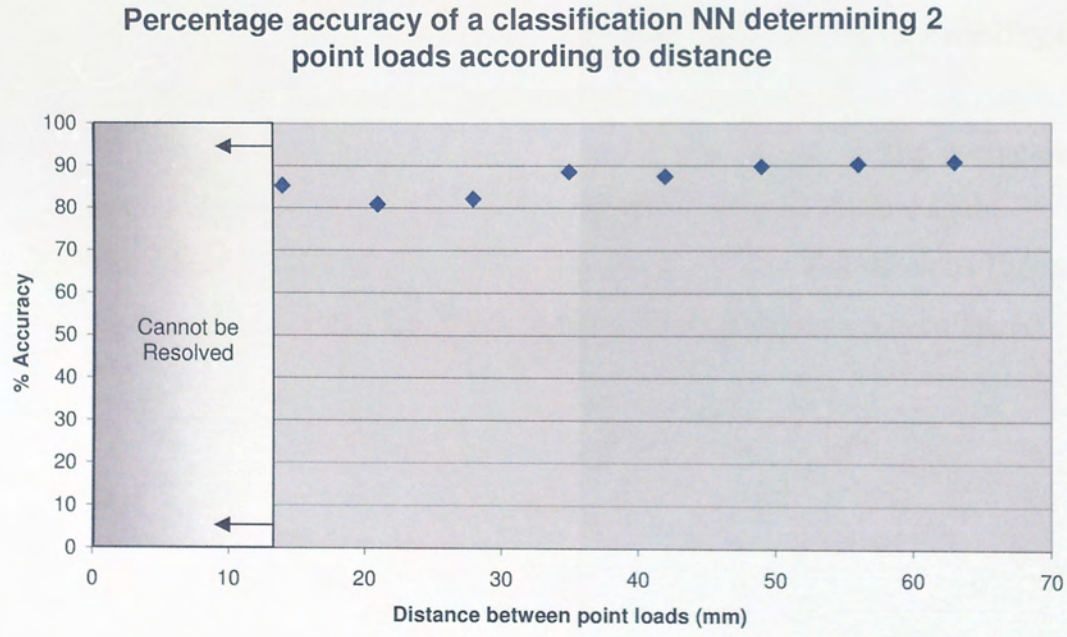

Figure 5. 8 Percentage accuracy of a two point load according to distance separator

5.2.2.3 Load Magnitude

In this experiment, the intensity of contact force on the digit is evaluated. The aim of is to determine if the digit can discriminate between different magnitudes of point loads. Since results of filtering non-contact data sets has been proved to be effective (Section 5.2.2.1), the data sets recorded for subsequent experiments assumes that non contact data sets have already been removed.

Method for evaluating load magnitude

1. The digit is clamped at the root with the sensors facing upward and the strains measured.
2. A load of 0.125 N is placed at the tip of the digit and the strain is measured again.
3. Step 2 is repeated with increasing number of loads until the digit has been loaded with 0.75 N in 0.125 N increments.
4. Each loading position was repeated five times to determine repeatability of results.
5. The load is then placed 3 mm (the next convolution on the corrugated tube) from previous loading point and steps 2 to 4 are repeated again.
6. The data is processed, as outlined in Chapter 3 and a continuous (linear) model neural network is optimised for evaluating the data sets collected.

Results for evaluating load magnitude

The architecture for the neural network for load magnitude has three inputs, one output and five nodes. Figure 5. 9 shows a graph of the neural network prediction of different intensities of static load magnitudes at different load positions. The left hand side of the x-axis is the tip of the digit and the right hand side the root of the digit. The graph shows that the digit is able to predict the load magnitude to an overall total root mean square error of 0.075 N. This corresponds to the predictions being within 10% of the maximum load placed at the tip of the digit. It also indicates that the accuracy falls as the load is placed closer to the root of the digit.

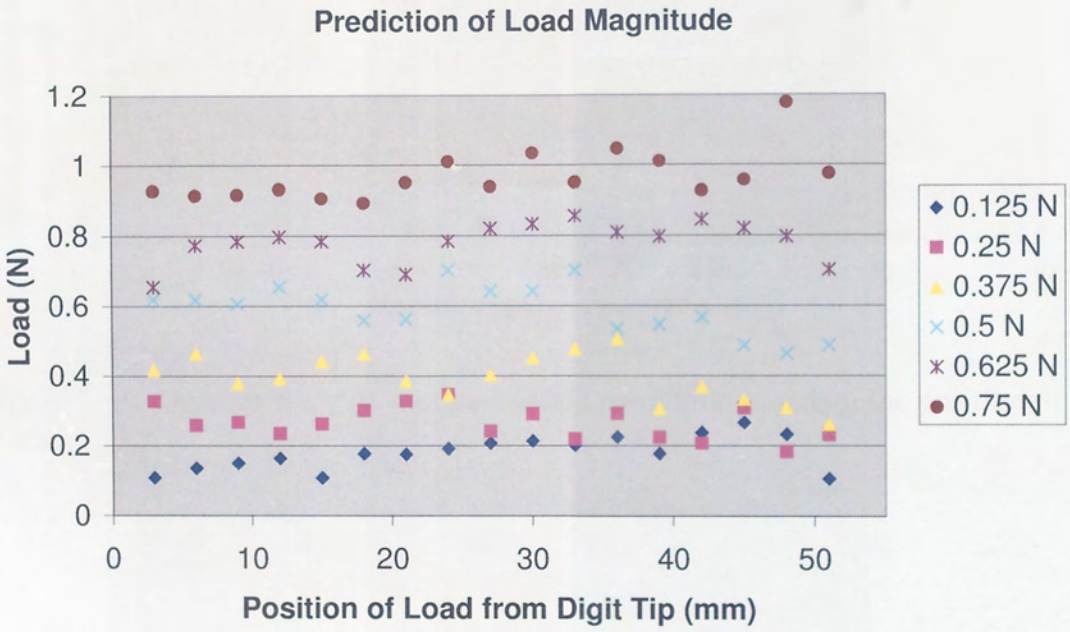

Figure 5. 9 Prediction of load magnitudes over the effect range of the digit

By determining the average absolute error of load magnitude detection and plotting this with the position of the load, Figure 5. 10 is obtained. This shows that the neural network becomes less accurate in deducing the magnitude of when the loading point is positioned past the last sensing element (20 mm) from the tip of the digit.

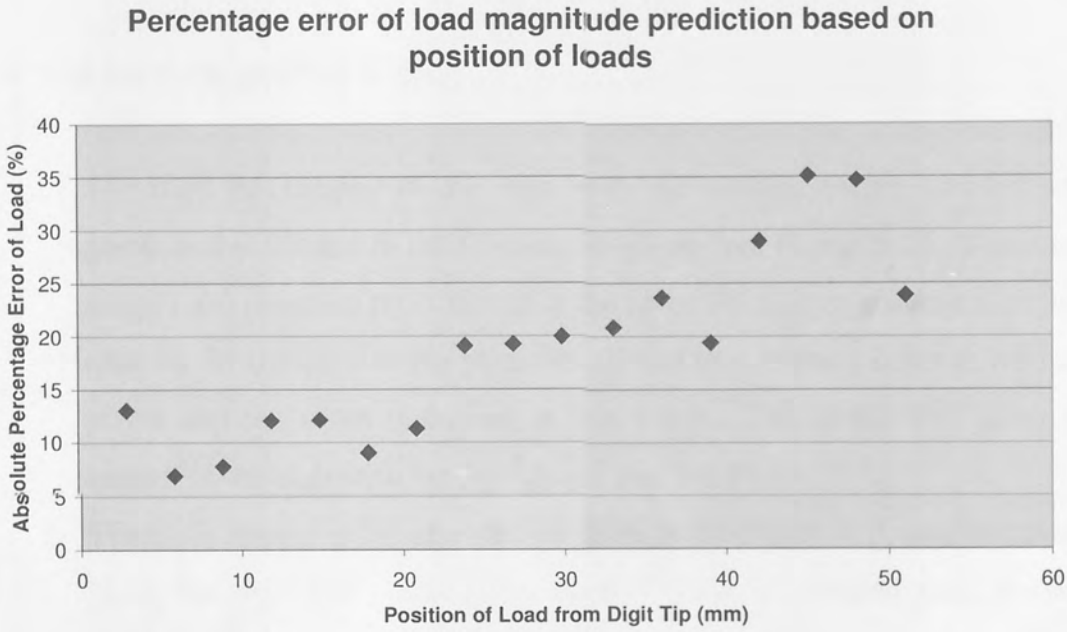

Figure 5. 10 Absolute error of load magnitude prediction based on the position of loads

5.2.2.4 Static Position Testing

The position of contact offers reference information about the location of the digit. The aim of this experiment is to determine the performance of the digit in the evaluation of the position of static contact.

Method for static position testing

1. The digit is clamped at the root with the sensors facing upward and positioned at the end of the linear drive platen (see Figure 5. 2). The force stepper and phantom rig is placed at the tip of the digit so that the digit just rests on the top edge of the phantom rig and this position is set to zero on platen and the strain measured at this point. This is the first point of contact of the digit with the rig. This is position P1
2. The force stepper is incremented by 30 steps (100 steps = 10 mm of travel) along the digit and strain is measured. This is repeated until the rig reaches 60 mm from the tip of the digit. This will yield positions P2 to P19.
3. Each loading position was repeated five times to check for repeatability of results.
4. By processing the data, as outlined in Chapter 3 and using a continuous (linear) model neural network.

Results of Static Contact Points

The architecture for the neural network is three inputs, one output and five nodes. Testing the neural network for static contact points show that the digit is able to predict the contact points to the root mean square error of 2.5 mm of the overall of the actual position. This equates to a percentage error of 2 % over the full range. Figure 5. 11 shows the root mean square error of the predicted position of the load plotted against the actual position of the load. As the contact point approaches the root of the digit, the accuracy of prediction tends to fall as the sensing elements closer to the tip of the digit become less sensitive to the contact.

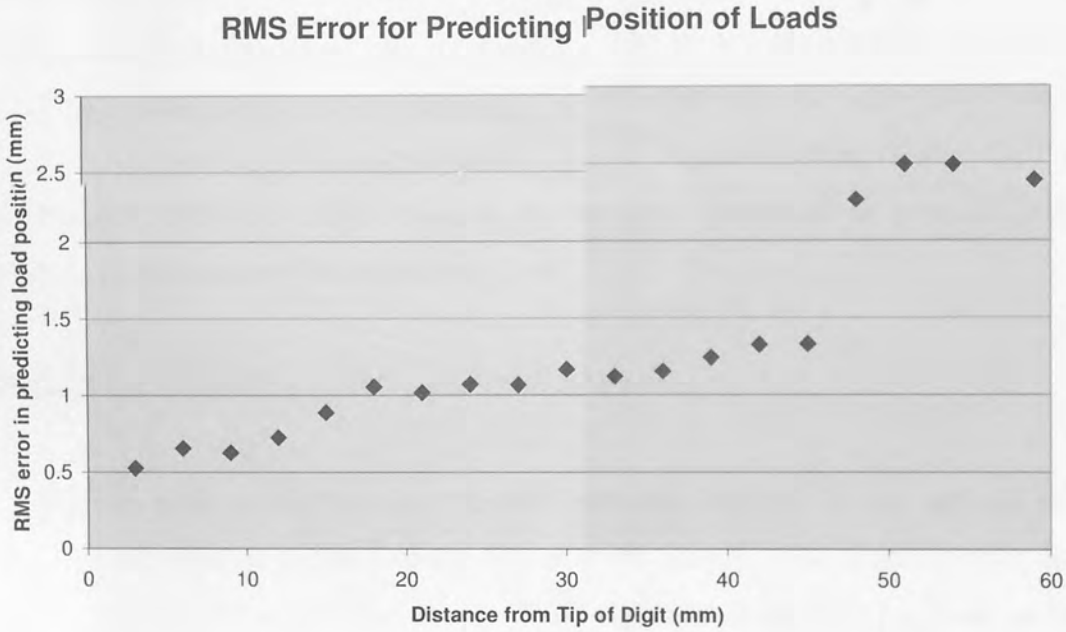

Figure 5. 11 A graph showing the root mean square error for predicting position of loads dependent on the distance of the load from the tip of the digit (left hand side).

5.2.3 Evaluating Navigation Characteristics

The experiment used to determine the performance of the digit in navigation is relative positioning by means of novel self-referencing the digit to tactile features.

5.2.3.1 Relative Positioning

Following on from the experiment to evaluate static load positions (Section 5.3.1.4), the neural network's response to dynamic positioning is tested. The aim of this experiment is to determine if the digit is able to determine the position of a contact when the contact point is moving. The experiment is carried out by applying a stroking contact on the digit at different speeds. The speed range chosen was between 20mm/s to 100 m/s. The performance of the digit is determined from the value of following the error produced in predicting the position of the contact with respect to time.

Method for evaluating relative positions of contact

1. The digit is clamped at the root with the sensors facing upward and positioned at the end of the linear drive platen. The force stepper and phantom rig is placed at the tip of the digit so that the digit just rests on the top edge of the phantom rig and this position is set as zero point on the force stepper platen.
2. The force stepper is programmed to move back and forth 50 mm from the tip along the digit at the speed of 20 mm/s. The positions of the force stepper and the strains on the digit are recorded.
3. The speed is then increased by to 30 mm/s and step 2 is repeated.
4. This procedure is repeated for 40 mm/s to 100 mm/s and all the data is recorded.

5. The strain data for each of the dynamic tests using the neural network trained for determining static positions (Section 5.3.1.4) and the predicted positions of contact can be plotted against the positions recorded from the force stepper.

Results Dynamic Contact Points (Stroke Test)

By plotting the true stroke position simultaneously with the predicted position, the following error can be seen (Figure 5. 12). At a speed of 20 mm/s, the digit is able to follow the stroke as it moves along with a following error of 5.8 % of the actual position.

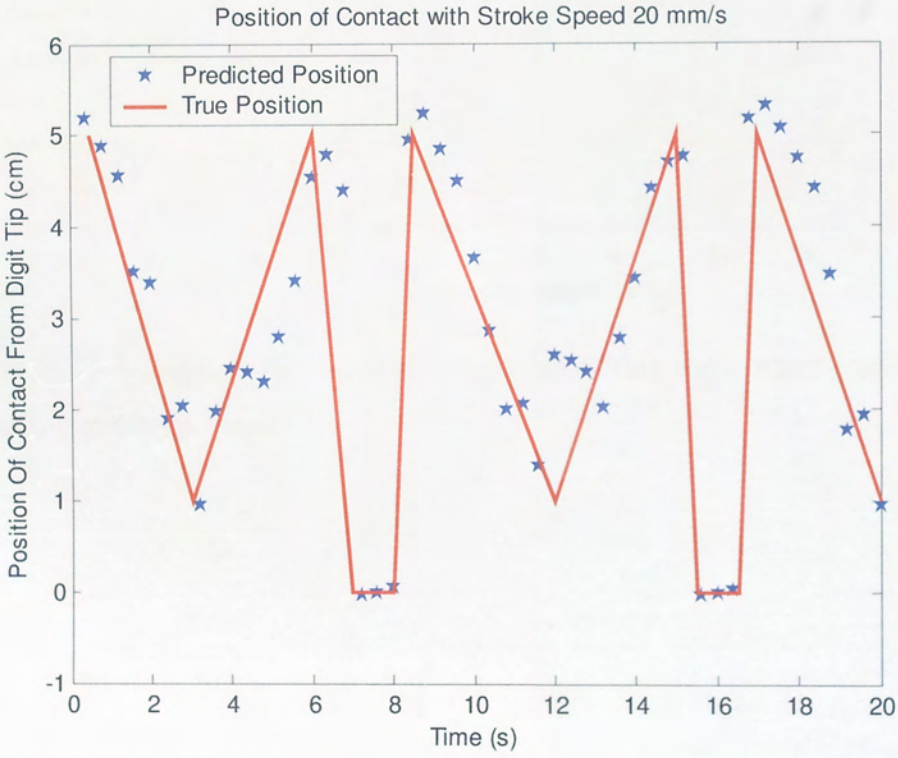

Figure 5. 12 Position of contact predicted for a stroke speed of 20 mm/s

As the speed increases, the sensors find it more difficult to keep up the motion of contact, as noted by the increasing drop in following accuracy. When the contact is moved too fast, data capture is not fast enough, leading to larger following errors. Figure 5. 13 shows how the percentage following error increases as the stroke speed increases.

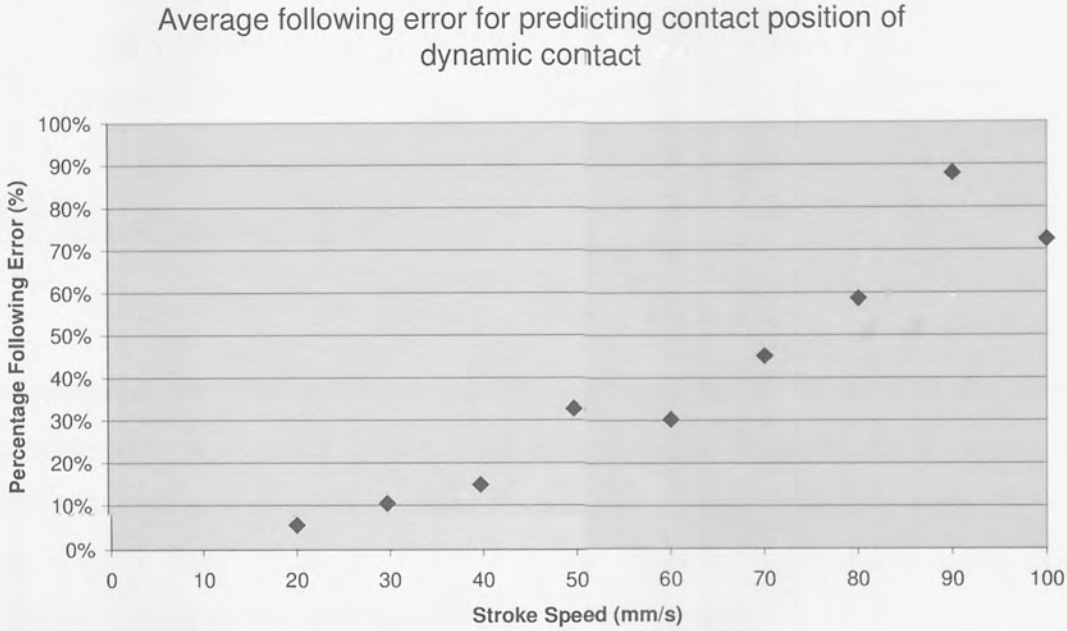

Figure 5. 13 A graph of following errors for predicting the contact positions according to stroke speed

5.2.4 Characteristics of Palpation

Palpation is a major function in diagnosis. For a flexible digit, it has a separate used to navigation. The experiments carried out in this phase are:

- Contact Stiffness
- Palpation

5.2.4.1 Contact Stiffness

In palpation, the digit is used to discriminate changes in stiffness of the tissue being examined. In order for the digit system to be evaluated for its ability to discriminate ranges in discrete stiffness, a range of three materials were chosen. The digit is then evaluated for its ability to discriminate stiffness under axial resistance when subjected to the same impact acceleration.

To validate the stiffness values of the contact materials, their spring rates are determined experimentally. The spring rate is the amount of force needed to compress the spring to a certain distance, or more specifically, the amount of weight required to compress a spring by one millimetre. Springs that have a low spring rate are soft and those that have a high spring rate are stiffer. However, in surgery, the value of the stiffness is less significant than its value in context to other stiffness.

Method for determining spring rate

1. To determine the spring rate of the test specimens for the stiffness test, three contrasting specimens of different material were prepared. Their dimensions are 30 mm x 30 mm x 30 mm cubes of soft expanded polystyrene foam, medium density rubber and Perspex.
2. 1 kg weights are placed on top of each sample and the amount of deflection caused by the weight were measured using a micrometer.

Results for contact material spring rates

The difference between the compressed and uncompressed specimens is used to determine the spring rate of the material (Table 5.4). These specimens could then be attached to the evaluation rig and tested on the digit (Figure 5. 14).

Material	**Stiffness Range**	**Deflection when subjected to a load of 9.8 N (mm)**	**Spring Rate (N/mm)**
Light Plastic Foam	Soft	9	1.1
Rubber	Medium	0.25	39.2
Perspex	Hard	Not Perceptible	100 +

Table 5.4 The spring rate of test materials to measure the stiffness

Method for Contact Stiffness

1. The digit is clamped at the root with the sensors facing downward and positioned at the end of the linear drive platen. The first test specimen is attached to the side of the phantom rig and is positioned 1mm from the tip of the digit. This is the starting point.
2. The test piece is then driven into the digit at a speed of 10 mm/s 5mm into the digit and the strains are measured before the test piece is retracted back to the starting point (Figure 5. 14).

3. This procedure was repeated five times in total before the procedure is repeated on another specimen of different stiffness.
4. A 3 input, 3 output classification type (Softmax) neural network optimised for use in the evaluation of the data.

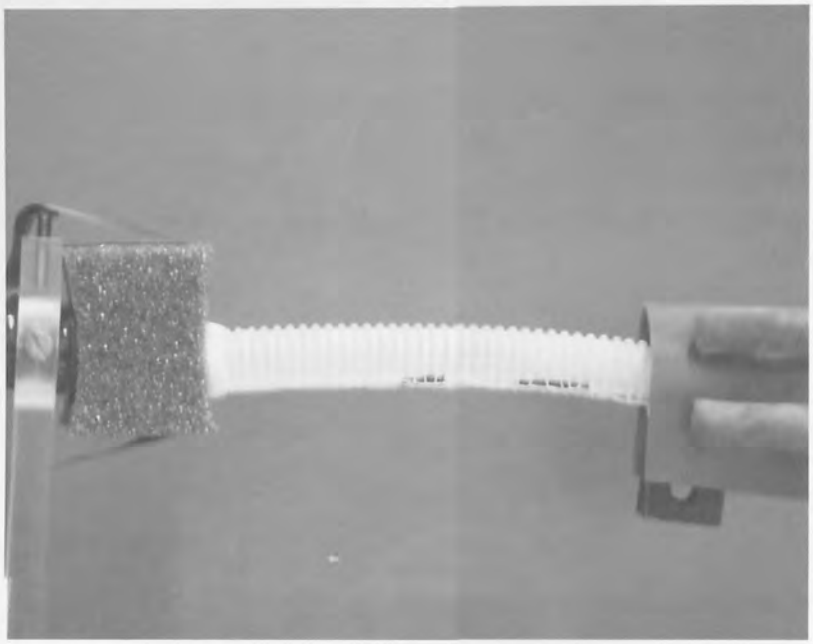

Figure 5. 14 Stiffness testing of digit under axial resistance

Results for Contact Stiffness

The optimised neural network architecture for determining contact stiffness is a 3 input, 3 output classification network using 40 hidden nodes and is able to predict three discrete contact stiffness ranges to a high degree of accuracy when the digit is not inflated and with axial resistance as shown in Table 5. 5.

Real/Predicted	Hard	Medium	Soft
Hard	181	0	0
Medium	0	208	0
Soft	0	0	236

Table 5. 5 The results show that the digit is able to distinguish between three contrasting different stiffness of materials.

5.2.4.2 Palpation Test

The motion of palpation is the pressing lifting of the hand and fingers (or digit in the case of an artificial palpation device). In this experiment, the aim is to evaluate the digit system's ability to discriminate contact stiffness on its traverse axis, whilst being subjected to inflation and deflation to mimic the movement of pressing and lifting. The same range of materials of different stiffness that were used in 5.2.4.1 is used for these experiments.

Method for evaluating palpation

1. The first contact stiffness test specimen is placed on the base of the evaluation rig and fixed into place with adhesive tape. The digit is clamped at the root with the sensors facing downward and positioned 50 mm vertically from, and 25 mm horizontally past the test specimen
2. The pressure in the digit is controlled inflate the digit from 0 to 2 bar in 20 seconds and strain on the digit when it is pressing against the test specimen is collected. This is repeated five times for repeatability.
3. The second and third contact specimens are subjected to the same procedure.
4. The data is processed in the method outlined in Chapter 3, and a three input, three-output classification (softmax) neural network is optimised.

Results for evaluating palpation

The optimised neural network architecture for this experiment is determined to be 40 hidden nodes for a 3-input, 3-output classification neural network. Out of 625 samples tested, the accuracies of the system in determining are 80.5 % for soft surfaces, 80.4 % for medium stiffness surfaces and 85.2 % for hard surfaces and the results are presented in Figure 5. 15. This graph shows the comparison of correctly and incorrectly identified instances of contact with materials of different stiffness.

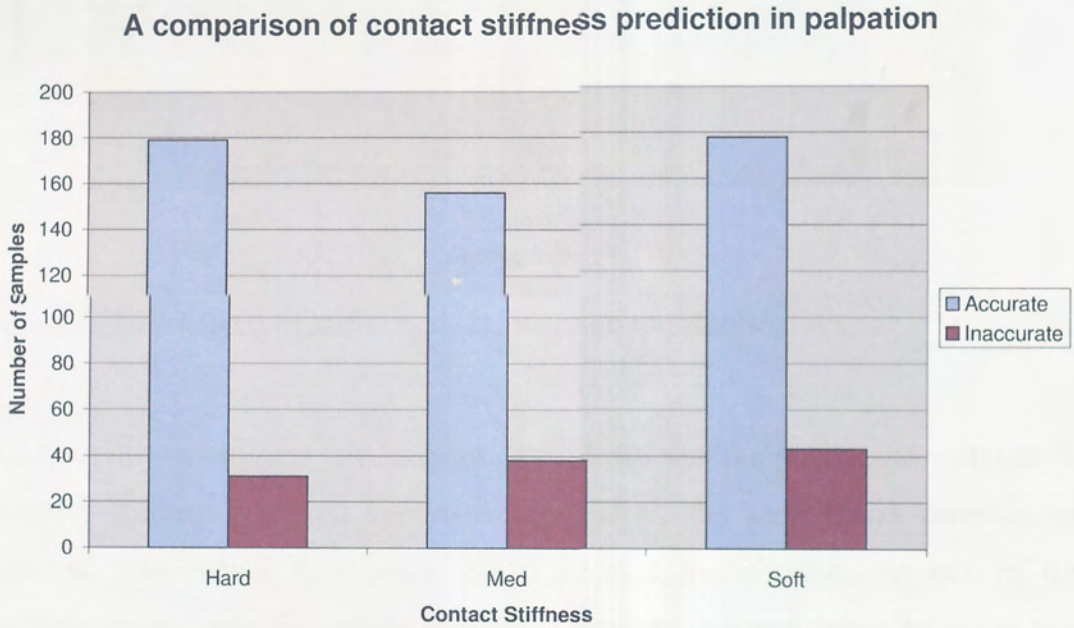

Figure 5. 15 A comparison of contact stiffness predictions in palpation

On further examination of the results more carefully, the results were grouped into the three regions of stiffness, with the proportion of each stiffness range identified and this is shown in Figure 5. 16. From this graph, it can be seen that there is a tendency for the errors in prediction to occur on the side closest to the next range in stiffness. The results for traverse palpation are not as accurate as for axial contact stiffness, but it is to be expected as inflation of the digit reduces the sensitivity of the strain sensors by opposing the strains induced by traverse

contact. Despite this, an overall accuracy of the system to discriminate stiffness in palpation is 82%.

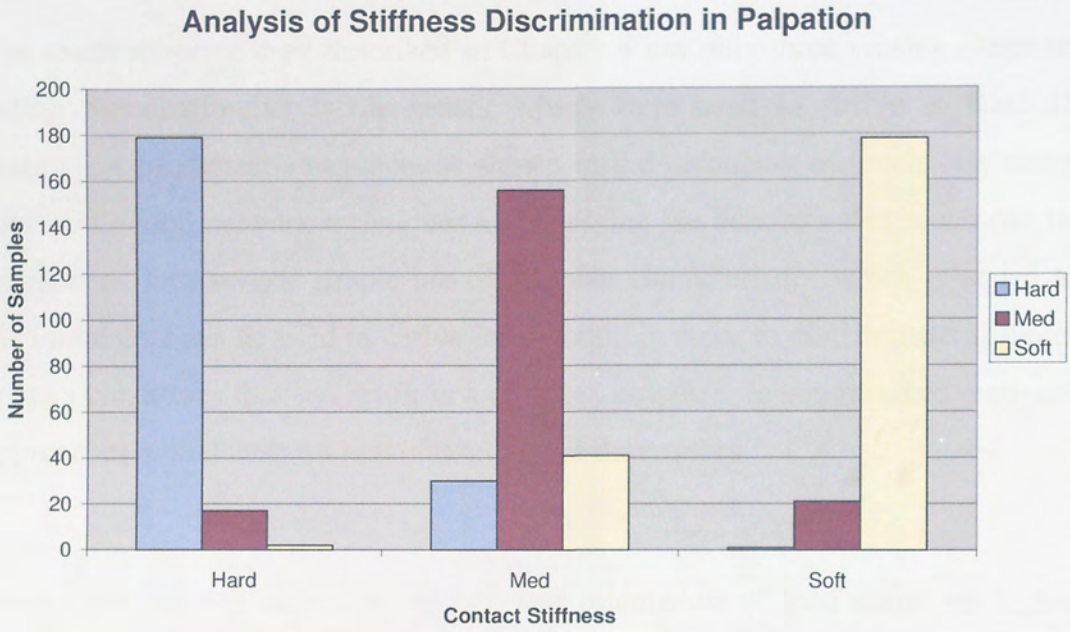

Figure 5. 16 Analysis of stiffness discrimination in palpation

For both this experiment and its prior, is expected that the greater the variation in material stiffness the digit system is exposed to, the accuracy in determining different classes will decrease. This is because the discrete step size of the stiffness ranges reduces and the difference between stiffness levels becomes less distinct.

Although an acceptable performance in a simplified phantom demonstration rig has been achieved, other features may compliment the discrimination of tactile conditions and therefore a more specific phantom for discrimination would be a future step in this research.

5.3 Conclusion

The touch sensitive digit described in Chapter 4 has only three sensing elements within the distributive tactile sensor which were used to derive at least 18 descriptors of contact and touch, as shown in the taxonomy of touch. By using cascaded neural network techniques and applying the concepts that touch can be categorised into several simple but identifiable characteristics which is added to the initial data can be used to derive information in order to discriminate different contact conditions that can result in a complex output. In contrast, conventional approaches would derive a maximum of three descriptors.

From three sensing elements, contact and orientation of load could be highly accurately determined using a *softmax* neural network. By assuming the neural network filtered out non contact situations, results in subsequent experiments in load magnitude and static load positioning showed an improvement in the accuracy of neural network predictions compared to the three sensing element configuration described in Section 4.3.6. These neural networks predicted load magnitude to 66.2% accuracy and load position to 75% accuracy with contact and non contact data sets, whereas using just the contact data, the accuracies are 90 % and 98 % for load magnitude and load position respectively.

The taxonomy of touch characterises the different elements of touch in a hierarchical form. By first isolating each of these characteristics and measuring the performance of the digit when subjected to each of these characteristics, the success of the data outputs from each of the results can be analysed.

By choosing the neural networks that discriminate with the least errors for the smallest number of input values, we obtain a table of performance (Table 5. 6)

that will indicate which order the neural networks can be cascaded. It has been shown that by separating contact and null contact data is vital for accuracy of subsequent parameters.

Contact Characteristics	**Number of Inputs**	**Accuracy**
Contact and Orientation	3	100 %
Position of Static Contact	3 + Contact	98 %
Number of Contact Points	3 + Contact	97.6 %
Position of Dynamic Contact	3 + Contact	94 %
Load Magnitude	3 + Contact	90 %
Stiffness of Contact	3 + Contact	82 %

Table 5. 6 Contact Characteristic Hierarchy

The consequence of these experiments in this chapter shows that a range of the touch parameters can be ordered in a hierarchical format of the taxonomy of touch. This is why the independent testing of parameters to demonstrate their accuracy using pragmatic assumptions of human tactile reception. The combination of resulting outputs gives indication of spatial awareness in two dimensions. This principle can also be applied to three dimensions.

The aim of the experimental investigation was to demonstrate how the performance of the digit could be measured and how the results compared with human models of touch recognition. For example the resolution for stiffness was only demonstrated for three categories, where in reality there are more than three types of stiffness. However, human perception of stiffness by touch is limited to only a few states determined through a process of comparison. The number of groups of stiffness can be increased, but the larger the number, the greater the number of discrepancies one can expect. The number of states of stiffness in the experiment described in this chapter is sufficient to demonstrate a suitable process for discriminating the value of stiffness.

Chapter 6

System Input, Feedback and Visualisation

The focus of the research has been on applying sensors to the distributive tactile sensing method to an envisaged master slave system to reference tactile output to the user. The final of step of this work was to implement a full working system to drive the slave digit from a master glove input device and obtaining feedback information to assist navigation and diagnosis and to determine how the information can be made useful to the operator. In this chapter, we look at the functions and development the input and feedback device to fulfil the complete system requirements for an intelligent actuated digit with tactile feedback. In addition, experimental visualisations were developed to explore the nature of the information that would assist the control of the operator. The exploration devised represents the pragmatic solutions to suit the needs of the actual environment.

The input device drives the end tool and is the point that the user interacts with. Currently, there are very few complete surgical systems that provide tactile feedback for tools. In this chapter, methods for introducing feedback are discussed, along with solutions for an input device, its construction and evaluation. The system response is slow; due to the limitations of the MatLab, Real Time Workshop and xPC Target software, hence the low actuation speeds are acceptable with the responses being much lower than the strain time constants of the materials used.

6.1 The System

A complete system for a device for a flexible digit actuator with tactile perception consists of a looped system (Figure 6. 1) of a clinician connected to an input device with tactile feedback. This input device connected to a central controller, which operates the unit for end tool control. The central controller is a supervisory system that enables the master-slave system to function correctly.

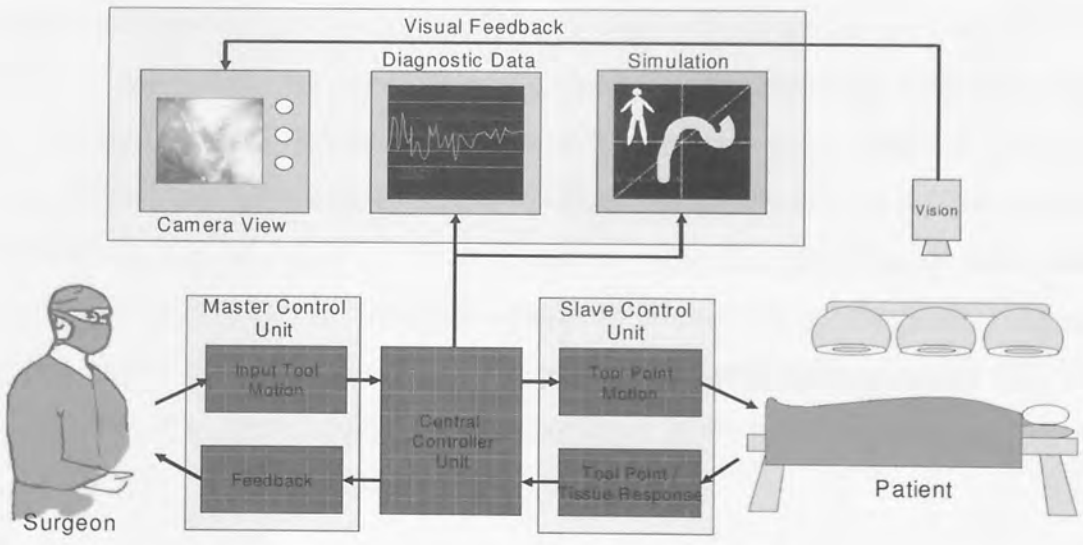

Figure 6. 1 A schematic diagram of the master-slave system

6.1.1 The Central Controller

In this work, the central controller was created on a PC running MatLab with Simulink, xPC Target and Real Time Workshop toolboxes. MatLab is a command interface for real time application control, signal acquisition, analysis and parameter tuning. Simulink provides the environment to model a physical system and controller as a block diagram.

xPC Target is a host target PC solution for prototyping, testing and deploying real time systems. xPC Target allows the system interface models to be replaced by I/O driver blocks that can be connected to the sensors and actuators on a real system. Real-Time Workshop converts the Simulink models of the control system into C code that can be compiled into a real-time executable control system, which is linked with the I/O driver in xPC Target. This allows for an environment where the host development PC and target real time controllers PC are different computers.

The central controller acquires sensory inputs from both the master and slave devices and gives instructions for controlling digit motion and deploying feedback. The central control consists of a number of sub systems (Figure 6. 2). Following the path of the central controller starting with the clinician, we see the flow of actions required to actuate the digit to reach a contact condition, judge the properties of the contact parameters which are converted into simulated visualisations, diagnostic data and tactile feedback prompts ready for the clinician to interpret and take action for. The features of each of the subsystems will be explained in the following sections.

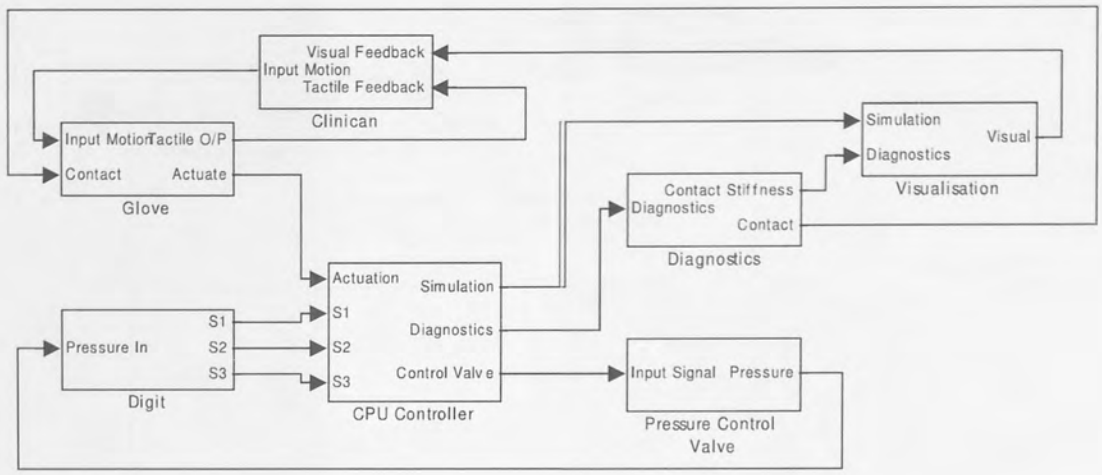

Figure 6. 2 The central controller is made up of several subsystems

6.1.2 The Central Processing Unit

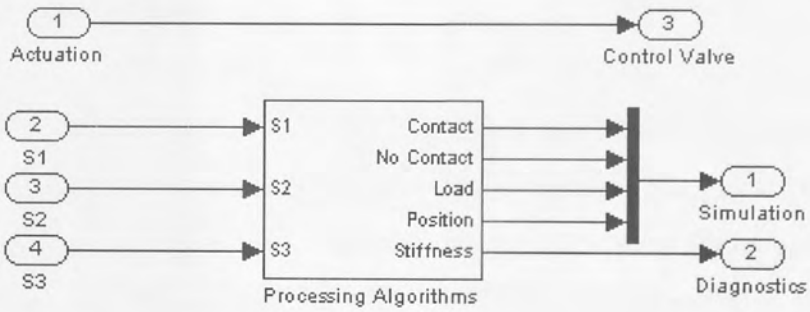

Figure 6. 3 Inside the CPU Subsystem

The CPU is the central processing unit that computes the controller demands (in practice a bypass to the control valve) and the flexible digit sensor signals processing algorithms that determine parameters such as contact, load, position and stiffness (Figure 6. 3).

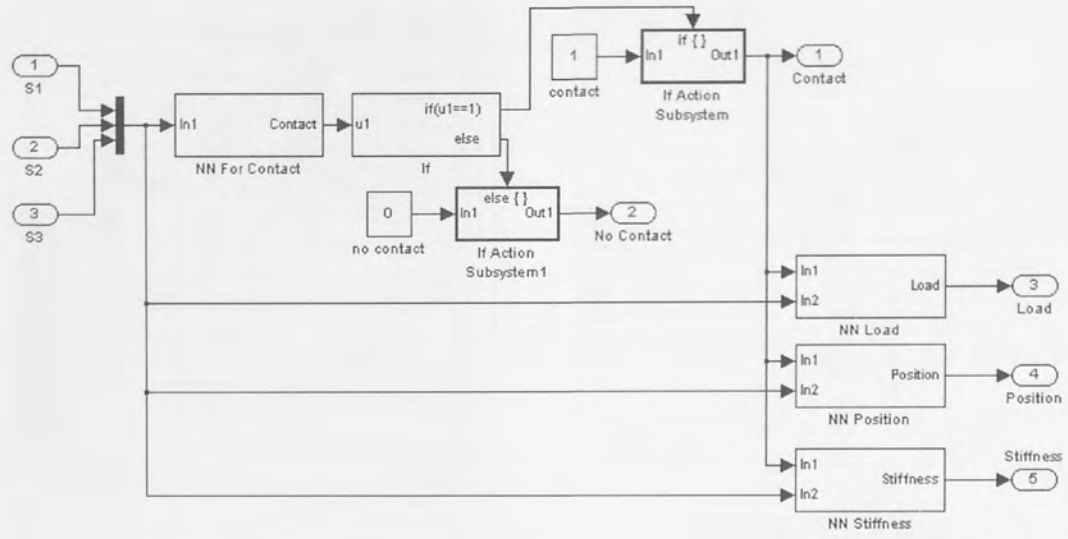

Figure 6. 4 Neural Network Cascaded within the system

If the Processing Algorithms subsystem is examined further, it can be seen they comprised of a cluster of cascaded neural networks that are dependent on the initial contact parameter being fulfilled before other touch parameters are initiated (Figure 6. 4) as described in Chapter 5.

The parameters of the neural networks developed and trained in Chapter 5 are built into Simulink neural network subsystems. For illustrative purposes, one such neural network is shown in Figure 6. 5. These Simulink neural networks are based on the coded versions in NetLab, but this format can be integrated with the rest of the control system.

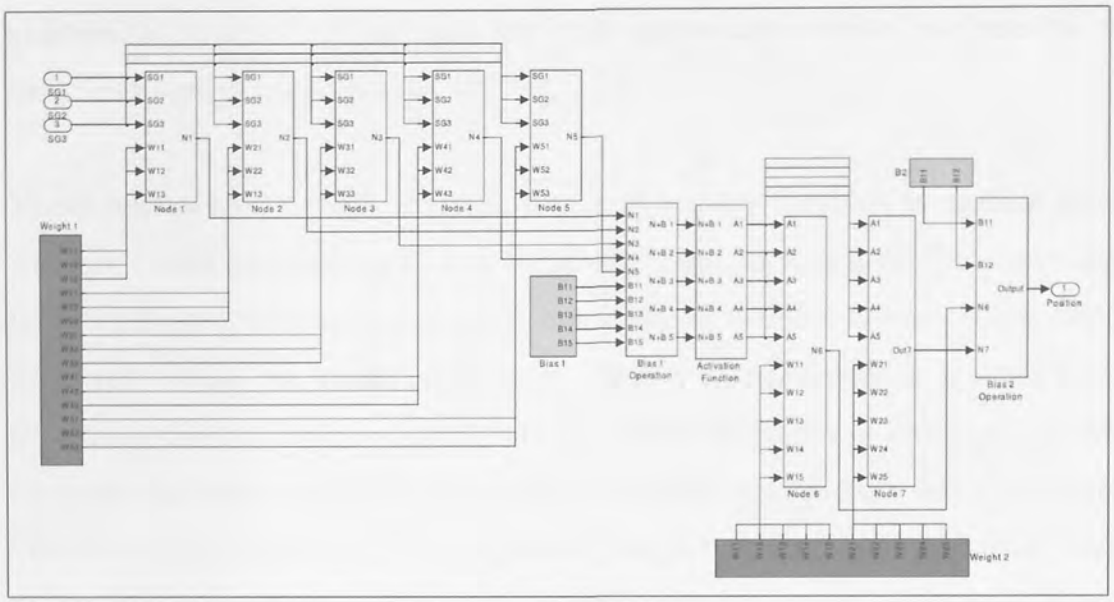

Figure 6. 5 The 5-node, 3-input, 1-output neural network used to detect load position

6.2 Feedback

The choices for sensory feedback are audible, visual and tactile, and whichever method of feedback that is chosen for clinical use needs to be clear and distinct. The most common feedback method is visual, and where input is remote, any steering is done with either a joystick, mouse or track ball as when moving a cursor or avatar on screen as commonly demonstrated with most contemporary PC and games systems. More advanced spatial motion can be achieved with a suitably instrumented glove. Audio cues offer an alternative form of information feedback and but rarer still are tactile feedback devices.

Out of the five human senses, audio, visual and tactile sensations are the most pragmatic for use in a clinical environment. Out of the three senses mentioned, difficulty in discriminating audio information sources may be a problem when for

example, a frequent false alarm at low risk state sounds similar to a rare but very dangerous state (Runciman et al, 1993)[72].

Visual feedback is currently the main source of sensory feedback in medical devices whereas tactile information is less frequently used, as much of the direct tactile feedback from the site of investigation in minimally invasive therapy is lost through the length of the instrument. The most common visual feedback is via a camera attached to the tool end, giving the clinician a view of the site of investigation. More advanced vision systems are digital, which use image sensors such as CCD (Charged Couple Device) to improve picture quality. Imaging systems currently show the site of investigation directly, but as the scope approaches a contact point, there is *white-out* in the field of vision.

Tests carried out on a mouse pointing device by Akamatsu et al (1995) [73] to compare tactile, auditory and visual feedback found there are no differences in overall response times, error rates, or bandwidths; however, significant differences were found in the final positioning times (from the cursor entering the target to selecting the target). Tactile feedback was the quickest, normal feedback (no additional feedback indicating the cursor was over the target) was the slowest for final positioning times. Tactile feedback allows subjects to use a wider area of the target and to select targets more quickly once the cursor is inside the target.

Tactile information can be incorporated with vision systems and offer a greater range of information at the fingertips to the clinician. In order to do this, we need to understand what is meant by the perception of touch.

6.2.1 The Perception of Touch

The skin is an active sensory system that covers the entire body. Skin is made up of a tough outer layer called the epidermis that protects the underlying dermis that contains sensory receptors. Sensory receptors are the specialized nerve endings designed to relay specific states or conditions in or around the body. There are many texts that describe the anatomy and physiology of the central nervous system in greater detail including Wyburn (1960)[74] and sensory perception is described by Schiffman (2001)[75].

Kinesthesis refers to perception of body position and movement, that is to say the posture, location and movement in space of the mobile skeleton such as fingers and vertebrae. This positional information is also referred to as proprioception. Two or more sources of mechanical stimulation; those from the joints and those from the muscles and tendons may contribute to kinesthetic sense. Kinesthetic information continually provides important spatial information concerning our bodies so that we can measure some objects or compare two objects on the basis of touch (Schiffman, 2001)[75].

> ***haptic*** */ 'haptɪk/*
> → ***adj.*** *(technical) relating to the sense of touch. - ORIGIN C19: from Gk haptikos 'able to touch or grasp', from haptein 'fasten'*
> Quoted from the Concise Oxford English Dictionary (haptic adj.)[76]

The combined input from the skin and kinesthesis provides haptic sense. The haptic system is responsible for the perception of geometric properties, such as shape, dimensions and proportions of objects handled. Furthermore manipulations such as

grasping, squeezing and hefting, the haptic system will give information on the weight and consistency of object (Schiffman, 2001)[75].

In the computer industry, haptic devices refer to interfaces that can provide the user with some kind of feedback regarding feel, usually by generating forces. Force-feedback controllers used in videogames are one example, provides feedback to illustrate events in a game. For example, in a shooting game, a force feedback joystick or game pad would recoil when a gun is fired.

Tactile sensing is used in perceptual tasks such as palpation where the clinicians evaluate tissue properties with their hands. In the absence of the access to remote tissue, haptic feedback devices can be employed in a master slave system. Tactile display or haptic feedback devices stimulate the skin to generate the sensation of contact. The skin responds to several physical quantities to convey the sensation of which the most common are vibrations, small-scale shape or pressure distribution and thermal.

Over a period of time, continued steady pressure in touching, results in a decrease or even elimination of sensation. Touch sensation undergo adaptation and adaptation to pressure is common. For example, we do not feel the pressure of wearing a watch after a short time. The time taken for adaptation will depend on a number of factors such as the intensity of the stimulus, the size and the region of skin contact. The time taken for the sensation to disappear is directly proportional to the intensity of the stimulus and inversely proportional to the size of the area of contact (Geldard, 1972)[77]. A brief movement or an abrupt change in stimulation is will restore the sensation of touch following a period of adaptation. Continuous changes in stimulation are caused by active touching and are used to obtain kinesthetic or haptic information about an object.

Howe (2002)[78] describes the various methods of providing haptic feedback. Vibrations can relay information about the surface texture, slip, impact and puncture. The frequency range of interest is between a few Hertz to the a few hundred Hertz. Small-scale shapes or pressure distributions are more difficult to convey and the most conventional approach is to use arrays of pins that can be lowered and raised against the skin. Thermal displays are more challenging because human fingers are generally warmer that their surrounding room temperature so thermal perceptions are based on a combination of thermal conductivity, capacity and temperature. In addition, the response is slower.

6.2.2 Tactile Feedback for Clinical Devices

Palpation is one of the fundamental skills used by clinicians in diagnosis. It is the act of touching, pressing and feeling the body in order to make an assessment of the state of the body without any instrumental intervention. In minimally invasive procedures, this skill cannot be used to its fullest extent when investigations go far beneath the surface of the skin. An anectodotal example from a surgeon describes the limitation of getting accurate information from inaccessible locations such as the inside of the bladder, where access is from the narrow tube of the urethra. External palpation of the area where the bladder is located will give some indication of the bladder status and if there are any indications of problems, only if the problem is near the surface. It may not be possible to feel for problems if the problem is located on the inside of the bladder. So by identifying more precise location by palpation, this can enable alignment ready for biopsy.

Tactile sensation is actuated in by the means of changes in displacement in reference to the surface. This can be done either through a force feedback, which offers the sensation of resistance for given output parameters, or by mechanical stimuli such as

vibration. The development of a dual purpose device that would serve as an input device interfacing the clinician with the tool tip and with as an output device providing feedback with minimal interference to the movement is necessary in order to move away from the bulky and expensive solutions currently available in the tactile feedback arena. The choice of input device is between a steering device such as a joystick or an intuitive glove. A glove input device was chosen over a steerable joystick, as the aim is to make a low cost, disposable input device for the system.

6.2.3 Contemporary Tactile Feedback Devices

Instrumented data gloves are a common solution to steering the tool end and there are several on the market. A survey of data gloves carried out revealed that the lowest cost data glove is the P5 Glove (Figure 6. 6) manufactured by Essential Reality (Essential Reality, 2003)[79] at the cost of $100 US (sold on Amazon.com in late 2003 dropping to a mere $10 by 2004) but this glove does not include any tactile feedback, though less bulky than other data gloves on the market, it is primarily used by computer gamers. There is also Pinch® Gloves developed by Fake Space Systems that integrate a sensor in each finger tip to detect contact between digits of either hand (2003)[80] but again, this does not include tactile feedback. This glove alone costs £1450 (Inition, 2004)[81]. A wireless data glove, such as the 5DT data glove captures motion and depending on its sensitivity, prices range from US$11,000 to US$22,000 (Metamotion, 2003)[82].

Figure 6. 6 The P5 glove: an example of a data input glove

Gloves that incorporate any sort of feedback multiply the cost. There are several tactile (haptic feedback) devices on the market at present. These include Immersion's Cyber Touch™ vibro-tactile glove that allows the user to feel sensation from computer generated 3D objects (Immersion, 2002)[83] which costs in the region of £14,000 for just feedback to the hand (Hendon, 2003)[84]. In addition to their cost, the complexity and weight of these gloves will infringe on freedom of the surgeon in the operating theatre.

Much of the other works on haptic feedback devices have been on sensory substitution for the disabled. This includes tactile pin arrays for conveying visual information to the blind and auditory information through vibrotactile displays for hearing impaired people. There are also haptic feedback devices used in virtual environments and in teleoperation that replicate stimuli of the original sense as opposed to replacing one sense modality with another. Tan & Pentland (1997)[85] describe the challenges in building a practical tactual displays wearable computing and provides a review of some of tactile devices available including TACTAID 7, which converts sounds to vibrations (TACTAID, c2002)[86].

Other haptic devices on the market are more development systems that computationally reproduce the feel of an object touched in virtual space. The Phantom® produced by SensAble offers high fidelity force feedback of virtual objects (SensAble Technologies, 2004)[87]. Reachin also offer a similar workstation system using the Phantom® haptic device but providing a different software platform called the Reachin Core. At the heart of each of the systems is the software, Ghost SDK in the case of SensAble and Reachin API for Reachin. However, this type of system would only provide part of the solution for this research project, as the force feedback would be based on modelled information in virtual space, whereas for this project, any interactions with the end tool would be real and physical.
Many of these devices have been developed for exploration of virtual systems. In particular in medical training where surgeons are trained to perform procedures such as laparoscopy in simulation programs (Reachin 2003)[88]. The tactile feedback often is generated by the system by computer (by modelling) and not from actual physical entities.

6.3 A Gloved Solution

Ideally any surgical instruments produced for the theatre would be disposable or at the bare minimum be able to withstand rigorous cleaning (Chapter 2). Sometimes this is not possible and in these cases, drapes or sheaths to shield instrumentation should be used.

The first actuation system trialled with the digit was operated by a resistive trigger (Figure 6. 7). This was connected to the control system and the output from the trigger was scaled to the proportions required for instructing the control valve. However, the output from this system did not repeat well and was uneven as the slide mechanism had a tendency to slip causing the output motion to be unsmooth and with

had low repeatability. Figure 6. 8 shows output voltage from the trigger when pulled at different positions. In addition, holding the trigger did not provide natural motion. A gloved solution was then approached as this input device is worn by the clinician, resulting in more intuitive natural motion.

Figure 6. 7 A resistive trigger input device

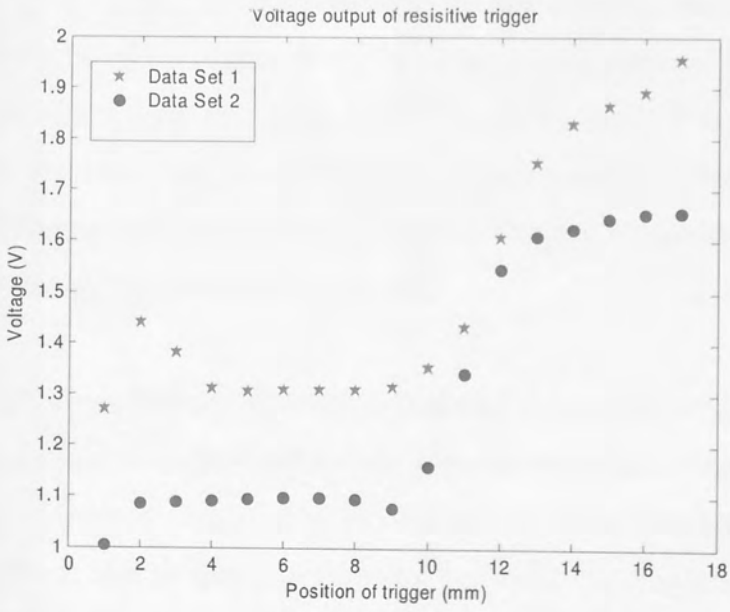

Figure 6. 8 Voltage output of the resistive trigger when pulled at different positions

What is novel about the glove developed in this project is the fact that it is a complete system that uses information obtained from real, not computer generated virtual

objects using the distributive sensors in the digit and fed back to a simple and potentially inexpensive and disposable glove. The whole system can also use virtual information for training purposes.

The aim of the glove is for it to be an integrated instrumented device, with input transducers which produce voltages to the circuit that drive the actuation of the digit in situ inside the body and having sensor derived feedback from the digit relayed in a vibro-tactile manner.

6.3.1 Material Choices

The choice of material for the glove in this prototype is cotton since earlier prototypes using latex gloves were unsatisfactory. Latex gloves are single use, and multiple applications lead to rupture. In the operating theatre, latex or vinyl gloves are used because they offer more touch sensitivity; however cotton gloves were chosen for the prototype because they would be more durable in experiments. It is intended that the sense detection technique will be verified using strain gauges for the sensing points; fibre bragg grating optical sensors as described in Chapter 3 could be embedded into the latex glove during the manufacture process.

A vibration device was chosen above force feedback for a glove as there is no way of reproducing resistance on a glove when it is difficult to choose a reference point from inside the body. Hence there are no force feedback mice or trackballs on the market for the same reason. For an initial prototype a small thin piezo transducer (Appendix 6.1) is used to produce vibro-tactile sensation. This is a low cost, thin and lightweight device suitable for experimental purpose, as it will allow for a highly mobile glove, ensuring little interference from a bulky actuation method and wires.

6.3.2 Inducing Vibro-Tactile Feedback

The actuator inducing the tactile stimulation in the glove is located at the back of the hand. The location is ideal as it is not a surface region generally used when operations are being performed. Using the Simulink and Real Time Workshop, the frequency of the piezo-transducer can be controlled. The threshold of detection depends on the frequency of stimulus and the size of the area of skin vibration is applied to.

Sensitivity to vibration begins to increase at 40 Hz and peaks at 250 Hz (Verrilo, 1991)[89]. Since any vibrations are intended to be unobtrusive, a frequency of between 50 and 200 Hz was chosen, which can be set according to the comfort of the wearer of the glove as the purpose of the vibrations is to indicate a change in a chosen parameter. For this initial stage tactile feedback is confined to a single touch parameter; that of the presence of contact to prove the concept of touch feedback and a frequency of 50 Hz was used for this research.

6.3.3 Glove Construction

A single strain sensor or an array of strain sensors, similar to those used in the distributive tactile sensor for the end tool can be applied to the glove to produce input signals to provide outputs for controlling the digit actuation. The construction of the. glove (Figure 6.9) is detailed below.

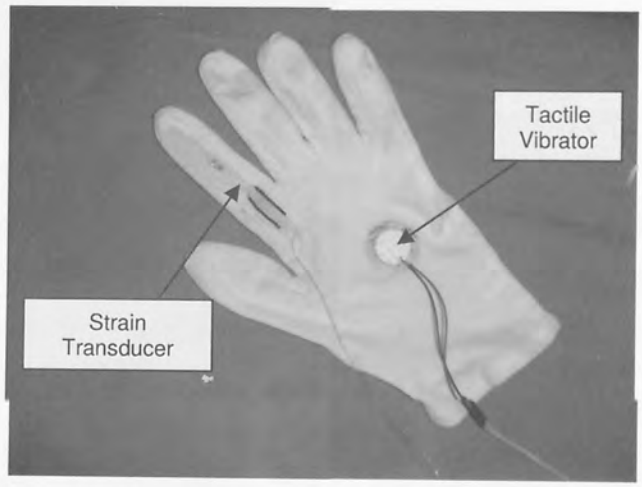

Figure 6.9 Input Glove Construction

A 2 mm strain gauge (Appendix 3.1) is attached to a thin strip of polypropylene 80 mm long at the mid point and then bonded to a strip of Rigiline boning before being sewn onto the back of a finger of a cotton glove. A weaving stitch is used to hold the strip in place.

On the back of the glove, a 28 mm diameter piezo-transducer (Appendix 6.1) is attached. The transducer sits close the back of the hand, which does not interfere with the movements of the fingers or with opening or closing.

The connecting wires are also sewn into the side of the glove until they reach a point where they can be conveniently connected to a data port.

The output from the strain gauge is amplified in a quarter bridge configuration using a Strainstall Ltd strain gauge amplifier (Appendix 3.2), which is then connected to a ADC board, connected to a computer to record the output using MatLab XPC Target. The tactile vibrator is controlled using MatLab Simulink with Real Time Workshop.

6.3.4 Calibration of the Input Glove

The input glove movement is calibrated by measuring the voltage output produced when the finger where the sensor is located is curled. An experiment was set up where a user, wearing the glove squeezes cylinders of differing radii and the output measured for each radius is distinctive (Figure 6.10).

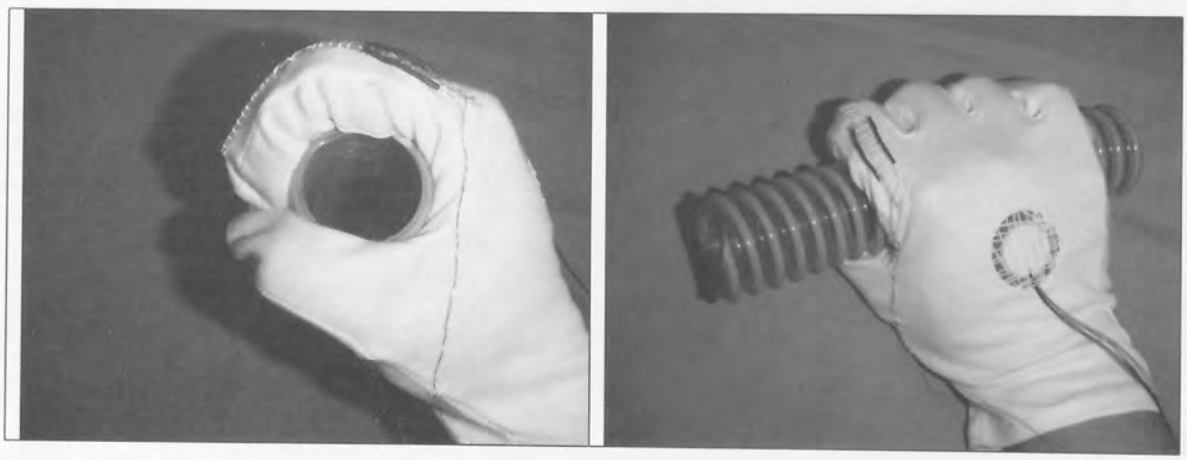

Figure 6.10 Calibrating the glove

At the point where the cylinder is very large and presumed as flat, the sensors reach a threshold, which causes the voltage to plateau out. From the data, a graph is plotted (Figure 6.11) showing that the outputs from curvature of radius of between 10 mm and 100 mm. The average values of these outputs give a close to linear voltage output for curvature with a mean linear approximation of the line is y=-0.004x-2.8. It is this region, which is used to control actuation. A calibration curve will have to be applied to each individual user as no two hands are the same.

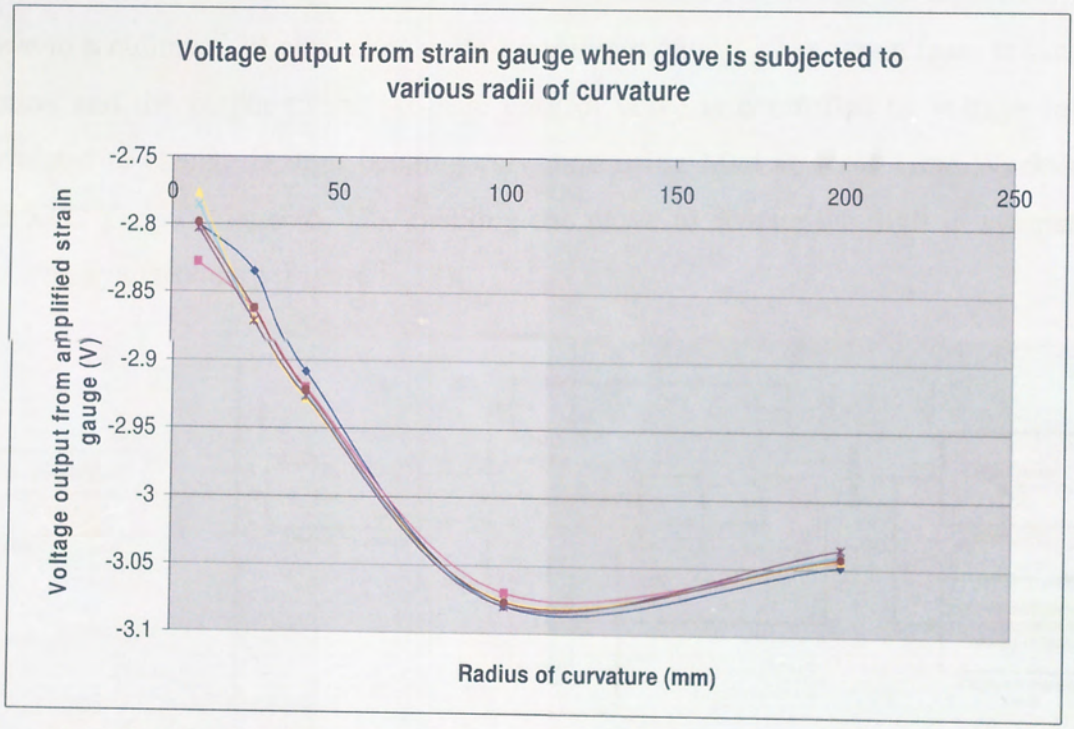

Figure 6.11 Graph of voltage outputs in multiple tests from strain gauge when glove is subjected to different radii of curvature.

6.3.5 Input Control

Input control is linked to the voltage input to the pressure control valve by a gain multiplier. The linear region is defined and limiters placed at the start and end of finger curving motion. The strain must reach a certain threshold before the system is activated. For this particular glove calibration, the strain output post amplification must exceed -3V before the pressure valve is activated. In addition, the maximum pressure exerted on the digit should be no more than 45 PSI so that the digit does not curve to a radius of 30 mm (almost 360° bend curvature). The strain from the input motion and the output to the pressure control valve is controlled as voltage input correlated to change in digit bending curvature using MatLab Real Time Workshop and XPC Target (Figure 6. 12), enabling the glove to actuate the digit in sympathy and with synchronicity (Figure 6. 13)

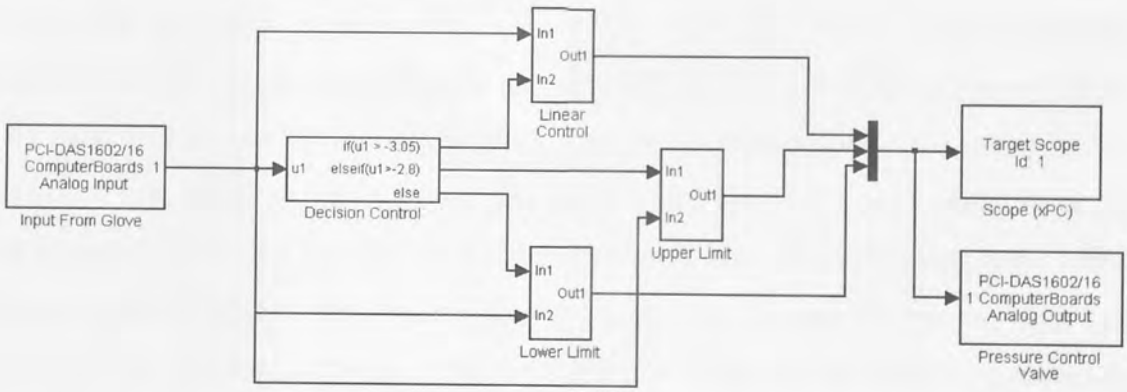

Figure 6. 12 Simulink Control System for Input

The Simulink control system for input (Figure 6. 12) describes the path of strain gauge input signals controlling the pressure control valve within upper, lower and linear control.

Figure 6. 13 Glove and digit synchronicity

6.3.6 Tactile Feedback Control

Combining the glove input control system (Figure 6. 12) with a tactile feedback mechanism, the final control loop for tactile feedback was developed (Figure 6. 14). The glove is actuated by the user, causing a change in the output on the strain sensor (s4) placed on the glove. This is indicative of a signal for actuation (V out), changing the pressure going into the digit to the required position. When the digit comes into contact with an object, the changes to the strains (s1, s2 and s3) on the digit are interpreted by a neural network. The interpretation of the contact status is signaled to operate tactile feedback when the correct parameters are indicated. In doing so, the piezo transducer on the back of the glove will vibrate to notify the user that contact has been achieved. By implementing a prompt in Simulink that was converted into a visual prompt in the Real Time Workshop screen, the reaction time of the glove user could be measured. When a tactile prompt (at 50 Hz) was added to the visual prompt, the reaction time measured was marginally quicker than by vision alone by an average of 0.02 seconds, over an average of five trials per prompt type.

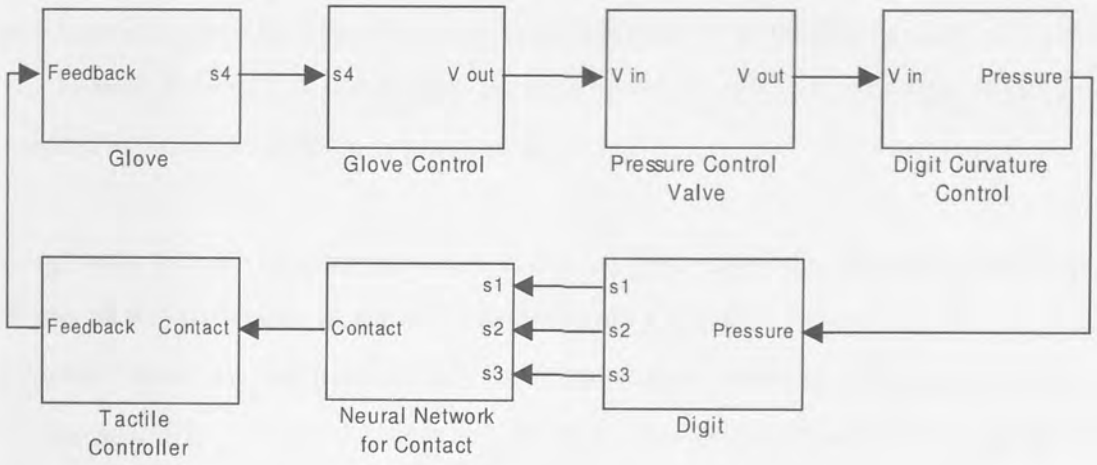

Figure 6. 14 Function Diagram of Glove Input and Feedback Control System

6.4 Visual Feedback

At present, the most common form of information feedback offered to clinicians is visual feedback, either in the form of direct sight or from scanning and imaging systems such as x-rays and MRI scans. In traditional endoscopy, examination, part of the diagnosis is made from observations from physical symptoms using camera systems. A lighted camera is incorporated into the tube of the endoscope and the picture is relayed back on visual displays, showing only the view of what the camera can see.

More advanced camera systems include Camera in a Capsule where the camera has been miniaturised to the extent that the system can be swallowed. On the outside, radio-receiving equipment is used to retrieve the data being sent from the capsule in-vivo as it travels along the intestinal tract. Once the capsule has passed through the body, the visual data can then be analysed for diagnosis (Rabenstein et al, 2002)[90]. However, with this method, there should be some considerations such as the location

and orientation of the camera whilst inside the body. The camera lens will point in one direction, but the capsule may rotate around as it travels, so the referencing visualisation software would need to be very powerful in order to tell the clinician the area and location the camera is pointing at.

Along with direct visualisation from cameras, there are other scanning techniques, which are strictly non-invasive. X-rays have been used for many years for diagnosis. However, there are some drawbacks such as overuse leads to exposure to radiation and the inability of x-rays to see soft tissues. Magnetic Resonance Imaging is an alternative method of scanning, and though it can read soft tissue, the presence of metallic (in particular ferrous) materials and electronics can lead to interference. Both these methods also require the patient to remain stationary.

Ultrasound, where high frequency sound is fired off at tissue and the amount of energy radiating back will give the reader an image of the surround area on a screen. This has been very successfully demonstrated in prenatal care in checking the development of growing babies in wombs. Highly delicate prenatal operations have been done in-vivo using this technology, where the instruments used in the operation can be viewed via ultra sound to check that they are reaching the intended targets. However, as with other types of scanning systems, the tactile feedback from instrument at site to the operating hand is negligible and ultrasound is unable to penetrate gas or bone.

The visualisation techniques described in this section are intended to be used in conjunction with tactile feedback to provide a more interactive map of sites of investigations that are in-vivo. Due to the information that the digit is able to extract using various neural network algorithms as shown in Chapter 5, it is possible to incorporate this data to create a map of the area in which the digit is examining.

Psudeo-haptic feedback using isometric input and a virtual handspring to determine stiffness has been used to simulate haptic information (Lecuyer et al, 2000)[91].

In addition to direct camera angle views from the end of the instrument, in this project novel side profile visualisations of the end tool has been developed, which will feedback the interactions of the side wall of the end tool. This enables the user of the system to know where along the end tool wall contact is being made. The visualisations were created in Virtual Reality Modelling Language (VRML) using V-Realm Builder v2.0 with the MatLab Virtual Reality Toolbox in SimuLink (Figure 6. 15) to generate the motion of bending based on collected real time data. The virtual world is explored using a standard web browser such as Internet Explorer or Netscape Navigator, which can be viewed and controlled from a remote computer through a TCP/IP connection via host and remote computers giving rise to opportunity for exploration of the actuated digit system being used in the field of telemedicine.

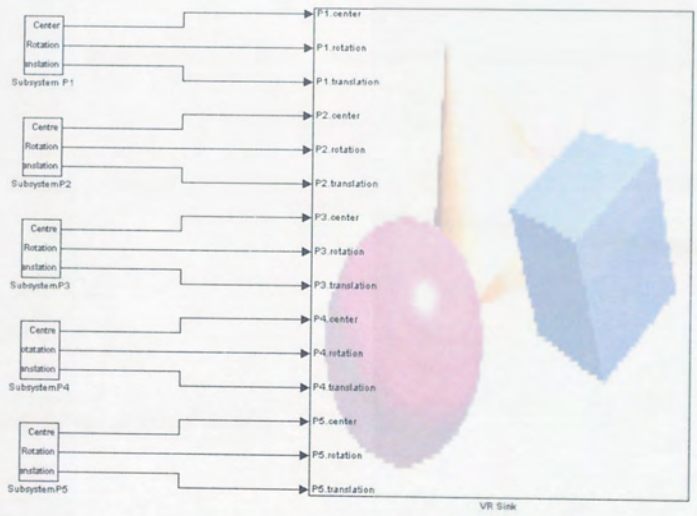

Figure 6. 15 Simulink interface for a virtual reality model where external input devices can be interfaced to control a real or VR model. The box on the right hand side of the diagram is the software portal to the VRML environment.

6.4.1 Visualisation of Tube Curvature

The movement exacted by the VR model depends on the visual characteristics required in for a particular application. The first attempt of visually modelling the digit in bending used the known equations of beam in bending. Mathematical modelling of the device is important to help understand and predict how a device might act. Work was carried out on how a flexible digit might deform when pressure is applied to it in actuation first without any external load being applied.

The shape of digit deformation can be determined by the following beam equations (6.1), (6.2) and (6.3) that can be found in many mechanical engineering textbooks such as (Case et al, 1999)[92] and considering a cantilever of length L and under load W at point a (Figure 6.16):

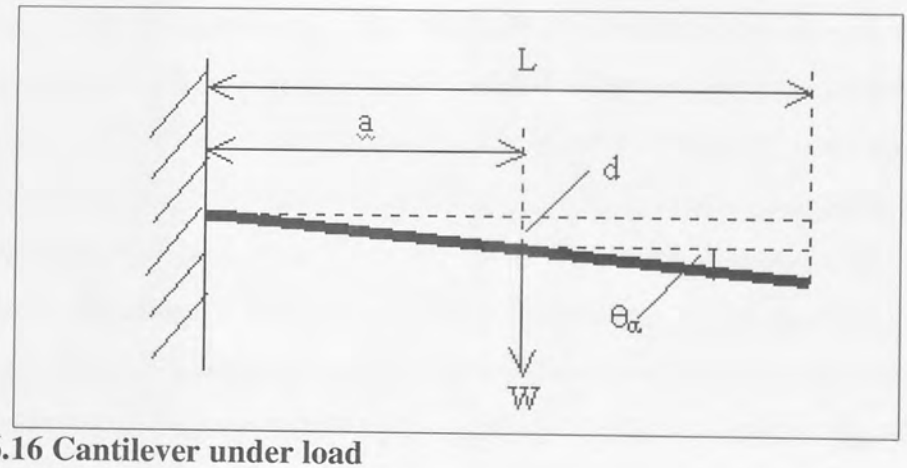

Figure 6.16 Cantilever under load

$$d = \frac{Wa^2}{3EI} \qquad (6.1)$$

$$\theta_a = \frac{Wa^2}{2EI} \qquad (6.2)$$

Where d = Deflection about from a load at a
W = Load
a = Distance of load W from the root of the beam
E = Young's Modulus
I = Second Moment of Area
θ_a = Angle of deflection at a

The second moment of area about the neural axis for a thin walled cylinder section:

$$I = \pi r^3 t \qquad (6.3)$$

Where r = Radius of the tube
t = thickness of tube

The modulus of elasticity (Young's Modulus), E for spring steel, used in the cantilever experiment is 205 GN/m^2 (Slack, 2005)[93], but Young's Modulus, for the polymer construction is unknown and was experimentally determined. It is assumed that when the digit is not inflated, it behaves elastically within a specific region. By assuming that the digit is a cantilever and that the deflections when it is loaded can be measured, E can be determined. The deflections measurements are obtained from still frames of the digit, which had been loaded at the tip with increasing loads of 0.12N. The vertical displacement of the end point is measured from graph paper placed behind digit. The information obtained from the still frames was plotted as shown in (Figure 6. 17) as a graph of load versus maximum deflection, and applied to the cantilever equation for deflection equation (6.1) where a=L as the load is at the tip of the digit, hence it is maximum deflection and the second moment of area for a thin walled cylinder, (6.3), an approximate value of Young's Modulus was derived in equation (6.4).

$$E = \frac{WL^3}{3\pi r^3 td} \qquad \mathbf{(6.4)}$$

Where L = Length

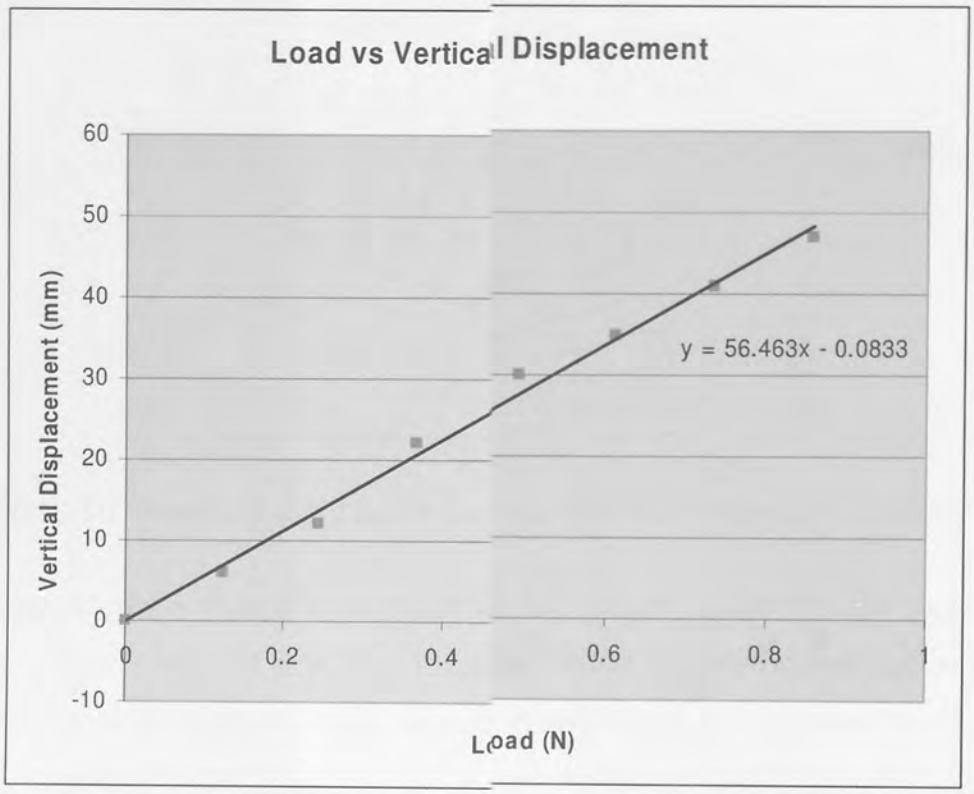

Figure 6. 17 Displacement caused by load on the digit is approximated from information taken from still frames of the digit under loading.

The resulting value of Young's Modulus obtained from equation (6.4) and the graph (Figure 6. 17) is 0.13 GN/m^2 and found to be comparable with rubbers and polyethylene (Ashby, 1980)[94].

However, when equations (6.1), (6.2) and (6.3) are applied to the entire length of the tube, the calculated deflection would be greater than the total length of the beam for large angles of deflections. Instead, since the predominant feature of the digit is that it is made from flexible convoluted tubing, the assumption that each length of the convolutions can be considered as individual short beams (Figure 6.18) and using the same equations (6.1), (6.2) and (6.3), the deflections calculated will also be small and when concatenated in a rotation matrix, the distance of the deflection is no longer greater than the total length of the tube.

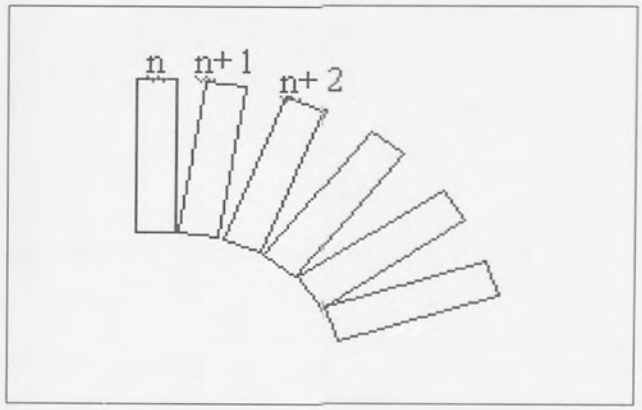

Figure 6.18 The beam is divided into n number of sections called convolutions

A rotation matrix is created in the plane of the body (6.5) and position vector (6.6) and applying the angle of deflection calculated from the beam equations, individual positions for each of the convolutions can be calculated by concatenation (6.7) and (6.8)

$$ {}^{n}_{n+1}R = \begin{bmatrix} \cos\theta & -\sin\theta & 0 \\ \sin\theta & \cos\theta & 0 \\ 0 & 0 & 1 \end{bmatrix} \qquad (6.5) $$

Where R = Rotation matrix
θ = Angle of deflection
$_n$ = Convolution number

$$ {}^{n}P = \begin{bmatrix} x \\ y \\ z \end{bmatrix} \qquad (6.6) $$

Where P = Position vector
x = Position in the x direction
y = Position in the y direction
z = Position in the z direction

For the position vector of convolution n+1:

$$ {}^{n}P_{n+1} = {}_{n+1}^{n}R\,{}^{n}P \qquad (6.7) $$

For the position vector of convolution n+2:

$$ {}_{n+2}^{n}P = \left[\begin{array}{ccc|c} & {}_{n+1}^{n}R\,{}_{n+2}^{n+1}R & & {}_{n+1}^{n}R\,{}^{n+1}P_{n+2ORG} + {}^{n}P_{n+2ORG} \\ 0 & 0 & 0 & 1 \end{array}\right] \qquad (6.8) $$

Where $_{ORG}$ = Position vector origin

This can be continued with subsequent convolutions until the positions of the whole digit have been determined.

The curvature of the digit is based on the moment effects caused by pressure, K being exerted on the inside of the inflated digit. We make the assumption that the pressure is constant all the way inside the tube and we can derive the load, W required for to calculate the deflection by using the pressure equation (6.9).

$$ W = KA \qquad (6.9) $$

Where W = Load
K = Pressure
A = Area of the cross section of the tube

This load is applied to equations (6.1) and (6.2) and the results applied to equation (6.7) to determine the curvature of the tube (Figure 6. 19). Each of the blue lines on this graph represents the shape of digit subjected to a certain internal pressure. This shows that curvature of the tube changes with pressure, but does not show the digit increases in length.

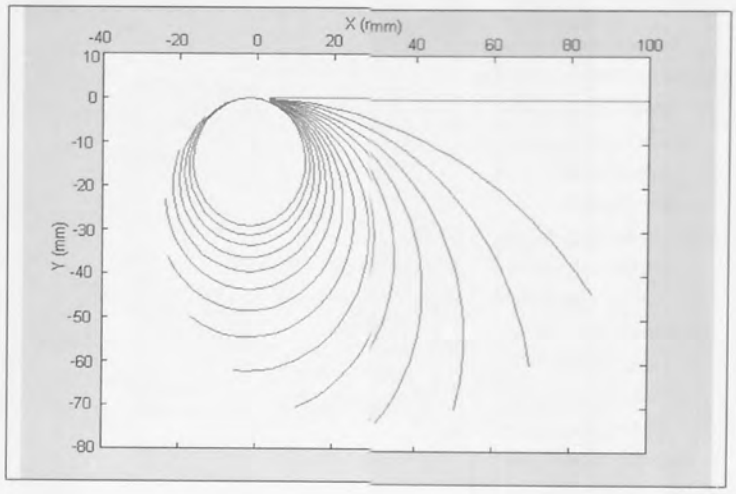

Figure 6. 19 The shape of the tube in bending when subjected to different pressures can be approximated.

6.4.2 Virtual Visualisation

Each position of the convolutions can be extracted from the program model, which was written in MatLab code (Appendix 6.2). From the values calculated from this model the positions where each of the convolutions will be after pressure is applied to the digit. A VRML model in Simulink (Figure 6. 20) of the tube can then be produced (Figure 6.21). A graphical representation of the digit curvature when in vivo presents the user with the opportunity to see what is happening inside the body from a different perspective compared to the conventional field of vision; that of direct line of sight from the tip of the endoscope.

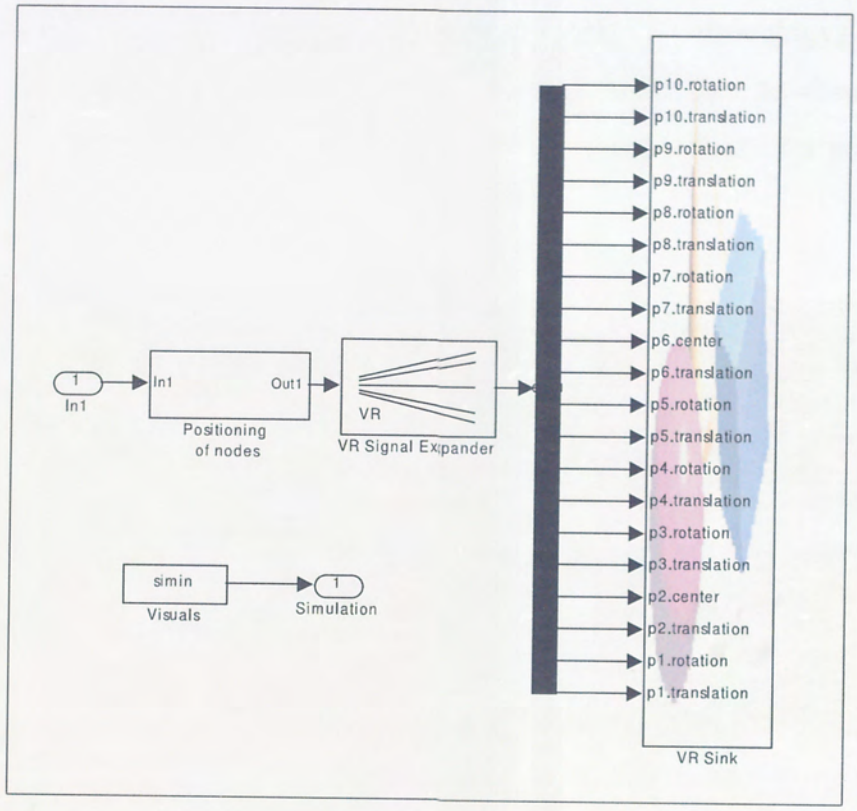

Figure 6. 20 Simulink subsystem for positioning nodes for visualisation of digit

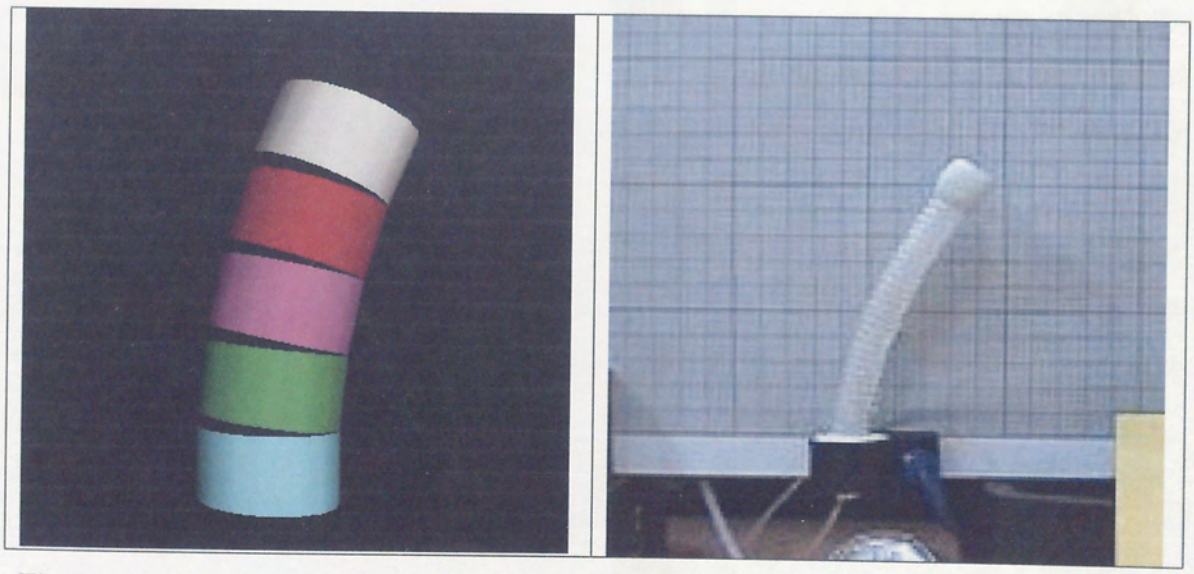

Figure 6.21 Real time computer generated visualisation (left) of the prototype digit (right)

By adding additional movable objects (nodes in VRML terminology) and linking them to displacement values, positioning of point loads can be displayed as is demonstrated in Figure 6.22. The screen shots show movement of a point load for relative positioning, as described in Chapter 5.3.2.1.

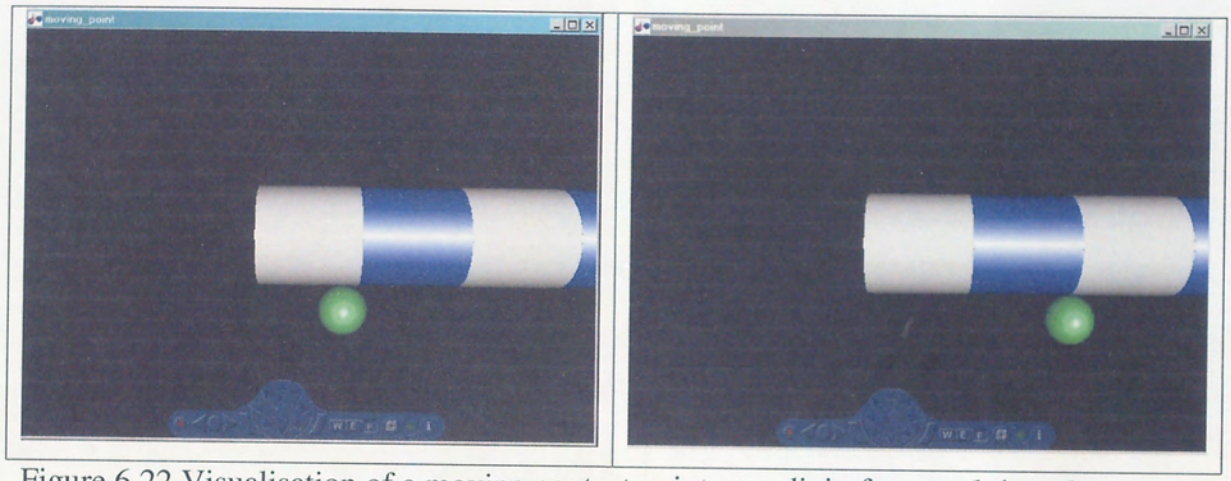

Figure 6.22 Visualisation of a moving contact point on a digit, from real time data obtained in relative positioning as detailed in Chapter 5.3.2.1

Finally, the clinician drives the digit using an instrumented glove. The use of a glove provides the clinician with a more organic method of inputting motion. The complete system demonstrates that the user responds to a tactile prompt that can be used to indicate a change or a new result, such as the time of contact between the digit and tissue. Figure 6. 23 describe an equivalent subsystem representation of clinician control in Simulink. The clinician makes decisions on controlling actuation of the glove based on the visual and tactile feedback he receives, and actuates the digit movement via the instrumented glove.

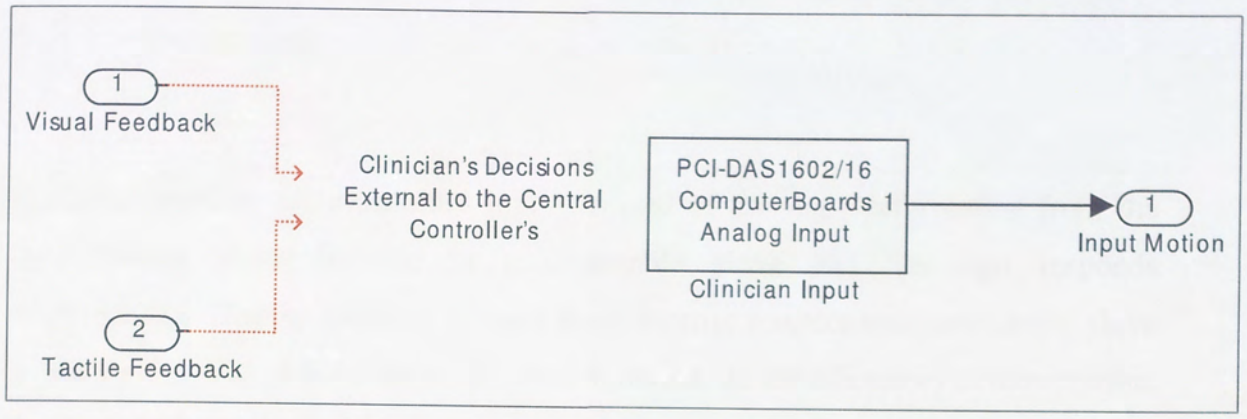

Figure 6. 23 Equivalent Subsystem Schematic Representation of Clinician Control

In addition to a tactile prompt, additional visual displays show the side view of digit's deflected shape that is derived from sensory data. Furthermore, visual diagnostic data such as classification of tissue stiffness can be displayed as values. This can be put into a simple and clear graphical user (Figure 6. 24). This will be used in conjunction with real visuals obtained from an on board camera that will be located along the axial constraint of the digit.

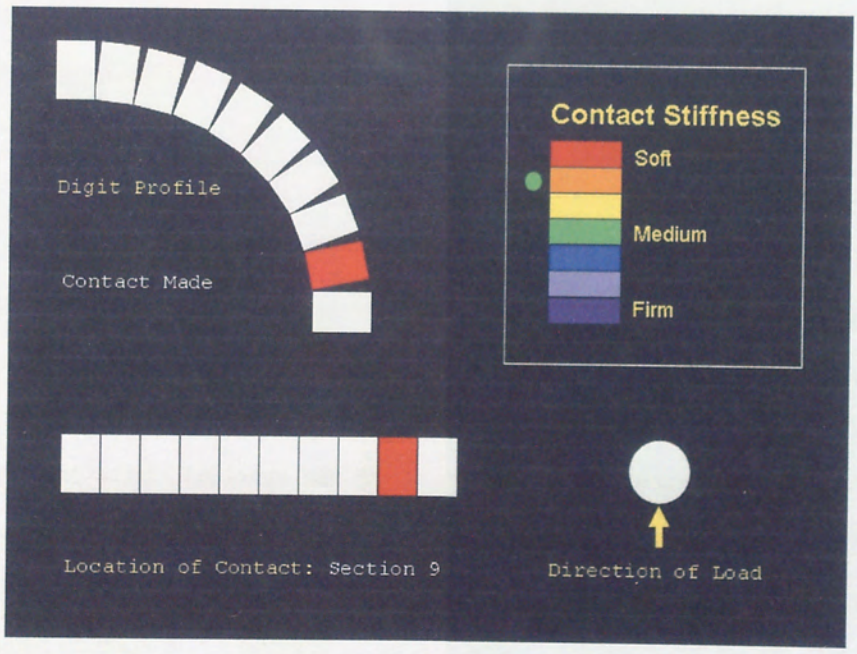

Figure 6. 24 Complete simulated visualisations including diagnostics

6.5 Conclusion

The user interface accommodates input demand of the digit deformation from the user through strain induced in a disposable glove and the digit responds automatically. Tactile feedback is via a piezo-electric actuator mounted on the glove to prompt the user of conditions they wish to detect. In the laboratory demonstration, the tactile feedback was used to give digit-contact information. Visual feedback complements any tactile feedback and provides additional information that cannot be extracted from the digit as tactile feedback. The use of a tactile prompt does marginally improve reaction time of the user to a visual prompt by 0.02 seconds (over a limited test range), however, the response time of the overall system is slow, and so the improvement in reaction time is minimal. The shape of the end tool digit can be predicted using modelling techniques and relayed back as a visual component, along with other diagnostic data extracted from neural networks and interpreted from a central controller. The work in this chapter demonstrates that a complete master slave actuated digit with tactile and visual feedback is achievable.

The point of the glove is that it is convenient and different to other solutions for input devices. This is a versatile, cost efficient for wider ranging healthcare and pragmatic solution, consequently it is mechanically simple. Further tactile sensory feedback could be achieved by either integrating actuating elements within the glove, or devices actuating external to the glove. However, this would lead to a more complex arrangement that would be more bulky, cumbersome and expensive for the operating room environment and surgical practice. In addition, there is the question of the need for further tactile feedback as there is potential for sensory overload when a simple solution would suffice.

Chapter 7

Conclusions

From the work done, the following achievements and conclusions have been made:

7.1 The Context of Clinical Procedures in Design Evaluation

The research was put into context of clinical procedures, with an evaluation of designing an instrument that would be multifunctional, versatile and offer a solution that will offer measurable and quantifiable diagnosis on a large scale, which would supply the need to diagnose a wide range of the population. A summary of the achievements is described on the following page.

- A review of the endoscopic clinical procedure was carried out from which general and specific needs were identified so that technological requirements could be judged in the perspective of general needs and impact.
- A taxonomy of endoscopic procedures was generated based on clinical needs and further identified needs on the technical functional capabilities required of endoscopic tools. The taxonomy could be divided into two sections: diagnosis and treatment. Focusing on diagnosis, the general functions of endoscopy were identified as:
    - Navigation to the site of investigation
    - Examination of the site by palpation
- Tactile examinations of variations in tissue stiffness would enhance procedures and enable discrimination of the targets or tissue types.
- Two clinical procedures for a novel device were selected on which to base representative studies of palpation and navigation needs through tactile sense. These were identified as a digit for use in transanal palpation of the prostate and a digit for use in intubation in anaesthesia. Variants of this device can also be used for other similar applications.
- The design requirements were examined and the specification identified as:
    - Scaling, size and access issues will affect which region of the body the device can operate. The range of lumen size in which a device could be scaled for was determined as being between 6.5cm for the size of the colon to 0.008mm for the size of a capillary.
    - Conventional fabrication technologies can be used to build devices for larger scale lumen, but more specialised technologies, potentially utilising micro fabrication and nanotechnology would be required for very small-scale devices.
    - A device that can work in an electromagnetic environment such as a magnetic resonance imaging (MRI) scanner so a device that is non-metallic and non-electrical device would be ideal.

- Sterility and disposability of clinical devices after use are of growing concern; hence there is motivation for a low complexity, low cost device.

7.2 Distributive Tactile Sensing

Greater understanding of the distributive tactile sensing technique was established during this research; in particular, work on minimising the number of sensing points used to deduce complex information about touch from limited sets of data. The work demonstrated that different types of sensing elements could be used in conjunction with Artificial Neural Networks to provide good results in determining characteristics of touch, and their success is enhanced if the data contains less noise, but nonetheless, successful detection of touch and contact characteristics can be made with noisier data. The success of the experiments on the distributive tactile sensing technique are summarised in the next few points:

- A distributive tactile sensor for a thin flexible beam was built using contrasting sensor elements of strain gauges and optical fibres.
- Feed-forward back propagation artificial neural networks (FFBP ANN) were deployed using different activation functions to optimise predictions of outputs by either classification or inference.
- A mathematical model calculating the strains induced on the beam were used to increase the number of sets of data used to train the ANNs.
- A distributive tactile sensor with resistive strain sensing elements provided successful predictions for determining contact presence, load magnitude and load position with accuracies of 98.5 %, 69.9 % and 74.6 % respectively.

- Use of fibre Bragg sensing elements in place of resistive elements in the distributive tactile sensor improved the reliability of ANN outputs overall by 8.2 %.
- Cascading the neural networks in a sequence provided improved accuracy of predictions lead to taxonomy for touch to be developed. The leading parameters that can be derived by tactile sensing are:
    - Contact
    - Shape
    - Orientation of loading on the digit
    - Position and length of contact
    - Multiple or single contact
    - Axial velocity and displacement relative to tissues
- The number and placement of the sensing elements on the sensor was initially designed with four elements positioned at 0.1L, 0.4L, 0.6L and 0.9L from the root of a beam of length L. It was later discovered that placement of an element at 0.9L from the root of the beam made a minor difference of +/- 3.5 % to the overall performance of the distributive tactile sensing system, leading to the adoption of an optimised three sensing element tactile sensor with sensing elements at 0.1L, 0.4L and 0.6L from the root of the digit.

7.3 The Tool End

Successful construction of an end tool was achieved after extensive experimentation of construction, adhesion and arrangement techniques. The focus of the end tool design is for a device with mass production potential, especially as one of the proposed clinical applications is that examination of the prostate, where mass screening of the target population is considered one of the best strategies for public health. This work shows that a digit like tool end would be able to satisfy

the specific functions for such a purpose and the achievements are summarised below:

- Several functioning prototype end tools, called digits were developed, including several incorporating the distributive tactile sensing system, optimised for the size of and application of the device.
- The versatility of the digit is enhanced by the addition of extra chambers to form steerable endoscopes for clinical investigations requiring more extensive navigation. Two and three chambered digits were produced and capable of providing greater range of movement in different directions depending on configuration.
- The resulting device has shown properties of mechanical simplicity, cost efficiency and suitability in magnetic clinical environments, particularly if the more effective fibre Bragg grating sensors are incorporated into the next version of the device
- Different sized versions of the digit were manufactured to examine the effects of scaling lead to the conclusion that the pressure required to actuate the digit increased as diameter of the digit chamber decreased, indicating that hydraulic pressure would be the preferred medium for smaller scale devices of this design.
- For a mass-produced device it has been identified that manufacturing methods such as blow moulding was justified. This would lead to a digit that can be considered disposable as the issue of sterility is of growing concern and this solution is of great significance.

7.4 Digit Performance

The aim of the experimental investigation is to demonstrate how the performance of the digit could be measured and how the results compared to human models. Clarification of touch was enabled by the development of the taxonomy of touch, which digit performance can be compared with. The taxonomy offers a new method of understanding what the different characteristics of touch are and how they are related to each other. A test rig was designed and built for the purpose of performing contact experiments both static and dynamic tests on the digit. A digit using three sensing elements was successful able to distinguish parameters for:

- Single as opposed to multi-point contact with 87.6 % accuracy with most of the inaccuracies due to multiple contact points being less than 14 mm apart.
- Discrimination of reaction force orientation with 100% for six categories of contact; left, right, top, under, end and no contact.
- Contact stiffness can be evaluated for use in palpation. The digit is capable of discriminating between three distinct ranges of stiffness; hard, medium and soft with 100% accuracy when the digit is not inflated, however, when air is introduced into the digit, the accuracy falls to 82% due to reduction in sensitivity of the sensors. For typical clinical applications, stiffness is deduced as relative phenomena by manual palpation, certainly without greater resolution.
- Discriminating axial motion of the digit with respect to contacting features can be used to assist navigation. The sensing scheme is able to evaluate motion within 5 mm even when moving at velocities of up to 20 mm/s. This following-error is very low for velocities between 20mm/s to 40 mm/s considering the stress relaxation nature of the structural materials of the digit. At the lowest velocities, the accuracy decreases due to overriding features of the test rig.

- Due to limitations of the test rig, it was not possible to test at the lowest velocities; however there is no reason to believe that the system would not perform well at very low speeds.

7.5 The User Interface

To complete a demonstration of a tactile system, an input mechanism was devised and the chosen methods were visual and mechanical input by means of an instrumented glove. To control the digit requires appropriate feedback of the digit shape and contacting conditions and a means to indicate changes in digit displacement; a master system to control feedback of the digit shape and contacting conditions was developed. The objective of the glove, as with the tool end, is for there to be a versatile and cost efficient device that would appeal to a wide range of health care solutions, and hence it is mechanically very simple. Other user interfacing is by visual stimulus, in addition to contemporary television displays offered by a camera at the tool end.

- Sensory information from the digit was translated into a visual feedback system, describing the deflections of the digit from a side profile, location of contact and the intensity of contact stiffness. This was programmed in VRML.
- A review of appropriate devices that could input the driver's demands and receive tactile feedback concluded in two potential methods; force feedback joysticks or instrumented gloves. The cost of commercial instrumented gloves was prohibitively high and joysticks do not offer a 'natural' input mechanism.
- A low cost disposable glove with tactile feedback was developed where finger gestures provides digit displacement and demands sensory information is sent back to the glove by means of tactile sensation.

- The glove's success in enhancing user performance was measured by comparable reaction times with visual stimulus alone, with slight improvement of 0.02 seconds in performance when tactile prompts were included.

7.6 The Master System and Resulting System Performance

A complete master-slave system was achieved, demonstrating the potential of an actuated digit system with tactile and visual feedback. Although the overall system is in its infancy, it is hoped that further work will be carried out in developing the graphical user interface and to optimise the response times available to the user.

7.7 Recommendations for further work

There are several ways in which this project can be developed and continued:

Digit Construction

- Further analysis of the materials used to build the digit, ensuring that they would be suitable for biomedical applications.
- Building a digit with fibre Bragg Grating optical sensing elements in place of the resistive strain gauges, with comparative measurement of performance would be a logical progression.

Modelling

- The modelling methods for digit deflection when subject to internal pressure could be refined and expanded to allow for other influencing factors such as the construction materials being composites of several types of polymers.

Intelligent Algorithms

- Artificial Neural Networks used in for this research could be improved in their classification and regression ability.
- Use of alternative intelligent algorithms such as fuzzy logic or the genetic algorithm could be investigated for comparison of performance.

Embedded system technology

- The interface for the central controller has been via a PC based system. This has controlled the digit actuation and navigation, sensor signal acquisition, provided intelligent sensing using neural networks in cascaded form and provided tactile and visual feedback of results. A next step would be to develop an application specific digital system implementation of the intelligent sensing digit. The System-On-A-Chip approach can be implemented to create a totally hardware based FPGA (Field-Programmable Gate Array) design as opposed to a PC based technology.

- To compare the two methods, the PC approach is broadly compatible with the pervasive computing solutions using the next generation PDA's (Personal Digital Assistant – small hand held computers) with sensor interfaces. The embedded systems approach is compatible with embedded micro controller implementations, System on chip (SoC) technologies and wireless sensor node implementations (Petra et al, 2004)[95].

7.7 Applications for the real world

The results of this work have generic implications for the surgical tools as a new range of system elements to increase the operator's perception of the working site when working through small or difficult access. The solutions produced are scalable with the potential to be applied to other clinical tools, and also in other clinical domains such as microbiology, biotechnology processing as well as other industrial and military applications.

References

Chapter 1

1. **Gray, Henry** (1995) The Anatomy of the Human Body, Lea & Febinger, 1985
2. **Li, X.** (2001) 'Endoscopic Surgery' in Minimally Invasive Medical Technology edited by Webster, J G, IOP
3. **Schmidt, R.A.** (1991) Motor Learning and Performance: from principals to practice, Human Kinetics Books
4. **Lee, M.H., Nicholls, H.R.** (1999) Tactile sensing for mechatronics - a state of the art survey, Mechatronics 9 (1-31), Pergamon,
5. **Harmon, L.D.** (1982)Automated tactile sensing, Int J Robotics Research, 1(2):3-31
6. **Nicholls, H.R., Lee, M.H.** (1989) A survey of robot tactile sensing technology, Int J Robotics Research, 8(3):3-30
7. **Nicholls, H.R. (editor)** (1992)Advanced Tactile Sensing for Robotics, World Scientific, Singapore
8. **Brett, P.N., Stone, R.S.W.** (1997) A technique for measuring contact force distribution in minimally invasive surgical procedures, Proc. IMechE, Part H, No. H4, Vol. 211, 1997

Chapter 2

9. **Ellis, H.** (2001) A History of Surgery, Cambridge University Press
10. **History Of Surgery** (c. 2004)Medicalbooks.com www.medicalbooks.com/historyofsurgery.htm [accessed 02/08/2004]
11. **Miller, R.A.** (1986) Endoscopic Instrumentation: Evolution, Physical Principles and Clinical Aspects, British Medical Bulletin, Vol.42, No.3, 1986, pp 223-225

12. **History of Minimally Invasive Surgery** (c. 2004) Minimally Invasive Surgery Center, Mount Sinai School of Medicine, www.mssm.edu/misc/history.shtml [accessed 02/08/2004]
13. **Dario, P., Carrozza, M.C., Allotta, B., Gugliemelli, E.** (1996) Micromechanics in medicine, IEEE/ASME Transactions on mechatronics, vol.1 no.2, June 1996, pp 137-148
14. **Wickham, J.E.A.** (1986) Endoscopic Surgery, British Medical Bulletin edited by Miller, R.A., & Wickham, J.E.A., Vol. 42, No. 3, July 1986, pp 222
15. **Minimally Invasive Surgery Defined** (c.2004) Minimally Invasive Surgery Center, Mount Sinai School of Medicine, www.mssm.edu/misc/defined.shtml [accessed 02/08/2004]
16. **Taylor, R.H., Lavallee, S., Burdea, G.C., Moesges, R.** (1996) Computer Integrated Surgery: Technological and Clinical Applications, Minimal-Access Surgery, MIT
17. **Tam, B., Brett, P., Holding, D., Griffiths, M.** (2004) The experimental performance of a flexible digit retrieving tactile information relating to clinical applications, IEEE Mechatronics & Machine Vision in Practice, Macau, 2004
18. **Li, X.** (2001) 'Endoscopic Surgery' in Minimally Invasive Medical Technology edited by Webster, J G, IOP
19. **Schiffman, H.R.** (2001) The Skin Senses, John Wiley & Sons, 2001
20. **Skuldt, D.H.** (2001A) 'X-Ray Based Imagining' in Minimally Invasive Medical Technology edited by Webster, J G, IOP
21. **Skuldt, D.H.** (2001B) 'MRI' in Minimally Invasive Medical Technology edited by Webster, J G, IOP
22. **Berghmans, F., Van Uffelen, M., Nowodzinski, A., Fernandez Fernandez, A., Brichard, B., Gusarov, Decréton, M.** (2000) Radiation effects in optical communication devices, Proceedings Symposium IEEE/LEOS Benelux Chapter, 2000, Delft, Netherlands
23. **Laroussi, M., Mendis, D.A., Rosenberg, M.** (2003) Plasma interaction with microbes, New Journal of Physics 5(2003) 41.1-41.10, April 2003
24. **National Institute for Clinical Excellence (NICE)** (2004) The Prevention of Surgical Transmission of Creutzfeldt-Jacob Disease (CJD) – Common Questions, http://www.nice.org.uk/page.aspx?o=221670 [accessed 10/12/2004]
25. **Gray, Henry** (1995) The Anatomy of the Human Body, Lea & Febinger, 1985
26. **Dario, P., Carrozza, M.C., Marcacci,M., D'Attanasia,S., Magnami, B., Tonet, O. and Megali, G.** (2000) A novel mechatronic tool for computer assisted arthroscopy.', IEEE Trans on Information Technology in Biomedicine, Vol.4, No1, March 2000.
27. **Dario, P.** (1996) Micromechatronics in Medicine, Transactions of Mechantronics, Vol. 1, No. 2, June 1996

28. **Rabenstein, T., Krauss, N., Hahn, E.G., Konturek, P.** (2002) Wireless capsule endoscopy – beyond the frontiers of flexible gastrointestinal endoscopy, Med Sci Monit, 2002; 8(6): RA128-132
29. **Anderson, V.H., Roubin, G.S., Leimgruber, P.P., Douglas Jr, J.S., King III, S.B., Gruentzig, A.R.** (1985) Primary angiographic success rates of percutaneous transluminal coronary angioplasty, The American Journal of Cardiology, Volume 56, Issue 12, 1 November 1985, Pages 712-717.
30. **Drake,J.M., Joy, M., Goldenberg, A., an Kreindler, D.** (1991)'Computer and robotic assisted resection of brain tumours.' Proc. 5th Int Conf on Advanced Robotics, 1991 ICAR, Pisa, 19-22 June 1991, pp888-892.'
31. **Taylor, R.H., Paul,H.A., Mittelstadt, B.D., Hanson, W., Kazanides,P., Zuhan,J.F., Glassman, E., Musits, B.L. and Bargar, W.L. and Williamson, W.** (1990)'An image based robotic system for hip replacement surgery.', J Robotics Soc of Japan, Oct 1990,111-116.
32. **Harris,S.J., Arambula-Cosio,F. Mei, Q., Hibberd, R.D., Davies, B.L.** (1997)' The PROBOT – An active robot for prostate resection.', Proc ImechE, Vol. 211, No H4, 1997, pp317-325.
33. **Davies, B.L., Ho, S.C. and Hibberd, R.D.** (1994) 'The use of force control in robot assisted knee surgery. Proc 1st Int conf on medical robotics and computer assisted surgery, pp258-262, Pittsburgh, September 1994.
34. **Miller, R.A.** (1986) Endoscopic Instrumentation: Evolution, Physical Principles and Clinical Aspects, British Medical Bulletin, Vol.42, No.3, 1986, pp 223-225
35. **History of Minimally Invasive Surgery** (c. 2004) Minimally Invasive Surgery Center, Mount Sinai School of Medicine, www.mssm.edu/misc/history.shtml [accessed 02/08/2004]
36. **A.D.A.M. Health Illustrated Encyclopaedia** (c2002) http:// www.adam.com (Accessed 10/01/2002)
37. **Martin, D.** (2002) 'Endometriosis' in A Practical Manual of Laparoscopy A Clinical Cookbook edited by Pasic, R.P. & Levine, R.L., Parthenon Publishing 2002
38. **Kirk, D.** (1999) BMA Family Doctor Guide to Prostate Disorders, Dorling Kindersley, 1999
39. **Cancer Research UK** (2002) CancerStats Incidence – UK September 2002, Cancer Research UK
40. **GLOBALCAN** (2000) GLOBALCAN 2000: Cancer Incidence, Mortality and Prevalence Worldwide Database version 1.0 (30-11-2000)
41. **Family Practice Notebook** (2000) Digital Rectal Examination, http://www.fpnotebook.com/GI50.htm [accessed 04/01/05]
42. **Limbs & Things** (c 2005) Diagnostic Prostate Trainer, http://www.limbsandthings.com/uk/products.php?id=60364 [accessed 15/04/05]

43. **Concise Medical Dictionary** (2002)"intubation *n.*" Oxford University Press, 2002. Oxford Reference Online. Oxford University Press. 19 September 2003 http://www.oxfordreference.com/views/ENTRY.html?subview=Main&entry=t60.005150
44. **Brett, P.N., Guild, F.** (2000) Investigations of operator response and interpretation of force stimulus at the user interface of master-slave minimal access clinical tools, *Proc. World Congress on Medical Engineering (IEEE EMBS)*, Track 4, Chicago, August 2000.

Chapter 3

45. **Lee, M.H., Nicholls, H.R.,** (1999) Tactile sensing for mechatronics – state of the art survey, Mechatronics 9 1999 1-31
46. **Ruocco, S.R.** (1987) Robot Sensors and Transducers, Open University Press: Milton Keynes
47. **Dargahi, J., Parameswararan, M., Payandeh, S.** (2000), A micromachined piezoelectric tactile sensor for an endoscopic grasper: Theory, fabrication and experiments, Journal of Microelectromechanical Systems, 9(3), 329-335
48. **Tekscan** (c 2004) Tekscan Technology, http://www.tekscan.com/technology.html [accessed 21/09/04]
49. **Woodburn, J., Helliwell, P.S.** (1997) Observations on the F-Scan in-shoe pressure measuring system, Clinical Biomechanics, Vol. 12. No. 3, 1997, S16
50. **Brett, P.N., Stone, R.S.W.** (1997) A technique for measuring contact force distribution in minimally invasive surgical procedures, Proc. IMechE, Part H, No. H4, Vol. 211, 1997
51. **Stone, R.S.W., Brett, P.N.** (1996) A sensing technique for the measurement of tactile forces in the gripping of dough like material, Proc. Inst. Mech. Eng. Part B: J. Eng. Manuf. 210 (3) (1996) 261–269
52. **Tongpadungrod P., Rhys T.D.L., Brett P.N.** (2003) An approach to optimise the critical sensor locations in one-dimensional novel distributive tactile surface to maximise performance, Sensors and Actuators A 105 (2003) 47–54
53. **Shinoda, H., Oasa, H.** (2000), Wireless Tactile Sensing Element Using Stress-Sensitive Resonator, IEEE/ASME Transactions on Mechatronics Vol.5 No. 3 September 2000
54. **Ma, X., Brett, P.N.** (2002) The performance of a 1-D Distributive Tactile Sensing System for Detecting the Position, Intensity and Width of a Contacting Load, IEEE Trans. Instrumentation and Measurement, vol 51(2), pp. 331-336, April 2002.
55. **Eberhart, R., Simpson, P., Dobbins, R.** (1996) Computational Intelligence PC Tools, Academic Press, pp 14-19
56. **Picton, P** (1994) Introduction To Neural Networks, MacMillan Press

57. **Bishop, M.C.** (2002) Neural networks for pattern recognition, Oxford University Press, pp119-127
58. **Morris, A.S.** (1993) Principals of Measurement and Instrumentation, Prentice Hall: Europe
59. **Orthonos, A. & Kalli, K** (1999), Fiber Bragg Gratings: Fundamentals and applications in telecommunications and sensing, Artech House Publishers: MA
60. **Yang, D., Tao, X., Zhang, A** (2001) Optical responses of FBG sensors under deformations, Smart fibres, fabrics and clothing edited by Tao, X, Woodhead Publishing
61. **Ezbiri, A., Kanellopoulos, S.E., Handerek, V.A.** (1998) High resolution instrumentation system for fibre-Bragg grating aerospace sensors, Optics Communications, v 150, n 1-6, May 1, 1998, p 43-48
62. **Nabney, I T** (2002) Netlab Algorithms for Pattern Recognition, Data Normalisation pp29, Springer, 2002
63. **Peine, W.J., Wellman, P.S., Howe, R.D.** (1997) "Temporal Bandwidth Requirements for Tactile Shape Displays," Proceedings, Sixth Annual Symposium on Haptic Interfaces for Virtual Environment and Teleoperator Systems, ASME International Mechanical Engineering Congress and Exposition, 61, pp.107-113, Dallas, 1997.

Chapter 4

64. **Olympus Industrial** (2005), Industrial Fiberscopes, Standard Range http://www.olympusindustrial.com/index.cfm/page/products.index.cfm/cid/323/navid/16/parentid/179 [accessed 21/02/05]
65. **Yamshita, H., Kim, D., Hata, N., Dohi, T.** (2003) Multi-Slider Linkage Mechanism for Endoscopic Forceps Manipulator, Proceedings of the 2003 IEE/RSJ International Conference on Intelligent Robots and Systems, Volume 3, pp 2577-2582, Las Vegas, Nevada, October 2003
66. **Lazeroms, M., La Haye, A., Sjoerdsma, W., Schreurs, W., Jongkind, W., Honderd, G., Grimbergen,C.** (1996) "A hydraulic forceps with force-feedback for use in minimally invasive surgery", *Mechatronics*, vol. 6, no. 4, June 1996, pp. 437-446.
67. **Stone, R.S.W., Brett, P.N.** (1996) A sensing technique for the measurement of tactile forces in the gripping of dough like material, Proc. Inst. Mech. Eng. Part B: J. Eng. Manuf. 210 (3) (1996) 261–269
68. **Buckingham, C.** (2002) Snake Arm Robots, Industrial Robot: An International Journal, Volume 29. Number 3, 2002 pp 242-245
69. **European Diagnostic Manufacturers Association** (2005), In Vitro Diagnostic Industry News, Medical Device Technology, May 2005

Chapter 5

70. **Russell, S.J., Norvig, P.** (1995) Artificial Intelligence: A Modern Approach (2nd Edition), Prentice Hall; Section 18.3; page 531
71. **Schiffman, H.R.** (2001), Sensation and Perception: An Integrated Approach, 5th Edition, John Wiley & Sons Inc

Chapter 6

72. **Runciman W.B., Sellen. A., Webb, R.K., Williamson. J.A., Currie, M., Morgan, C., Russell, W.J.** (1993) Errors, incidents and accidents in anaesthetic practice, Anaesthesia and Intensive Care, Vol. 21, No. 5, October 1993
73. **Akamastu, M., MacKenzie, I. S., & Hasbrouq, T.** (1995). A comparison of tactile, auditory, and visual feedback in a pointing task using a mouse-type device. *Ergonomics, 38,* 816-827
74. **Wyburn, G.M.** (1960) The Nervous System: An outline of the structure and function of the human nervous system and sense organs, Academic Press, London and New York
75. **Schiffman, H.R.** (2001), Sensation and Perception: An Integrated Approach, 5th Edition, John Wiley & Sons Inc
76. (**haptic adj.**) The Concise Oxford English Dictionary. Ed. Catherine Soanes and Angus Stevenson. Oxford University Press, 2004. Oxford Reference Online. Oxford University Press. Aston University http://www.oxfordreference.com/views/ENTRY.html?subview=Main&entry=t23.e25055 [accessed 13/12/04]
77. **Geldard, F.A.** (1972) The Human Senses (2nd Edition), John Wiley
78. **Howe, R.** (2002), Introduction to Haptic Display: Tactile Display, The Haptic Community Website, http://haptic.mech.northwestern.edu/TactileDisplay.html [accessed 29/09/2004]
79. **Essential Reality** (2003), P5 Specification, http://www.essentialreality.co/specifications.asp [accessed 13/03/2003
80. **Fake Space** (2003), Pinch®Glove, http://www.fakespacesystems.com [accessed 14/05/2003]
81. **Inition** (2004), Fakespace Labs PINCH Gloves, http://www.inition.co.uk/inition/product_glove_fakespace_pinch.php [accessed 09/12/2004]
82. **Metamotion** (2003) 5DT Datagloves, http://www.metamotion.com/hardware/motion-capture-hardware-gloves=Dataglove.htm [accessed 07/03/03]
83. **Immersion** (2002), CyberTouch™, http://www.immersion.com/3d/docs/cybertouch_datasheet.pdf [accessed 13/05/2003]

84. **Hendon, D.** David.Hendon@vrweb.com (2003), 5DT Data Glove 5/5-W, 13/05/2003, Email to B.K.Y.Tam (B.K.Y.Tam@aston.ac.uk)
85. **Tan, H.Z. & Pentland, A.** (1997) Tactual displays for wearable computing, Proceedings of the International Symposium on Wearable Computers, Cambridge, Massachusetts, USA (October 1997) pp 84-89
86. TACTAID, (c2002) TACTAID 7, http://www.tactaid.com/tactaid71.html [accessed 20/05/2002]
87. **SensAble Technologies** (2004) Phantom® Devices, http://www.sensable.com/products/phantom_ghost/phantom.asp [accessed 12/12/04]
88. **Reachin** (2003) Reachin Laparoscopic Trainer 2.0, http://www.reachin.se/products/reachinlaparoscopictrainer/ [accessed 02/02/2004]
89. **Verrilo, R** (1991) Vibration and sensation in humans, Music Perception, 1991, 9,3, 281-302
90. **Rabenstein, T. Krauss, N., Hahn, E.G., Konturek, P.** (2002) Wireless capsule endoscopy – beyond the frontiers of flexible gastrointestinal endoscopy, Med Sci Monit, 2002; 8(6): RA128-132
91. **Lecuyer, A., Coquillart, S., Kheddar, A., Richard, P., Coiffet. P.** (2000) Pseudo-haptic feedback: Can isometric input devices simulate force feedback?, IEEE Virtual Reality 2000 Conference 03 18 – 03, 2000, New Bruswick, Jersey
92. **Case, J., Chilver, A.H., Ross, C., Ross, C.T.F.** (1999) Strength of materials and structures, Butterworth-Heinemann
93. **Slack, P.S.**, 2004 A Cable Actuated Flexible Digit with Tactile Feedback for Use in Clinical Applications, Aston University, Master of Philosophy Thesis
94. **Ashby, M. F., Jones, D.R.H.**, 1980, Engineering Materials 1: An introduction to their properties and applications, Pergamon Press, 1980

Chapter 7

95. **Petra, I., Holding, D.J., Tam, B., Ma. X., Brett, P.N.** (2004) The design of a flexible digit towards wireless tactile sense feedback, ICARCV 2004, Eight International Conference on Control, Automation, Robotics and Vision, Kunming, China, 6 – 9 December 2004

Appendices

96. **Williams, C.H.** (1986), Colonscopy, British Medical Bulletin: Endoscopic Surgery Vol. 42, No. 3 pp 2265-269, July 1986
97. **Semm, K.** (1986) British Medical Bulletin: Endoscopic Surgery Vol. 42, No. 3 pp 284-295, July 1986
98. **Carr-Locke, D.L.** (1986) Biliary Tract and Pancreas, British Medical Bulletin: Endoscopic Surgery Vol. 42, No. 3 pp 257-264, July 1986
99. **Rodeck, C.H., Nicolaides, K.H.** (1986) Fetoscopy, British Medical Bulletin: Endoscopic Surgery Vol. 42, No. 3 pp 296-300, July 1986
100. **Sanborn, T.A.** (1986) Vascular Endoscopy: current state of the art, British Medical Bulletin: Endoscopic Surgery Vol. 42, No. 3 pp 270-273, July 1986

Appendix 1

List of Publications

Brett, P.N., Ma, X., Tam, B., Griffiths, M.V., Holding, D.J. A flexible digit with tactile feedback for invasive clinical applications (Keynote Address), 10th IEEE Conference on Mechatronics and Machine Vision in Practice, Perth, December 2003

Petra, I., Holding, D.J., Blow, K.J., Tam, B., Ma, X., Brett, P.N., The design of a flexible digit towards wireless tactile sense feedback, Proceedings 8th International Conference on Control, Automation, Robotics and Vision (ICARV 2004), pp 468-473, Kunming, China, 6-9 December 2004. ISBN 0-7803-8654-X

Tam, B., Brett, P.N., Holding, D.J., Griffiths, M.V., The experimental performance of a flexible digit retrieving tactile information relating to clinical applications, Proceedings 11th IEEE International Conference on Mechatronics and Machine Vision in Practice, Macao, 30 November – 1 December 2004

Cowie, B., Webb, D.J., Tam, B., Slack, P. Brett, P., Optical sensors capable of providing an endoscope with tactile sensitivity, Optical Sensors in Physiological Measurements, Institute of Physics, London, 11 May 2005

Tam, B., Brett, P.N., Holding, D.J., Griffiths, M., An experimental investigation of the distributive tactile sensing method applied to discriminate contact and motion of a flexible digit typical of invasive clinical environments, ASME 2005, International Design Engineering Technical Conferences and Computers and Information in Engineering Conference, Long Beach, California, USA 24-28 September 2005

Appendix 2: Clinical Notes

Appendix 2.1

Bibliography of references for range in human lumen

Beattie, J M, Dickson, W E C, Drennan, A M, Oliverm J O, A Textbook of Pathology, General and Special, William Heinemann, 1943

Cunningham D J (Romanes, G J (editor)), Cunningham's Manual of Practical Anatomy, English Language Book Society, 1986

Gray, H, Anatomy of a Human Body, Lea & Febinger, 1985

Knight, B, Forensic Pathology, Arnold, 1986

Sappey, P C, Anatomie, physiologie, pathologie des vaisseaux lymphatiques considérés chez l'homme et les vertébrés (Deuxième partie, comprenant, l'ensemble des planches, etc.) 1874-1886

Snell, R S, Dolan, T, Atlas of Clinical Anatomy, Little Brown, 1973

Snell, R S, Dolan, T, Clinical Anatomy for Medical Students, Little Brown, 1973

Wischnitzer, S, Atlas and Dissection Guide For Comparative Anatomy, W H Freeman, 1993

Appendix 2.2

Categorisation of Disciplines

The range of medical procedures that can be carried using a minimally invasive method is extensive, and could be categorised by the areas of the body involved. Some of the medical disciplines that use or could use endoscopic examination and surgery are listed below

The range of medical disciplines using minimally invasive methods

- **Anaesthesiology**
- **Andrology** (Male Reproductive System)
- **Embryology and Foetology** (Prenatal)
- **Gastroenterology** (Digestive System)
- **Gynaecology and Obstetrics** (Female Reproductive System)
- **Neurology** (Brain and Nervous System)
- **Orthopaedics** (Bones and Joints)
- **Otolaryngology** (ENT: Ear, Nose and Throat)
- **Thoracic and Pulmonary System including Cardiology** (Lung and Heart)
- **Urology and Nephrology** (Excretion)

Neonatal and Paediatric medicine could also be included in the above, but generally on a smaller scale.

Appendix 2.3

Types of Endoscopy

- **Arthroscopy:** examination, diagnosis and treatment of joints
- **Bronchoscopy:** examination of the trachea and lung's bronchial trees for abscesses, bronchitis, carcinoma, tumours, infection and inflammation
- **Colonoscopy:** examination of the inside of the colon and large intestine to detect polyps, tumours, ulceration, inflammation, colitis diverticula, Chrohn's disease, and discovery and removal of foreign bodies (Williams, 1986)[96].
- **Colposcopy, pelviscopy:** direct visualisation of the vagina, cervix and pelvis to detect cancer, inflammation, and other conditions (K Semm, 1986)[97].
- **Cystoscopy:** examination of the bladder, urethra, urinary tract, uteral orifices, and prostate with insertion of the endoscope through the urethra.
- **Endoscopic Retrograde Cholangio-Pancreatography) (ERCP)** uses endoscopic guidance to place a catheter for x-ray fluorosocopy with contrast enhancement to investigate the bile duct, the gallbladder, the pancreatic duct and other local anatomy to check for stones, obstructions and other malignancies (Carr-Locke, 1986)[98].
- **Fetoscopy**: under ultrasound guidance, endoscopic procedures are performed transabdominally with local anaesthetic. It provides access to the foetus for diagnosis such as blood and tissue sampling and for therapeutic purposes such as blood transfusion (Rodeck, 1986)[99].
- **Gastroscopy:** examination of the upper gastro-intestinal (GI) tract including the lining of the oesophagus, stomach, and duodenum. Gastroscopy is often used to diagnose ulcers and other sources of bleeding and to guide biopsy of suspect GI cancers and is also called **EGD Esophogealgastroduodensoscopy**
- **Laparoscopy:** visualisation of the stomach, liver and other abdominal organs including the female reproductive organs.
- **Laryngoscopy:** examination of the larynx (voice box).
- **Proctoscopy, proctosigmoidoscopy and sigmoidoscopy**: examination of the rectum and sigmoid colon.
- **Thoracoscopy:** examination of the pleura (sac that covers the lungs), pleural spaces, mediastinum, and pericardium.
- **Vascular Endoscopy:** examination of the blood vessels such as the arteries for build up of plaque knows as coronary angioscopy (Sanborn, 1986)[100] and treatment by coronary angioplasty.

Appendix 2.4

Functions of Endoscopy

Diagnosis Type

Visual diagnosis
: Examination for internal lesions, bleeding, change in colour or size, etc

Biopsy
: Removal of tissue for testing

Brush Cytology
: Examination of cells obtained from swabs

Tactile
: Palpation

Therapy Type

Palliative Care
: Retaining sections,
Removal of foreign bodies - large objects are lassoed with silk and forceps.
Localised management of tumours – phototherapy, laser cauterisation, cryotherapy (freezing)
Dilatation of strictures
Drainage – e.g. of the billary duct – stones
Endoprostheis – e.g. intubation of the billary duct

Laser Endoscopy
: In gynaecology for hysterectomy, genital warts, division of pelvic adhesions, fallopian tubes
In ENT for ablation of lesions
In Gastro for haemorrhage, vascular abnormalities, tumours
In Pulmonary for occlusions

Bibliography of References

Brune, I. B., Laparo-Endoscopic Surgery, Blackwell Science, 2nd Edition, 1996
Miller, R.A., Wickham, J.E.A. Endoscopic Surgery, British Medical Bulletin, Volume 42, No. 3, July 1986
Stammberger, H., Kopp, W., Denkomfeld, T. (Translator) Functional Endoscopic Sinus Surgery – The Messerklinger Technique, BC Decker, 1991

Appendix 3

Equipment Information for Distributive Tactile Sensor Construction

Appendix 3.1
Data Sheet for 2 mm Strain Gauges

Technical Specification
Gauge Length: 2 mm
Measurable Strain: 3 to 4 % Max
Temperature Range: -30 °C to +180 °C
Gauge Resistance: 120 Ohms +/- 0.5 %
Gauge Factor: 2.00 (nominal), temperature coefficient +/- 0.015 %/°C
Thermal Induced: O/P +/- 2 micron strain/°C (20 to 160 °C)*
Fatigue Life: > 10^6 reversals at 1000μ strain
Material: Foil (Copper nickel alloy), Base (Polyimide)
Linear Expansion: Mild steel; 10.8 x 10^{-6}/°C

* 1 micro strain is equal to an extension of 0.001 %

Appendix 3.2
Data Sheets for Strain Amplifiers

In this project, the amplifiers used are manufactured by RDP Electronics Ltd. and Strainstall Ltd.

3.2.1 Manuals for RDP Strain Gauge Amplifiers

Further information can be found online at:

RDP Technical Manual for Strain Module Type 628
http://www.rdpe.com/support/technical-manuals/cd2017k-628.pdf
[accessed 03/06/05]

RDP Technical Manual for Monitor 635 & 636
http://www.rdpe.com/support/technical-manuals/cd2004f-635-and-636.pdf
[Accessed 03/06/05]

Appendix 3.2.2 Strainstall Gagemeter 160/8 Operating Instructions

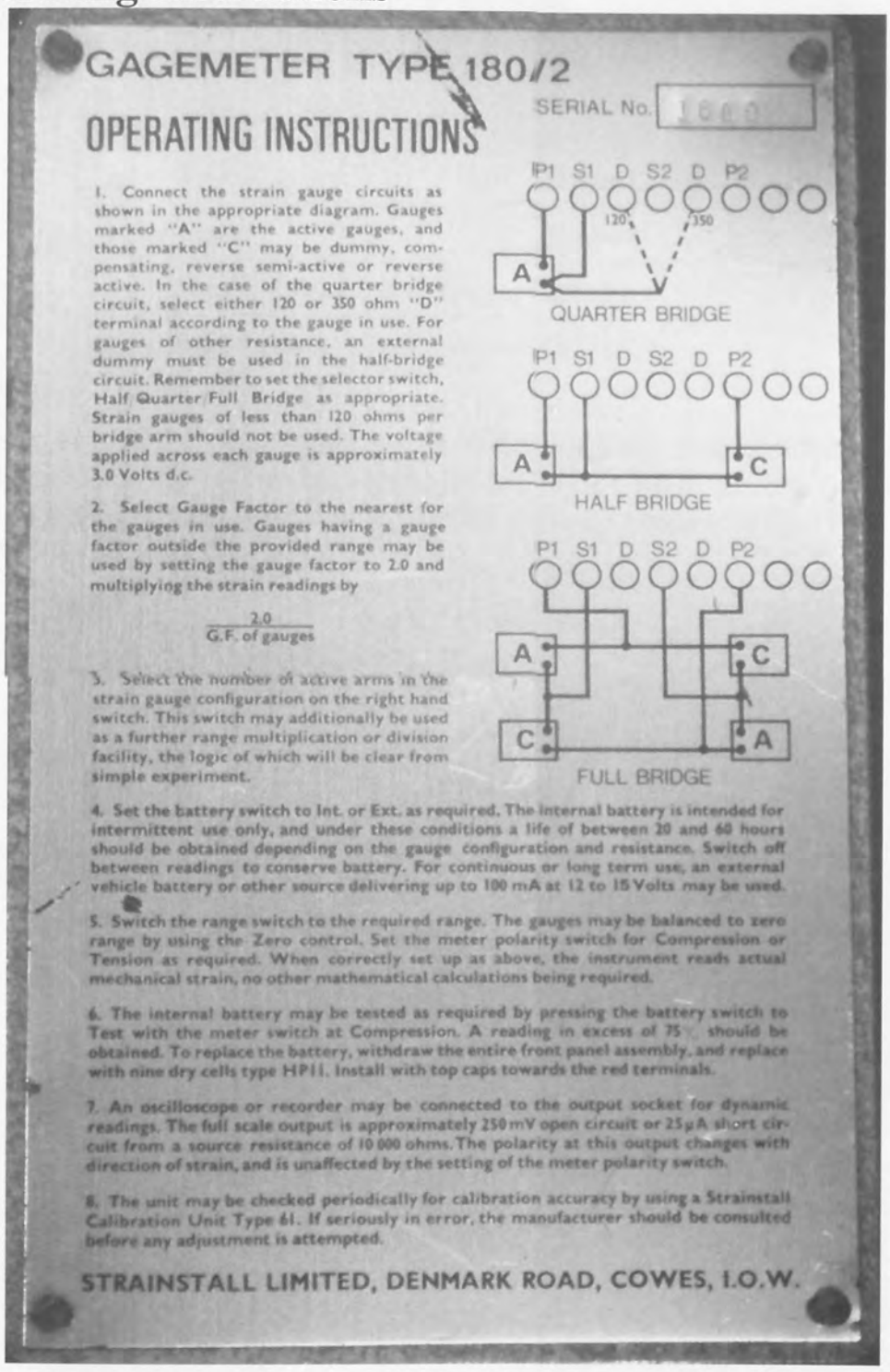

GAGEMETER TYPE 180/2

SERIAL No. 1000

OPERATING INSTRUCTIONS

1. Connect the strain gauge circuits as shown in the appropriate diagram. Gauges marked "A" are the active gauges, and those marked "C" may be dummy, compensating, reverse semi-active or reverse active. In the case of the quarter bridge circuit, select either 120 or 350 ohm "D" terminal according to the gauge in use. For gauges of other resistance, an external dummy must be used in the half-bridge circuit. Remember to set the selector switch, Half Quarter Full Bridge as appropriate. Strain gauges of less than 120 ohms per bridge arm should not be used. The voltage applied across each gauge is approximately 3.0 Volts d.c.

2. Select Gauge Factor to the nearest for the gauges in use. Gauges having a gauge factor outside the provided range may be used by setting the gauge factor to 2.0 and multiplying the strain readings by

$$\frac{2.0}{\text{G.F. of gauges}}$$

3. Select the number of active arms in the strain gauge configuration on the right hand switch. This switch may additionally be used as a further range multiplication or division facility, the logic of which will be clear from simple experiment.

P1 S1 D S2 D P2
120 350
A
QUARTER BRIDGE

P1 S1 D S2 D P2
A C
HALF BRIDGE

P1 S1 D S2 D P2
A C
C A
FULL BRIDGE

4. Set the battery switch to Int. or Ext. as required. The internal battery is intended for intermittent use only, and under these conditions a life of between 20 and 60 hours should be obtained depending on the gauge configuration and resistance. Switch off between readings to conserve battery. For continuous or long term use, an external vehicle battery or other source delivering up to 100 mA at 12 to 15 Volts may be used.

5. Switch the range switch to the required range. The gauges may be balanced to zero range by using the Zero control. Set the meter polarity switch for Compression or Tension as required. When correctly set up as above, the instrument reads actual mechanical strain, no other mathematical calculations being required.

6. The internal battery may be tested as required by pressing the battery switch to Test with the meter switch at Compression. A reading in excess of 75 should be obtained. To replace the battery, withdraw the entire front panel assembly, and replace with nine dry cells type HP11. Install with top caps towards the red terminals.

7. An oscilloscope or recorder may be connected to the output socket for dynamic readings. The full scale output is approximately 250 mV open circuit or 25 μA short circuit from a source resistance of 10 000 ohms. The polarity at this output changes with direction of strain, and is unaffected by the setting of the meter polarity switch.

8. The unit may be checked periodically for calibration accuracy by using a Strainstall Calibration Unit Type 61. If seriously in error, the manufacturer should be consulted before any adjustment is attempted.

STRAINSTALL LIMITED, DENMARK ROAD, COWES, I.O.W.

Figure A 1 Operating Instructions for Strainstall 160/8 Strain Amplifier

Appendix 3.3
Data Sheet for Cantilever Beam

Technical specification	
Type	Feeler Gauges
Brand	Starrett
Imperial steel feeler stock,	0.015in
Manufacturer's part number	667-15

The cantilever beam is made from Starrett feeler stock which is manufactured to BS957.1969 and finished to size, length 304mm (12in), width 12·7mm (1/2 in). Made of tempered steel with smooth rounded ends and punched 3/16 in hole for hanging.

Appendix 3.4

PCI DAS1602/16 Data Sheet

- 8 ch differential / 16 single-ended
- 16-bit resolution
- Dual 16-bit D/As (100KHz)
- 512 sample FIFO for analog inputs and analog outputs
- 6 counters, 24 digital I/O
- Auto-calibration of A/D, D/A

Complete manual and specification can be found at:

http://www.measurementcomputing.com/pdfs/pci-das1602_16.pdf

and

http://www.measurementcomputing.com/pdfmanuals/PCI-DAS1602_16.pdf

[Accessed 01/08/2005]

Appendix 4

Digit Construction

Appendix 4.1

Digit Tubing Information

Corrugated PTFE tubing

Cuff ID	10 mm / 22 mm
Cuff OD	12 mm /24 mm
Wall	0.4 mm
Max PSI at 70°F	170 / 100

Appendix 4.2

Other flexible tubing considered

- **Merlett Oregon PU (code 340) 25 mm inner diameter**

A white PVC helix embedded in clear non-toxic polyether polyurethane.

I.D. mm.	Weight gr./mtr.	Bending Radius mm.	Vacuum $m.H_20$	Coil Length mtr.
25	140	25	4	20

- **Merlett Superflex PU-L (code 410) 30 mm inner diameter**

A zinc plated spiral helix trapped between two layers of crystal clear flexible polyurethane. A lightweight ducting which has excellent internal and external abrasion resistance.

I.D. mm.	Weight gr./mtr.	Bending Radius mm.	Vacuum $m.H_20$	Working Pressure bar
30	130	7	0.30	0.60

- **Merlett Alaska Antistatic (code 360) 35 mm and 40 mm inner diameter**

A grey PVC helix embedded in a clear anti-static flexible PVC compound. Totally wire free. Static conductive compound ROE $1x10^{p1}$ Ohm

I.D. mm.	Weight gr./mtr.	Bending Radius mm.	Vacuum $m.H_20$	Coil Length mtr.
20	150	20	5	50
25	185	25	5	50

- Bellowed tubing can also be custom made and require a combination of polymers added in different ratios will give different stiffness. Combinations of Polymethylhydrosiloxane (PMHS) and Polymethylsiloxane (PDMS) were tested. These are stretchy polymers that can be stiffened with a cross linking agent, Ethylene dimethacrylate (EGDMA). However, all of the compounds made were insufficiently stiff for the digit purposes.

Appendix 4.3

Data Sheet for Norgren Proportional Pressure Control Valve

Technical Specification	
Medium	Compressed air, filtered to 40
	micron, non lubricated
Max. supply pressure	14 bar
Setting pressure range	0·1 to 10 bar (VP5010)
	0·1 to 6 bar (VP5006)
Operating temperature range	-5℃ to +50℃
Port size	G1/4
Air consumption	< 5 1/min
Supply voltage	24V dc ±25%
Power consumption	< 1W
Input signal	4-20mA or 0-10V factory set
Feedback signal	0-10V full scale
Supply sensitivity	Better than 0·75% span output
	change per bar supply presssure
	change
Response time	< 80ms (10-90% step into 0·1
	litre load)
Total error	Max.error < ± 1% of span
	(independent error includes the
	combined effect of non
	linearity, hysteresis, deadzone
	and repeatability)
Temperature effect	Typically better than 0·03% of
	span/℃ for span and zero
Vibration Immunity	< 3% output shift 3g 10-2000Hz
Protection rating	IP65

Appendix 5

Phantom Test Rig

Appendix 5.1
Baldor Linear Drive Specifications

- **Single-Axis Linear Stepper Motor Technical Data**

	Units	LMSS1302-2WW1
No of phases		2
Static force	Lbs (N)	5.0 (22.2)
Force @ 40 in/sec	Lbs (N)	2.5 (11.1)
Resistance/Coil	Ohms	2.2
Inductance/Coil	mH	2.6
Amps/Phase	Amps	2.0
Weight	Lbs (kg)	0.7 (0.32)
Bearing type		Wheel
Air bearing requirements	CFM (L/min)	n/a
Attractive force	Lbs (N)	40 (178)

Repeatability = + 0.0004 in (10 μm)
Resolution = + 0.0001 in (2.5 μm)
Cyclic Error = +/- 0.0002 in (+/- 5 μm) dependent on drive electronics and system implementation
Wheel Bearing Airgap – 0.0008 in (20 μm)

- **Stepper Motor Linear Bar Platen = 21 in (525 mm)**
  The platen is photo-chemically etched on a steel bar filled with epoxy, ground and hard chrome plated.

- **Controller + 3 Stepper Drives = Baldour Nextmove ST**

Technical Data:
Number of Axes 3 internal stepper, 1 external stepper (step & direction @ 400 Hz)
Axis Type
Stepper control with 3 built in stepper drives: 2A @ 37VDC, half stepping
Provision to drive 4 external axes via header—pulse, direction and boost. 400 kHz max. frequency.
5V open collector Darlington
On-board Memory
2MByte Flash for firmware and program storage
2MByte SRAM. 32kBytes FRAM (non-volatile RAM) for parameter storage
Connectors Two part screw terminals.
Digital Inputs
24 inputs. 5V TTL
Software configurable for limits, home, stop and error
Software configurable level and edge triggered
1ms sample rate
Digital Outputs
16 outputs. 5V open collector Darlington
Software configurable for drive enable
50mA per channel, 350mA max. current sink per channel, 500mA max. for 8 channels
Analog Inputs
2 differential ±10V inputs
12-bit resolution
Analog Outputs
1 output 0-10V at 8 bit resolution
Optically isolated
Pulse/Timer Input
Accepts pulse train input with direction. For following type applications.
5V TLL level inputs. 4 MHz max. input frequency
Serial Ports
RS232 via 9-pin D-type. Maximum Baud rate of 115,200
USB 1.1 (12 Mbit/sec) supported by Windows 2000/XP. A 2m USB cable is supplied.
CANbus Ports
Single CAN port via RJ45 connector. Software configurable for CANopen or Baldor CAN via firmware
download
CANopen DS301. Support for CANopen DS401 I/O devices
Master functionality for peer-to-peer communications with other Mint nodes
Baldor CAN. Support for Baldor's range of digital I/O expansion units
Maximum of 63 nodes supported on the network.
Input Voltage: Drive Stage 12-37VDC @ 150W
9-30VAC @ 150VA
Input Voltage: Control Logic 24VDC @ 60W
Environmental Limits Operating temperature 0°C to 40°C (32°F to 104°F) ambient
Weight 0.98 kg (2.16 lb.)
Dimensions L: 262mm/10.3"; W: 140mm/5.5"; H: 54mm/2.13"
Programming
MintMT – Multi-tasking Motion Basic
Windows 9X/NT/2000/XP via ActiveX control

Appendix 5.2
Phantom Rig Drawings

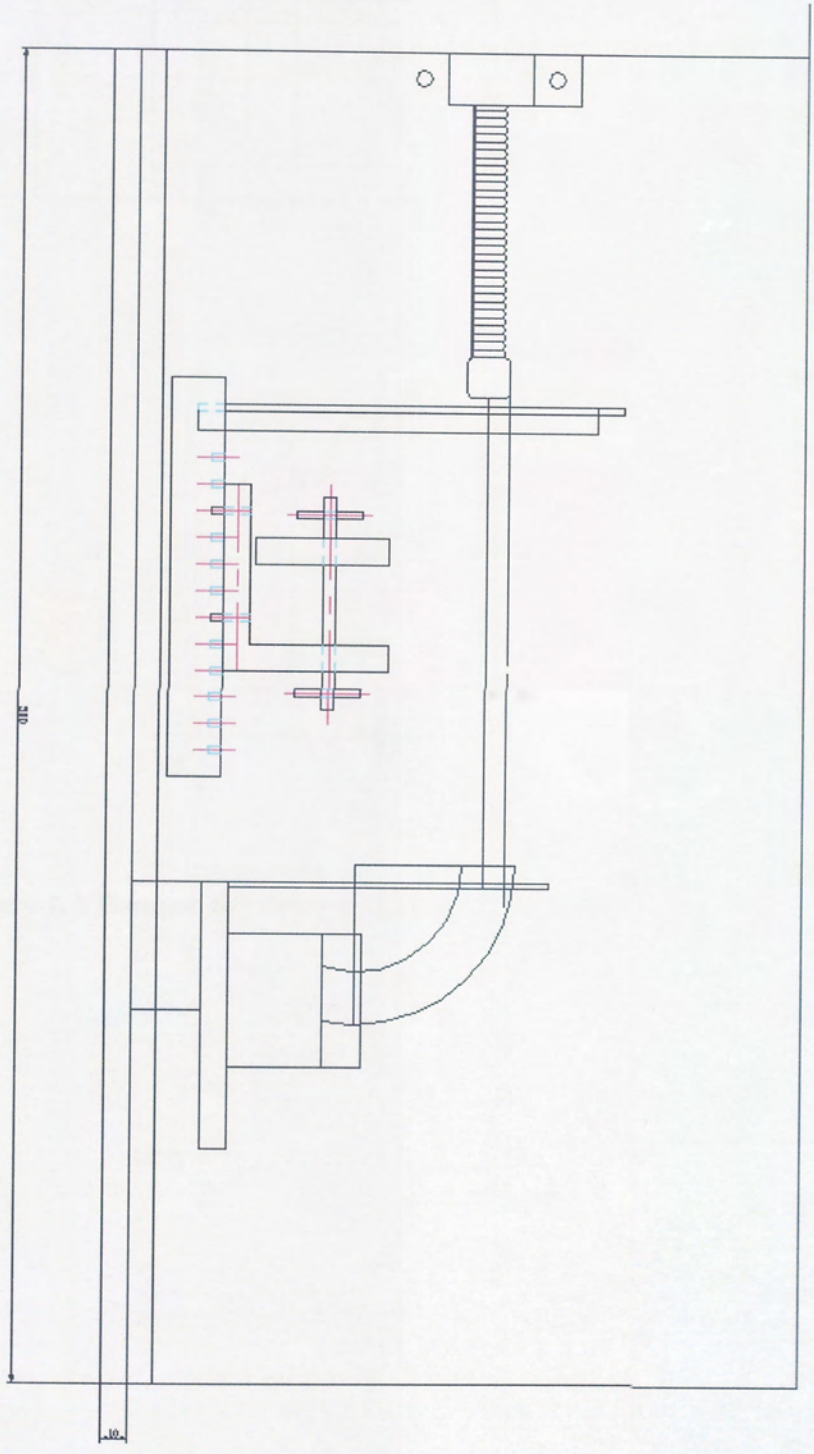

Figure A 2 Impression of phantom rig

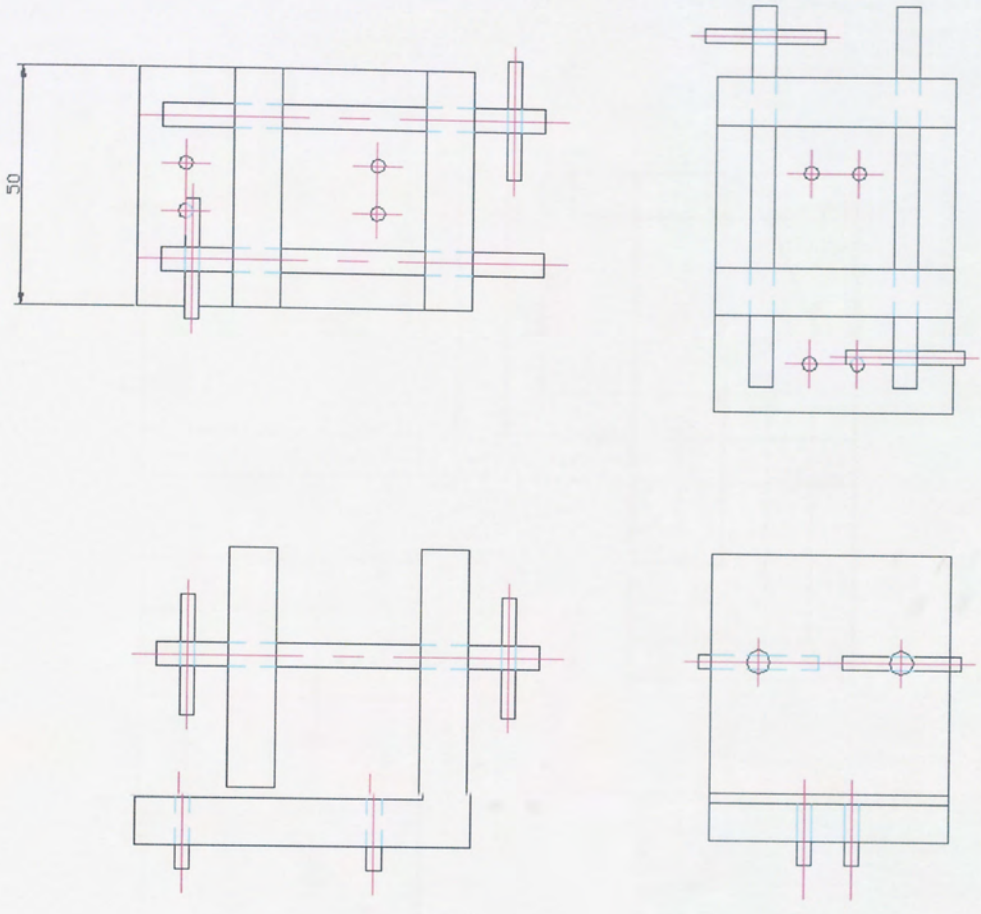

Figure A 3 Phantom Rig Bracket Overall Construction

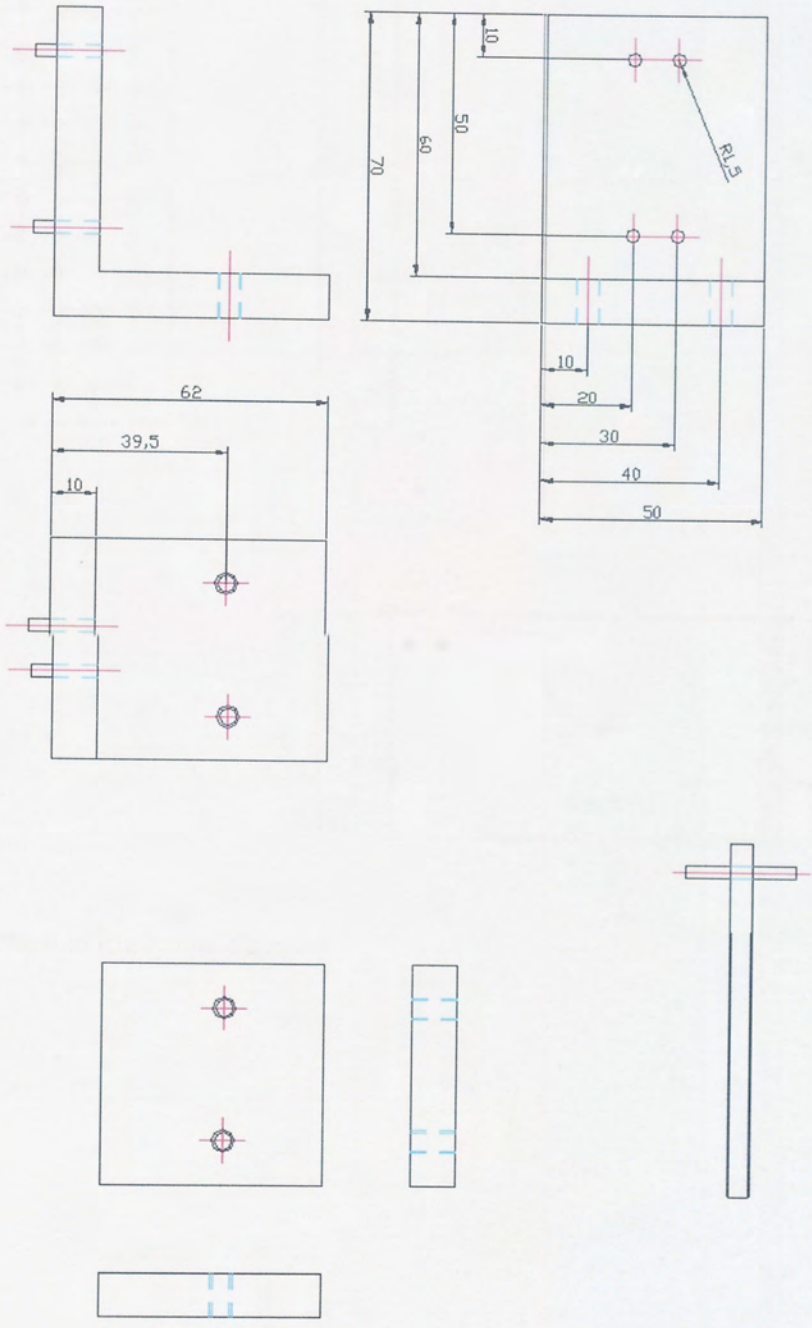

Figure A 4 Phantom Rig Bracket Construction

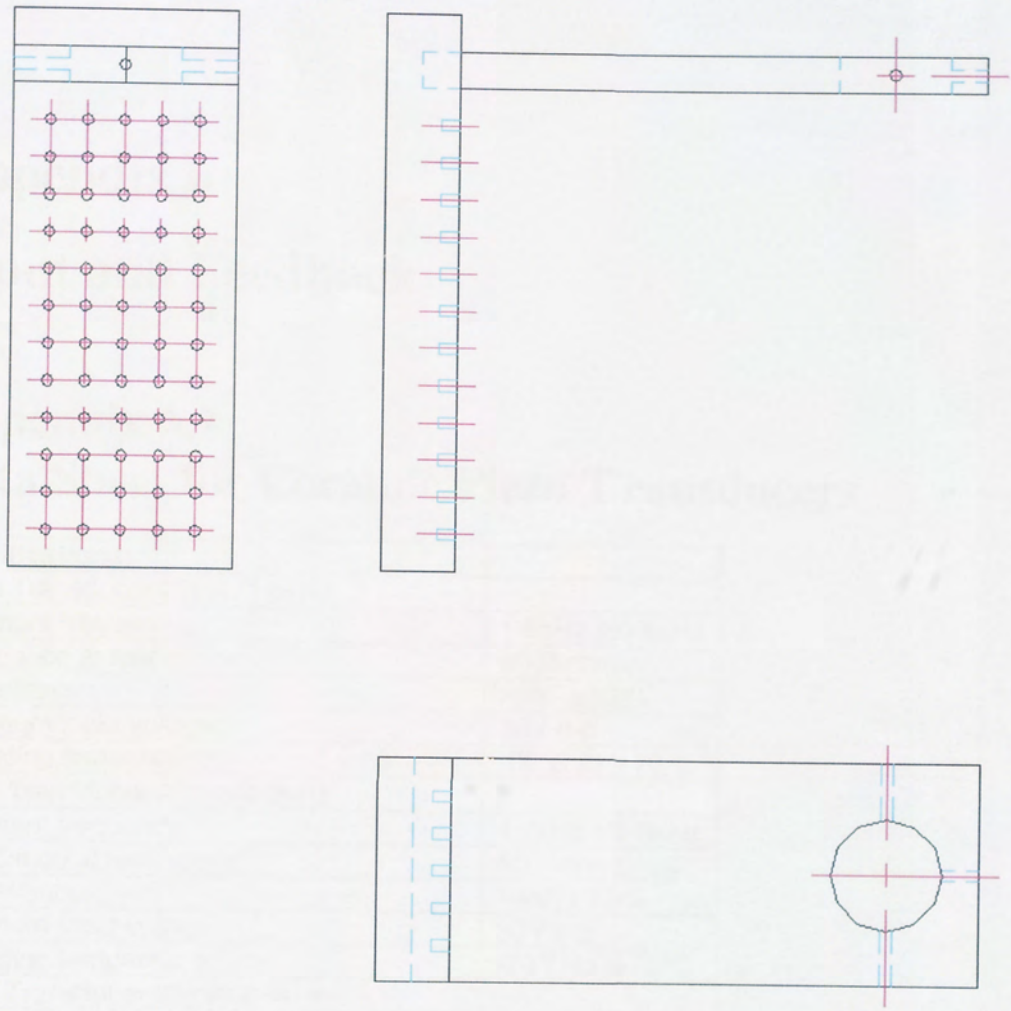

Figure A 5 Phantom Rig Lumen Support

Appendix 6

Input and Feedback

Appendix 6.1
Data Sheet for Ceramic Piezo Transducers

Specifications:	
Piezo Transducer 27mm/1·8kHz	
Resonant frequency:	1·8kHz ±0·5kHz
Impedance at resonance:	800Ω
Capacitance:	25nF ±30%
Maximum input voltage:	30V p-p
Operating temperature:	-20℃ to +70℃
Piezo Transducer 27mm/4·2kHz	
Resonant frequency:	4·2kHz ±0·5kHz
Impedance at resonance:	500Ω
Capacitance:	14nF ±30%
Maximum input voltage:	30V p-p
Operating temperature:	-20℃ to +70℃
Piezo Transducer 35mm/2·8kHz	
Resonant frequency:	2·8kHz ±0·5kHz
Impedance at resonance:	450Ω
Capacitance:	20nF ±30%
Maximum input voltage:	30V p-p
Operating temperature:	-20℃ to +70℃
Piezo Transducer 41mm/2·0kHz for speech	
Resonant frequency:	2·0kHz ±0·5kHz
Frequency range:	750Hz to 20kHz
Impedance at resonance:	600Ω
Capacitance:	40nF ±30%
Maximum input voltage:	15V p-p
Operating temperature:	-20℃ to +70℃
Piezo Transducer 50mm/2·8kHz	
Resonant frequency:	2·8kHz ±0·5kHz
Impedance at resonance:	500Ω
Capacitance:	20nF ±30%
Maximum input voltage:	30V p-p
Operating temperature:	-20℃ to +70℃
Nodal ring diameter:	34mm

Further information can be found at
http://www.maplin.co.uk/Module.aspx?ModuleNo=3202&doy=16m5D[accessed 28/07/2005]

Appendix 6.2
MatLab code for the determining the radius of curvature

```
%Determining the radius of curvature R where the
equation is 1/R = Ws/EI

% Tube Dimensions
clear all;
D=12;      %Diameter of tube in mm
r=D/2;    %Radius of tube in mm
t=1;      %Thickness of tube in mm
r2=r-t;   %Inner radius of tube in mm
IA=pi*(r2.^2);    %Interior Area

L=20;     %Length of tube in mm
n=50;     %Number of sections
s=L/n;    %Length of section

I=(r.^3)*t; % Second Moment of Area for a Thin Walled
Tube
E=1.3;      % Young's Modulus 0.13 GN/m2

%Pressure
Pbar=0;
%Pbar=input('What is the pressure in Bar? ');
for j=1:50
    Pbar=Pbar+0.01;
P=Pbar*(100034.1396/1000000);
W=P*IA;

%Radius of Curvature
R=((W*s)/(E*I))^(-1);

% ThetaA
ThetaA=s/R;
ThetaAdeg=ThetaA*57.295;

%Chord A
A=sqrt((2*R^2)-((2*R^2)*cos(ThetaA)));

% ThetaD
ThetaDdeg=90-((180-ThetaAdeg)/2);
ThetaD=ThetaDdeg/57.2958;
```

```
x=A*cos(ThetaD);     %Horizontal Displacement
y=A*sin(ThetaD);     %Vertical Displacement

%%%%%%
%Reference Matrix
count=1;
%x=Length;
y=0;
z=0;
power=1;
P = [0;0;0];
P(:,count)=[x;y;z];
Rmat=[cos(ThetaD) sin(ThetaD) 0; -sin(ThetaD)
cos(ThetaD) 0; 0 0 1];
% Rmat = [1 -0.0086 0; 0.0086 1 0; 0 0 1];

while count<=n
    count=count+1;
    P(:,count)=(Rmat^(count-1))*P(:,count-1);
end

final = [0;0;0];
for i=1:n;
    sum = [0;0;0];
    for j = 1:i
        sum = sum + P(:,j);
    end
    final(:,i) = sum;
end
final;
figure(1)
plot(final(1,:),final(2,:))

axis([0 20 -10 0]) %axis dimension
%axis equal
pause(0.001) %time taken for each iteration hence
0.001s per iteration
end %end repeat pressure loop
```